

ISSN 1607-8829

Journal of

THERMOELECTRICITY

International Journal

- General problems
- Theory
- Materials research
- Technology
- Design
- Metrology and standardization
- Reliability
- Thermoelectric products
- News
- Discussion

2013

1

Institute of Thermoelectricity, Academy of Sciences and Ministry of Education and Science of youth and sports of Ukraine

Journal of THERMOELECTRICITY

International Research

Founded in December, 1993

published 6 times a year

No. I

2013

Editorial Board

Editor-in-Chief LUKYAN I. ANATYCHUK

Petro I. Baransky

Bogdan I. Stadnyk

Lyudmyla N. Vikhor

Vilius Ya. Mikhailovsky

Ivan V. Gutsul

Elena I. Rogacheva

Stepan V. Melnychuk

Andrey A. Snarskii

International Editorial Board

Lukyan I. Anatychuk, *Ukraine*

A.I. Casian, *Moldova*

Steponas P. Ašmontas, *Lithuania*

Takenobu Kajikawa, *Japan*

Jean-Claude Tedenac, *France*

T. Tritt, *USA*

H.J. Goldsmid, *Australia*

Sergiy O. Filin, *Poland*

L.P. Bulat, *Russia*

M.I. Fiodorov, *Russia*

L. Chen, *China*

D. Sharp, *USA*

T. Caillat, *USA*

Yuri Gurevich, *Mexico*

Yuri Grin, *Germany*

Founders - National Academy of Sciences, Ukraine
Institute of Thermoelectricity of National Academy of Sciences and Ministry
of Education and Science of youth and sports of Ukraine

Certificate of state registration № KB 15496-4068 ПР

Editorial office manager D. Taschuk

Editors:

L. Vikhor, L. Kosyachenko, A. Farion, V. Kramar, V. Katerynchuk

Published by decision of Scientific Board of Institute of Thermoelectricity
of National Academy of Sciences and Ministry of Education and Science of youth
and sports of Ukraine

Address of editorial office:

Ukraine, 58002, Chernivtsi, General Post Office, P.O. Box 86.

Phone: +(380-3722) 7 58 60.

Fax: +(380-3722) 4 19 17.

E-mail: jt@inst.cv.ua

[http:// www.jt.cv.ua](http://www.jt.cv.ua)

Signed for publication 25.02.13. Format 70×108/16. Offset paper №1. Offset printing.
Printer's sheet 11.1. Publisher's signature 9.2. Circulation 400 copies. Order 6.

Printed by "Bukrek" publishers,
10, Radischev Street, 58000, Chernivtsi, Ukraine.

Copyright © Institute of Thermoelectricity, Academy of Sciences
and Ministry of Education and Science, Ukraine, 2013

CONTENTS

General Problems

- A.O. Teut, N.A. Kulenova* The role of thermoelectricity in self-organization processes of polysulfide ores 5

Theory

- P.V. Gorsky, V.P. Mikhachenko* Reduction of thermoelectric material lattice thermal conductivity using shape-forming element optimization 18

Material Research

- E.M. Godzhayev, G.S. Dzhafarova, S.I. Safarova* Band structure of $TlInTe_2$ and thermoelectric figure of merit of solid solutions on its basis 26

Technology

- L.D. Ivanova, L.I. Petrova, Yu.V. Granatkina, V.G. Leontyev, A.S. Ivanov, S.A. Varlamov, Yu.P. Prilepo, A.M. Sychev, A.G. Chuiko, I.V. Bashkov* Melt spinning as a promising method for preparation of bismuth and antimony telluride solid solution materials 31

Design

- S. Yamaguchi, Y. Ivanov, A. Sagara, M. Emoto, Y. Okamoto, H. Nakatsugawa, H. Kitagawa, M. Hamabe, F. Watanabe, J. Sun, T. Kawahara* A proposal of thermoelectric divertor by using silicon carbide in nuclear fusion experiment 41

- L.I. Anatychuk, R.R. Kobylanskyi* Computer design of thermoelectric heat meter readings under real-service conditions 47

- Yu.M. Lobunets* Performance evaluation of OTEC with thermoelectric power converter 55

- V.R. Bilinsky-Slotylo, L.N. Vikhor, V.Ya. Mykhailovsky* Design of thermoelectric generator modules made of Mg and Mn silicide based materials 60

- L.I. Anatychuk, R.V. Kuz, A.V. Prybyla* The effect of heat exchange system on the efficiency of thermoelectric air conditioner 67

Thermoelectric products

- V.S. Gischuk* Electronic recorder with processing signals from heat flux thermoelectric sensor 74

News

- Uemura Kin-ichi* (Dedicated to the 90-th anniversary) 79

- G. Pastorino* (Dedicated to the 75-th anniversary) 80

- V.O. Semenyuk* (Dedicated to the 75-th anniversary) 81

- S.V. Melnychuk* (Dedicated to the 65-th anniversary) 82

- T. Huber* (Dedicated to the 65-th anniversary) 83

Discussion

- Kh.O. Khoshdurdyev* The Earth's thermoelectricity as the basis for power supplies of mankind 84

A.O. Teut¹, N.A. Kulenova²



A.O. Teut

¹The Eastern Mining and Metallurgical Research Institute for Non-Ferrous Metals (VNIITSVETMET),

1, Promyshlennaya Str., Ust-Kamenogorsk,
070002, Republic Kazakhstan

²D. Serikbayev East Kazakhstan State Technical University, 19, Serikbayev Str., Ust-Kamenogorsk, 070012, Republic Kazakhstan



N.A. Kulenova

THE ROLE OF THERMOELECTRICITY IN SELF-ORGANIZATION PROCESSES OF POLYSULFIDE ORES

The purpose of this work was to study the correlation between the electrical and chemical parameters of ore bodies and their role in the restoration of geosystem balanced state. The investigation was concerned with studying the material composition, the electrical and thermal properties of polysulfide ores and the laws of their change with a destabilization of geological formation. A close correlation between the electrophysical and electrochemical properties of sulfide materials has been established. It has been shown that synergism effects contribute to restoration of a disbalance between the material and energy components of the ore system due to development of electrochemical reactions and thermoelectric effect resulting in the active formation of oxidation zone. The results of research can be used to control the processes of crude ore treatment and to prevent its self-ignition.

Key words: polysulfides, synergism, oxidation zone, geosystem stability, electric dipole, galvanocouple, thermoEMF.

Introduction

Natural bodies, including geological ones, by definition of academician V.I. Vernadsky, are formations combining two substances: material and energy. They are in close correlation and, under stable external conditions, in a balanced state. With a change of external conditions in the natural systems, this balance is disturbed, bringing about the processes aimed at its restoration with a new state of environment. The synergetic effects are distinctly traced by the results of analysis of the material characteristics of ore bodies, their composing ore minerals, the electrophysical, electrochemical properties of these formations and the electrical fields produced by them [1, 2].

The nature of energy effects

There are two main types of reasons for destabilization of geological systems: natural, related to development of different geodynamic, metamorphological, etc. processes, and antropogenic, caused by human technological activity.

Ore accumulations and bodies of pyrite-polymetal deposits are nonuniform in the distribution of material and physico-chemical parameters in them, which is caused by polygenesis and polychronism

of their formation. When ore bodies of deposits are formed in several stages, the distribution of ores in them has a zone structure, in the form of stripes or layers. In so doing, the ore materials in each zone are characterized by their unique physico-chemical properties leading to a drastic difference in the electrophysical properties of the layers formed. Owing to this, in terms of energy, they are natural thermoelectric elements combined with micro- and macrogalvanic elements located on different hierarchical levels. In the open environment such thermoelectric elements are generally arranged in subconformity with the occurrence of the ore bodies. The higher is temperature difference on the ends of these elements, the higher is thermoelectromotive force with which they generate current.

For many millions of years the established deposits have been under stable conditions with a balanced state between the material and energy components. In the case of blind ore bodies the difference in temperatures between the upper and lower parts is determined by the temperature gradient of the Earth. Under Rudny Altai conditions this temperature difference with a vertical drop of the ore body and its length to 2 km is 20 to 30 °C. With such temperature difference, the intensity of emerging electrical field does not exceed tenths of a microvolt and thermal currents are minor.

Reaching the erosive truncation changes the environmental conditions (humidity, oxygen concentration, etc.) for micro- and macrogalvanic elements which initiates development of electrochemical reactions with formation of secondary minerals. This process is accompanied by heat release and heating up the upper part of ore body to temperature beyond 100 – 150 °C (almost five-fold increase). Creation of high-power thermal gradient results in the origination of considerable thermoelectric effect and re-formation of natural dipole electrical system: position of ore body heating area is changed and potential difference of the upper and lower dipoles is increased considerably. In the former case heating area was concentrated in the fringe zone, whereas in the latter case it migrates to the head of the ore body. In so doing, due to a large temperature difference between the upper and lower areas of the ore bodies, the intensity of natural electrical field is much in excess of the intensity of electrical fields of the ore bodies that are in a stable state. Such deposits have a well-developed oxidation zone whose formation is related to bringing the material and energy components into a balanced state and which is frequently a seat of sulfide fires.

Antropogenic reasons leading to destabilization of geological systems during extraction and treatment of ores are represented by a continuous process including consecutive steps of development of ore bodies and accumulations by mining; storing of mass in the stockpiles of mines and dressing works; preparation of charge for dressing; dressing; subsequent treatment.

Development of ore accumulation by mining brings about synergism effects similar to those that emerge when an ore body reaches the erosive truncation. Synergism is most conspicuous in places of self-ignition of ores. These processes first appear in the ores enriched with macrogalvanic elements. The temperature in places of ignition reaches 90 – 110 °C, which contributes to launching of local thermoelements. Thermal currents resulting from the work of thermoelectric element, in turn, produce a significant influence on the work of micro- and macrogalvanic elements and intensify oxidation processes. The work of described system of electric elements results in formation of secondary minerals.

Ore excavation disturbs the balance between the material and energy components in total break pieces. Transition to a new stable state during this stage is accompanied by self-organization processes aimed at establishing the balance by transformation of material component due to the effect of micro- and macrogalvanic elements. Transformation of material component changes, in turn, the energy component, cancelling part of natural galvanic elements.

Synergism effects are also observed in the ore stacks of homogenizing yards at the mines and dressing works with a layer by layer formation of ores with different electrophysical (electrochemical)

properties. Crushing and grinding of ores being prepared for flotation enlarges the total surface of natural galvanic elements which intensifies their work.

Results of research on the composition and properties of ores

This paper presents the results of research on pyrite-polymetal and gold-sulfide deposits of Rudny Altai which are notable for their polygenetic nature. It is shown [3, 4] that each step of formation of such deposits took place under specific thermobarogeochemical conditions, unique to this step. This determined zonal distribution of the natural types of ores within ore bodies, as well as the polymorphism of same-name minerals and, hence, the impurity composition and quantitative relations of impurities therein. In Tables 1 and 2 are given compositions of various types of ores and impurity distribution in the depth of occurrence of the ore deposit. Deviations of crystal lattice shape of minerals (including same-name) from perfect one, as well as different composition of impurities in them account for the difference in their electrophysical properties.

*Chemical composition of typical ores of East Kazakhstan
gold-bearing deposits*

Table 1

Components	Content, % (mass)		
	Average for the upper horizons	Deep horizons ("Central" area)	Deep horizons ("Intermediate" area)
<i>SiO₂</i>	60.0 – 65.0	66.0 – 67.0	55.0 – 56.0
<i>Fe general</i>	4.1 – 4.3	5.0 – 6.0	2.8 – 3.0
<i>Al₂O₃</i>	12.1 – 12.5	12.0 – 13.0	14.0 – 15.0
<i>CaO</i>	1.0 – 2.0	2.0 – 2.1	2.2 – 2.3
<i>MgO</i>	1.0 – 2.0	1.3 – 1.4	1.4 – 1.5
<i>Cu</i>	0.010 – 0.015	0.01 – 0.015	0.010 – 0.015
<i>Pb</i>	0.04 – 0.07	–	0.001 – 0.0015
<i>Zn</i>	0.10 – 0.15	0.009 – 0.011	0.007 – 0.009
<i>As</i>	0.90 – 0.93	1.0 – 1.1	0.6 – 0.7
<i>Sb</i>	0.05 – 0.07	0.05 – 0.07	0.01 – 0.02
<i>S general</i>	1.85 – 1.90	1.3 – 1.4	1.8 – 1.9
<i>S sulfide</i>	1.65 – 1.68	1.2 – 1.3	–
<i>C</i>	3.0 – 3.5	1.2 – 1.3	2.1 – 2.5
<i>Au, g/t</i>	9.0 – 10.0	10.0 – 11.0	8.0 – 9.5
<i>Ag, g/t</i>	3.3 – 3.6	1.0 – 2.0	–

According to their electrophysical properties, sulfide minerals are classified as semiconductors. This is directly related to the Fermi level position in the surface layers of mineral-semiconductors

which determines such important surface characteristic as electrode potential representing potential drop at the interface of mineral and ionic medium (for instance, leaching solution) or other mineral forming an aggregate with it.

Table 2
Chemical composition of various types of ores of the Nikolayevskoye deposit

Component	Crystalline ores			Metacolloidal ores	
	Sulphuric-pyrite	Copper pyrite	Copper-zinc pyrite	Copper-zinc pyrite	Zinc pyrite
<i>Cu</i> , %	2.5	7.8	23.4	25.45:8	9.95
<i>Pb</i> , %	0.55	0.5	1.1	4.8	4.55
<i>Zn</i> , %	1.55	3.25	11.65	26.45:5	37.1
<i>S_{sulfate}</i> , %	2.03	0.44	0.48	0.84	2.03
<i>S_{general}</i> , %	44.89	37.99	43.96	46.00	40.53
<i>Fe_{general}</i> , %	39.39	32.50	34.49	38.58	31.75
<i>Al₂O₃</i> , %	2.41	1.75	0.34	1.36	0.17
<i>BaO</i> , %	0.06	0.86	0.11	2.3	4.56
<i>CaO</i> , %	0.36	0.13	0.08	0.15	0.07
<i>MgO</i> , %	0.20	0.54	0.13	0.48	0.14
<i>Bi</i> , %	0.01	0.0021	0.008	0.012	0.0062
<i>Ga</i> , %	0.001	0.00044	0.0003	0.002	—
<i>Ge</i> , %	Not detected	0.0002	0.00032	0.0005	0.0002
<i>In</i> , %	Not detected	0.0001	0.00005	0.0009	0.0009
<i>Cd</i> , %	0.002	0.0108	0.004	0.014	0.003
<i>Mo</i> , %	0.002	0.0018	0.002	0.002	0.0018
<i>As</i> , %	0.07	0.11	0.10	0.22	0.22
<i>Ni</i> , %	weak	0.00098	0.0009	0.0012	0.0038
<i>Sn</i> , %	0.001	0.003	0.003	0.009	0.010
<i>Sb</i> , %	0.004	0.0032	0.002	0.0016	0.022
<i>Se</i> , %	—	0.009	weak	0.006	weak
<i>Tl</i> , %	0.0005	0.0029	weak	0.004	0.004
<i>Te</i> , %	0.0020	0.00174	weak	0.001	0.0016
<i>Ti</i> , %	—	0.0106	0.082	—	0.042

Tables 3 and 4 present the electrophysical properties of the ore minerals of the main deposits of Rudny Altai [5]. The estimates of semiconductor properties of minerals were made on the basis of results of measuring the thermoelectric, galvanomagnetic effects, the electrical conductivity and studying the volt-ampere characteristic of minerals. As can be seen, the thermoEMF T_{EMF} and electrical resistivity ρ of minerals vary within wide limits. The largest variation range is peculiar to iron sulfides (pyrite, markasite) composing, as a rule, a matrix of pyrite-polymetal and gold-sulfide ores (from 60 to 95% of mineral composition). Among them there are species possessing both electron- and hole-type conductivity.

Chalcopyrites are mostly characterized by electron-type conductivity. Grains with hole-type conductivity are extremely rare in the metamorphized ores of the Maleyevskoye deposit.

Among the ores of studied deposits, galenite mainly possesses the electron-type conductivity. Grains with hole-type conductivity are sometimes found in the ores of the Orlovskoye, Maleyevskoye and Tishinskoye deposits.

Table 3
Electrophysical properties of the main ore minerals of the Nikolayevskoye and Orlovskoye deposits

Minerals	Deposits					
	Nikolayevskoye			Orlovskoye		
	T_{EMF} , mV/degree		ρ , $\Omega \cdot \text{m}$	T_{EMF} , mV/degree		ρ , $\Omega \cdot \text{m}$
	n -conductivity ($-T_{\text{EMF}}$)	p -conductivity ($+T_{\text{EMF}}$)		n -conductivity ($-T_{\text{EMF}}$)	p -conductivity ($+T_{\text{EMF}}$)	
Markasite	—	$\frac{0.1; 9.0}{2.43}$	$\frac{5 \cdot 10^{-3}; 3.4}{—}$	—	—	—
Pyrite	$\frac{18; 7}{13}$	$\frac{7; 28}{16.22}$	$\frac{12.5 \cdot 10^{-4}; 1.8}{3.5 \cdot 10^{-3}}$	$\frac{18; 6}{12}$	$\frac{0.1; 15}{7.8}$	$\frac{9.4 \cdot 10^{-4}; 1.1}{4.18 \cdot 10^{-2}}$
Chalcopyrite	$\frac{48; 20}{32}$	—	$\frac{1.8 \cdot 10^{-4}; 0.81}{5.1 \cdot 10^{-5}}$	$\frac{32; 18}{28}$	—	$\frac{9.7 \cdot 10^{-4}; 0.14}{2.3 \cdot 10^{-3}}$
Sphalerite	$\frac{3.0^*; 0}{—}$	$\frac{0.1; 2.5^*}{—}$	$\frac{3.1 \cdot 10^{-2}; 48 \cdot 10^4}{9.2 \cdot 10^3}$	$\frac{8.2^*; 0}{—}$	$\frac{0.2; 12^*}{—}$	$\frac{0.16; 1.1 \cdot 10^7}{5 \cdot 10^5}$
Galenite	$\frac{42; 5}{28}$	—	$\frac{7.2 \cdot 10^{-4}; 0.1}{—}$	$\frac{48; 0}{32}$	$\frac{0.1^*; 3.4^*}{—}$	$\frac{13.2 \cdot 10^{-5}; 0.72}{—}$
Pyrrhotine	—	$\frac{8; 32}{—}$	$\frac{2.8 \cdot 10^{-6}; 0.7}{—}$	—	—	—
Melnikovite; melnikovite-pyrite	—	$\frac{12; 27}{18}$	$\frac{6.7 \cdot 10^{-2}; 1.42}{0.35}$	—	—	—

Note. In the numerator – the minimum and maximum values, respectively, in the denominator – the average value;
^{*} – is of limited occurrence.

ThermoEMF of sphalerites rarely exceeds tenths and even hundredths of mV/degree. In so doing, the hole-type conductivity is mostly recorded. In the ores of the Nilolayevskoye deposit the varieties of sphalerite are sometimes found (marmatite with increased iron content), characterized by thermoEMF value within 5 to 9 mV/degree.

Table 4
*Electrophysical properties of the main ore minerals of the Tishinskoye
 and Maleyevskoye deposits*

Minerals	Deposits					
	Tishinskoye			Maleyevskoye		
	T_{EMF} , mV/degree		ρ , $\Omega \cdot m$	T_{EMF} , mV/degree		ρ , $\Omega \cdot m$
	n -conductivity ($-T_{EMF}$)	p -conductivity ($+T_{EMF}$)		n -conductivity ($-T_{EMF}$)	p -conductivity ($+T_{EMF}$)	
Pyrite	$\frac{30; 16}{21}$	$\frac{2; 13}{6}$	$14 \cdot 10^{-4}; 8.1$ 0.24	$\frac{17; 0}{8}$	$\frac{0.1; 27}{-}$	$1.1 \cdot 10^{-4}; 0.13$ $8.4 \cdot 10^{-2}$
Chalcopyrite	$\frac{48; 20}{32}$	—	$3.6 \cdot 10^{-4}; 1.3 \cdot 10^{-2}$ $15 \cdot 10^{-3}$	$\frac{42; 20}{22}$	$\frac{0.1^*; 3.8^*}{-}$	$4.6 \cdot 10^{-5}; 4.8 \cdot 10^{-2}$ $2.5 \cdot 10^{-3}$
Sphalerite	$\frac{-}{0.4^*}$	$\frac{-}{0.9^*}$	—	$\frac{0.8; 0}{-}$	$\frac{0.27; 6.3^*}{-}$	$1.8 \cdot 10^3; 9.3 \cdot 10^6$ —
Galenite	$\frac{34; 18}{-}$	$\frac{6^*; 18^*}{-}$	—	$\frac{49; 16}{32}$	$\frac{1.4^*; 3^*}{-}$	$8.8 \cdot 10^{-5}; 2.6 \cdot 10^{-3}$ —
Pyrrhotine	—	—	—	—	$\frac{2.4; 12}{-}$	$3.1 \cdot 10^{-5}; 6.6 \cdot 10^{-3}$ $2.8 \cdot 10^{-4}$

Note. Notation is the same as in Table 3

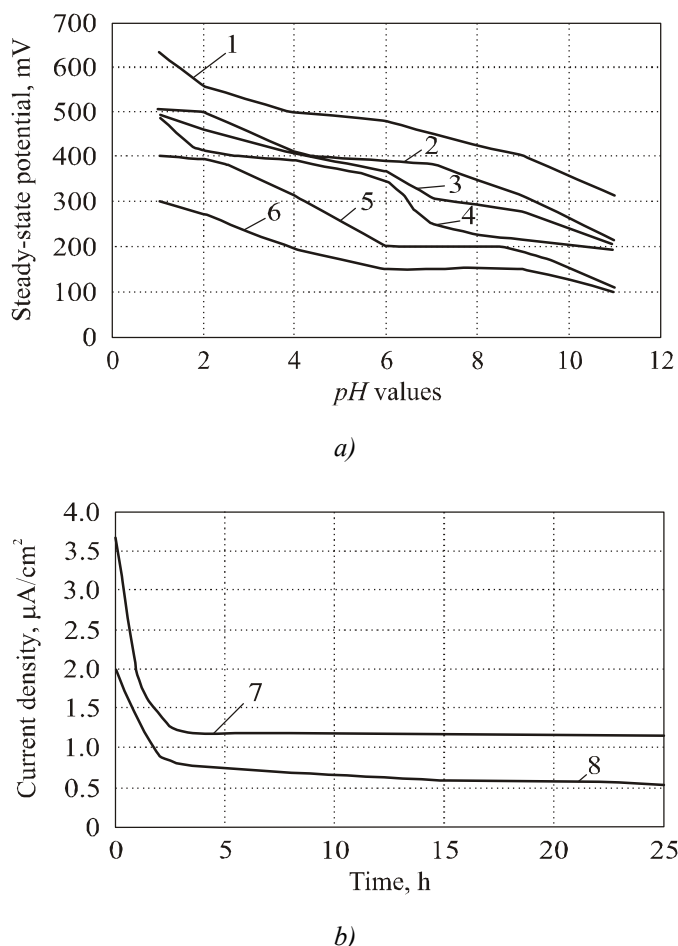
Thus, ores under study are a complex electrode “composed of individual mineral electrodes having relatively positive and negative values of electrode potential” [6]. In so doing, the minerals electrochemically interact and form complex microgalvanic elements. Experimental studies aimed at simulating the work of galvanic elements formed by natural mineral aggregates have shown [5] that electrode potentials of grains as part of polymetallic ores differ considerably from steady-state potentials of isolated monominerals (Table 5).

Table 5
*Effect of “sphalerite – chalcopyrite” galvanic element from the ores of the Nikolayevskoye
 deposit on passing of copper and zinc into solution*

Experiment	Minerals	Content in solution, mg/dm ³			
		without pulp aeration		with aeration	
		Cu	Zn	Cu	Zn
1	Chalcopyrite – sphalerite	$\frac{0.31}{0.49}$	$\frac{1.57}{1.77}$	$\frac{0.35}{0.54}$	$\frac{1.70}{1.85}$
2	Chalcopyrite, sphalerite	$\frac{0.18}{0.23}$	$\frac{0.64}{0.77}$	$\frac{0.20}{0.25}$	$\frac{0.75}{0.88}$
3	Chalcopyrite (n -type)	$\frac{0.17}{0.19}$	—	$\frac{0.18}{0.19}$	—
4	Sphalerite (p -type)	—	$\frac{0.21}{0.28}$	—	$\frac{0.25}{0.33}$

Note. In the numerator – within 24 hours, in the denominator – within 48 hours.

From Table 5 it is seen that with formation of a short-circuited galvanocouple (experiment 1) passing of copper and zinc into solution is increased almost twofold as compared to separate leaching of chalcopyrite and sphalerite (experiments 3 and 4). Some increase of extraction of metals to solution with a simultaneous location in it of non-contacting electrodes of chalcopyrite and sphalerite (experiment 2) is apparently related to formation of ionic electrical bond. Fig. 1 shows a change in electrode potentials on different mineral electrodes in acid and alkali media. The run of potential curves indicates that the work of galvanocouples is controlled by anode process which is retarded both due to products of direct oxidation of sulfides and of secondary reactions on the anode surface, particularly in alkaline medium.



*Fig. 1. Results of measuring steady-state electrode potentials of the main minerals of the Maleyevskoye pyrite-polymetal deposit at different pH values of medium (a) and a change in current density of chalcopyrite-sphalerite galvanocouple with time, mV/degree (b):
 pyrite: 1) +14; 2) -6,3; 3) -15; chalcopyrite: 4) -21; 5) -60; sphalerite:
 6) -2,5; 7) with air purging; 8) without purging.*

Electrochemical oxidation processes related to the work of microgalvanic elements, are rather widespread in nature in the formation of hypergenesis zones. Electrochemical processes and chemical oxidation processes are interrelated and mutually enhancing. Current strength of galvanocouples made of mineral electrodes (simulating natural aggregates), under conditions of active aeration contributing to chemical oxidation of mineral surface, is increased (for the case in Fig. 1, b by a factor of about 2). The generated electrochemical currents, in turn, intensify chemical oxidation of electrodes accompanied by

formation of secondary minerals (Fig. 2). It was established that the electrochemical properties (electrode potential) and the Seebeck coefficient depending on specific features of mineral crystal structure, the character of impurity atoms entry into crystal lattice of sulfides, are closely correlated [7].

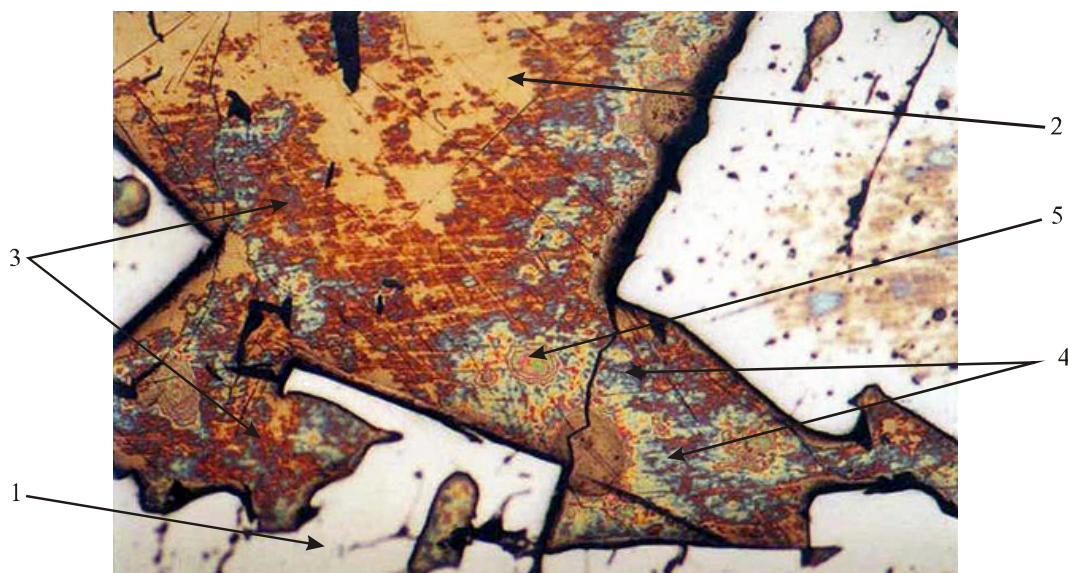


Fig. 2. Result of work of microgalvanic elements formed by p-type pyrite (position 1, light-yellow, relief) and n-type chalcopyrite (position 2, orange, oxidized) in the ore of the Rubtsovskoye deposit: bornite (position 3, brick-red), covellite (position 4, blue), chalcocite (position 5, crimson).

The fact that pyrites qualitatively prevail in polysulfide ores allows singling them out as a mineral which is most responsible for semiconductor properties of ores. From comparison of the composition of pyrites of metacolloidal and crystalline ores in Table 6 it follows that despite the identical collection, the concentration of impurity elements differs considerably, and dependence thermoEMF of pyrites on the content of individual elements in them (Fig. 3) permits a conclusion to be made on the impurity nature of iron sulfides conductivity. Hence it follows that there exists a certain relation between thermoelectric characteristics of pyrite matrices of ores and microsystems of carrier minerals comprised in them (sphalerite, chalcopyrite) with emulsion or microimpregnated inclusions of other minerals (pyrite, chalcopyrite, galenite).

Table 6
Content of the main elements-impurities in the pyrites of ores of the Nikolayevskoye deposit

Elements	Crystalline ores, $n \cdot 10^{-4} \%$	Metacolloidal ores, $n \cdot 10^{-4} \%$
Copper	1568.7	523.5
Zinc	430.0	318.8
Lead	78.9	617.9
Silver	6.2	47.9
Cobalt	286.4	31.8
Nickel	80.7	10.6
Arsenic	534.1	1169.7
Titanium	218.4	674.3

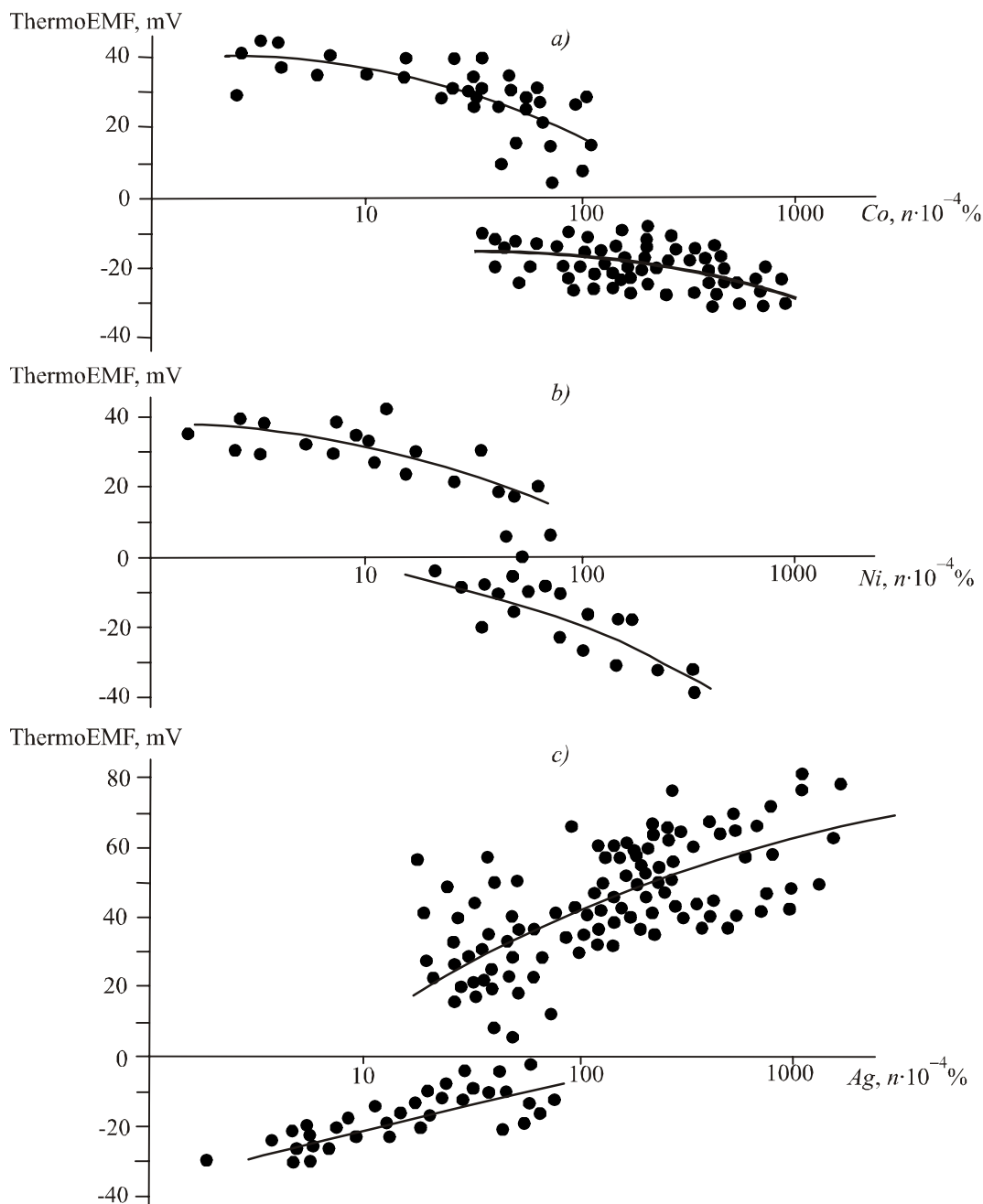
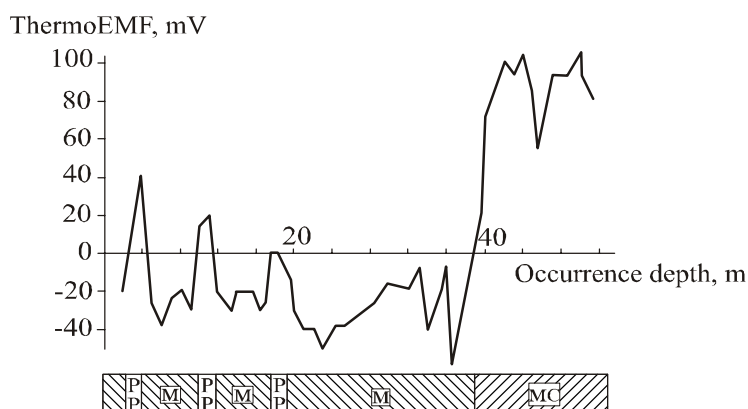


Fig. 3. Correlation dependence of electrophysical properties of iron disulfides of the Nikolayevskoye deposit on the content of elements-impurities
 (a – dependence of thermoEMF of pyrites on cobalt content;
 b – the same, on nickel content; c – the same, on silver content).

To characterize the thermoelectric properties of ores, P.S. Revyakin [8] proposed a term “the Seebeck effect” denoting the total thermoEMF value of minerals in the ore which is a resultant of this parameter with a simultaneous measurement of thermoEMF value of crystal grains composing the ores (including those with different conductivity type) and is proportional to the share and thermoEMF value of predominant-sign crystals.

Practical use of this parameter makes it possible not only to separate and trace different types of sulfide ores in the mine workings (Fig. 4, Table 7), but also to localize zones corresponding to different stages of deposit ore formation (Fig. 5).



*Fig. 4. Results of measuring the Seebeck effect in the quarry of the Nikolayevskoye ore mine:
M – crystalline copper-pyrite ores; MC – metacolloidal copper-zinc ores; P – veinlets of barite-polymetal ores.*

Table 7
The Seebeck effect in the ores of pyrite-polymetal deposits of Rudny Altai

Deposit, Natural types of ores	Conductivity type, $\mu\text{V}/\text{degree}$	
	Prevalence of electron conductivity	prevalence of hole conductivity
Nikolayevskoye deposit		
Metacolloidal ores	— —	$\frac{98; 510}{275}$
Transient ores	$\frac{-258; -0.63}{-125}$	$\frac{18.7; 420}{110}$
Crystalline ores	$\frac{-520; -110}{-315}$	— —
Orlovskoye deposit		
Polymetal ores	$\frac{-480; -18}{-276}$	$\frac{5; 520}{206}$
Copper-pyrite ores	$\frac{-590; -127}{-360}$	— —
Maleyevskoye deposit		
Polymetal ores	$\frac{-510; -12.8}{-260}$	$\frac{34; 490}{211}$
Copper-zinc ores	$\frac{-605; -208}{-418}$	— —
Rubtsovskoye deposit		
Polymetal ores	$\frac{-390; -23}{-186}$	$\frac{11.8; 620}{316}$
Note. In the numerator – the minimum and maximum values, respectively, in the denominator – the average value.		

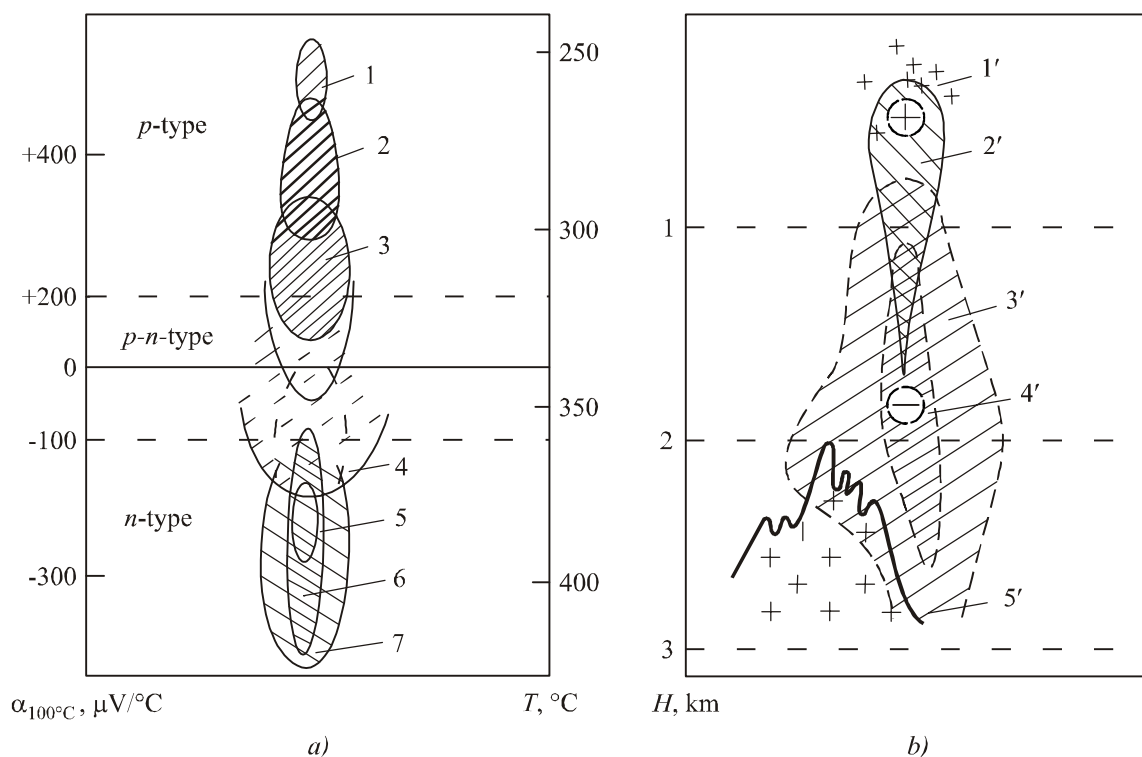


Fig. 5. Schematic of thermoEMF versus crystallization temperature of pyrites (a) and schematic of through-tier zoning of the electrical properties of pyrites of pyrite-polymetal deposits (b). Areas: 1 – low-temperature barite-polymetal ores; 2, 3 – medium-temperature polymetal and copper-zinc ores, respectively; 4 – chlorite-quartz metasomatites of iron-magnesium metasomatism area; 5, 6 – relatively high-temperature pyrite and copper-pyrite ores, respectively; 7 – cericite-quartz metasomatites of acid leaching zone. Areas of change in electrical properties: 1' – barite- and carbonate-polymetal veinlets with p-type pyrites; 2' – chlorite metasomatites and quartzites with p-type pyrites; 3' – sericite-quartz metasomatites with n-type pyrites (external zone); 4' – the same, internal zone; 5' – granitoids. Sign "+" corresponds to positive thermoEMF values, sign "-" to negative.

From the represented data it is seen that the natural types of ores are characterized by different electrophysical properties. Such distribution is exemplified by the ores of the Nikolayevskoye deposit. According to electrophysical properties, in the ores of this deposit there are zones with prevalent hole conductivity, prevalent electron conductivity and mixed conductivity. Localization of contacting ore bunches with different conductivity type causes formation of natural thermoelectric elements.

The technological properties of studied ores have the following specific features:

- in combination, the natural microgalvanic and thermoelectric elements in potential-forming medium are the reason for ignition of sulfide ores in their natural occurrence and in ore stockpiles or dumps. Isolation in the wells and minings during different prospecting stages of ores with different electrophysical properties allows estimating their fire hazard [9]. It is established that if the potential of natural electric field formation is 500 \div 700 mV, the fire hazard of the deposit is high;

- the presence of natural microgalvanic elements (aggregates) in the ores has a negative effect on flotation processes, due to which by the results of determination of electrophysical properties one can recognize the rebellious ores;

– electrochemical reactions occurring in operation of natural thermoelectric and microgalvanic elements, have a beneficial effect on hydrometallurgical ore dressing techniques, intensifying oxidation processes. Owing to this, as early as at the stage of studying the electrophysical properties, one can estimate the advisability of using a hydrometallurgical technique for ore dressing.

Conclusions

Geological formations, just as any natural bodies, tend to retention of equilibrium state. Any external exposures disturbing geosystem stability, initiate a response in the form of chemical and energy processes in crystal mass aimed at restoring the equilibrium.

Electrophysical properties of sulfide minerals belonging to semiconductor class due to peculiarities of material composition and structure are of considerable importance both in formation and life cycle of pyrite-polymetal and refractory pyrite and arseno-pyrite gold-bearing ore deposits. The zone structure of such deposits corresponds to thermobarogeochemical conditions of mineralization at each stage of ore body formation. With a change in the external conditions of stable existence of polysulfide ore deposit, getting its head into erosive truncation zone exposed to potential-forming medium (water, atmosphere air), the process of chemical oxidation of ore minerals is intensified by microgalvanocouples coming into operation (mineral aggregates with different conductivity type). The emerging electrochemical currents many times intensify the oxidation process, which raises essentially the temperature of ore body in oxidation zone. As a result, there is not only a reversal of temperature gradient direction (earlier determined by geothermal heating in the ore body fringe), but the gradient value itself is also considerably increased. A synergistic effect takes place which is manifested in the work of thermoelement formed by ore layers with different conductivity types. Currents generated thereby form an electrical field with a dipole structure activating the work of natural galvanocouples and intensifying mineral oxidation process. Such self-organization process goes on until there is full conversion of sulfide minerals contacting with potential-forming medium into secondary minerals and a new balance is established between the material and energy components of geological system.

Semiconductor properties of sulfides are the most important characteristic of pyrite-polymetal deposit ores. In combination with other geophysical methods of parameter estimation (electrode potentials, early stage of induced polarization), contact method of polarization curves, measurement of thermoelectric properties of ores and ore minerals yields information on the ontogeny, genesis of accumulation helpful in the search, exploration and estimation of explored deposits. On the other hand, thermoEMF measurements allow classifying the ores by technological types, predicting the history of ore treatment processes, in particular, flotation and hydrometallurgical ore dressing methods, estimating the degree of fire hazard of polysulfide deposits.

The Authors express their deep gratitude to professor V.D. Bortsov and other collaborators of VNIITSVETMET for submission of materials for this publication.

References

1. I.N. Plaksin, *Some Problems of Theory and Technology of Interaction of Reagents and Minerals. Flotation Properties of Semiconductor Minerals* (Moscow: Nedra, 1966), p.5-10.
2. I.N. Plaksin, R.Sh. Shafeyev and V.A. Chanturia, Interaction of the Energy Structure of Mineral Crystals and Their Properties, *Proceedings of VIII International Mineral Processing Congress*

(Leningrad, 1969, Vol. 2), p. 235-245.

3. V.V. Popov, N.I. Stuchevsky and Yu.I. Demin, *Polymetal Deposits of the Ore Altai* (Moscow: Nedra, 1995), p.414.
4. D.I. Gorzhevsky, V.B. Chekvalidze and I.Z. Isaakovich, *Types of Polymetal Deposits of the Rudny Altai, Their Origin and Exploration Methods* (Moscow: Nedra, 1977), p.197.
5. V.D. Bortsov, V.P. Naumov, L.B. Kushakova and S.S. Lozhnikov, Natural Galvanic Elements in the Ores of Pyrite-Polymetal Deposits of the Ore Altai, *Tsvetnye Metally* 6, 11-14 (2004).
6. G.B. Sveshnikov, *Electrochemical Processes in Sulfide Deposits* (Leningrad: Leningrad State University Publ., 1967), p.160.
7. V.D. Bortsov, N.V. Sulakvelidze, D.V. Titov, I.F. Kudinov, E.I. Sukhorukova, A.S. Filatov and L.E. Lagutova, Some Peculiarities of Oxidation Processes in the Eastern Kazakhstan Gold-Sulfide and Pyrite-Polymetal Deposits, *Geologiya i Okhrana Nedr* 3, 72-76 (2008).
8. P.S. Revyakin, E.A. Revyakina, Electrical Properties of Pyrites and Their Exploration Significance, *Razvedka i Okhrana Nedr* 7, 45-50 (1978).
9. Patent 41667 Republic Kazakhstan. Method for Establishing Potential Fire Hazard of Pyrite-Polymetal Ores/ V.D. Bortsov, N.I. Degtyar, A.A. Mikheyev, N.V. Sulakvelidze, L.B. Kushakova, V.P. Naumov, A.C. Filatov; Publ. 15.10.04.

Submitted 02.07.2012.

P.V. Gorsky, V.P. Mikhachenko



P.V. Gorsky

Institute of Thermoelectricity of NAS and MESYS
of Ukraine, 1, Nauky Str., Chernivtsi, 58029, Ukraine



V.P. Mikhachenko

**REDUCTION OF THERMOELECTRIC
MATERIAL LATTICE THERMAL
CONDUCTIVITY USING SHAPE-FORMING
ELEMENT OPTIMIZATION**

Within the four different model approaches the lattice conductivity of Bi_2Te_3 was calculated for a physical model of shape-forming element of thermoelectric material structure, namely two hemispheres contacting in a circle with regard to phonon scattering on the contact boundary as applied to Bi_2Te_3 . The calculated data is briefly discussed from the general physics and applied standpoints of thermoelectric material science.

Key words: thermoelectric material, extrusion, figure of merit, lattice thermal conductivity, shape-forming element, contact, boundaries, phonons, scattering, normal processes, U -processes.

Introduction

The most widely used thermoelectric materials nowadays are Bi - Te based alloys (Bi_2Te_3 compounds). They are prepared by different methods, namely zone recrystallization, Czochralski pulling and oriented crystallization process. These three methods yield thermoelectric figure of merit Z in the range of $(2.8 \div 3.1) \cdot 10^{-3} K^{-1}$. Such Z values are achieved with heat flux and electric current orientations in the directions normal to Bi_2Te_3 trigonal axis. Whereas in the direction parallel to trigonal axis the Z values are essentially lower. This situation is due to the fact that Bi_2Te_3 is uniaxial anisotropic crystal whose conductivity values σ_{11} in the direction normal to trigonal axis are $\sigma_{11} = (800 \div 1000) \Omega^{-1}cm^{-1}$ and are considerably higher than σ_{33} – conductivity along trigonal axis. The values of thermal conductivity χ_i are also anisotropic and make $\chi_{11} = 1.45 W/m\cdot K$ and $\chi_{33} = 0.58 W/m\cdot K$. At the same time, the thermoelectric coefficients α_{11} and α_{33} are little different and make $210 \div 220 \mu V/K$. Therefore, $Z_{11} = (2.4 \div 2.5) \cdot 10^{-3} K^{-1}$. For this reason, practical use is found by materials oriented normal to trigonal axis.

Thermoelectric instruments and devices are also manufactured with the use of Bi_2Te_3 based materials prepared by extrusion method whose thermoelectric figure of merit is about $3 \cdot 10^{-3} K^{-1}$, that is, rather close to that of single crystal materials.

It should be noted that the macroscopic structure of extruded materials is a combination of arbitrarily oriented powder particles of size $(40 \div 80) \mu m$ whole properties are close to those of oriented crystalline thermoelectric materials. For extruded thermoelectric materials $\sigma_{ef} = \sqrt{\sigma_{11}\sigma_{33}}$ and $\chi_{ef} = \sqrt{\chi_{11}\chi_{33}}$. Therefore, thermoelectric figure of merit of extruded material must be lower than that of single crystal. Taking into account that electric conductivity anisotropy of Bi_2Te_3 depending on conductivity type is 2.7 for p -type and $4 \div 6$ for n -type, and thermal conductivity anisotropy is $2 \div 3$, the figure of merit can be reduced by a factor of $\sqrt{2} - \sqrt{3}$, that is, by 30 – 40 %. However, in the best

case for *p*-type material it can even grow by about 5 %. In practice, no figure of merit reduction is observed. Hence, there must be a mechanism leading to thermoelectric figure of merit increase in going from single crystal to extruded material structure due to a change in the character of phonon and current carrier scattering. Research on this mechanism would provide for helpful information as to the ways of radical improvement of thermoelectric figure of merit of said materials.

The physical concept of thermoelectric figure of merit improvement in extruded material is that thermal conductivity in going from a bulk to porous or fine-dispersed structure is reduced considerably and the electric conductivity – essentially weaker.

The authors of [1] who were among the first who paid attention to this fact, made evaluation calculations of the electric and thermal conductivity of model structure of thermoelectric material rods divided by vacuum gaps. From the evaluation formulae it follows that if the characteristic dimensions of the rods are small, then the electric and thermal conductivity of the structure is proportional to these dimensions. However, with the large rod dimensions said characteristics tend to parameters of the bulk material. Moreover, in the estimation of thermoelectric figure of merit in this work it was considered that the lattice conductivity of such structure is zero. The electric and thermal conductivity of the structure caused by free charge carriers is essentially dependent on the coefficient of electrons passage through the vacuum gap which does not affect, however, the thermoelectric figure of merit. Said approach did not yield quantitative estimates of rod dimensions and gaps between them that are optimal in terms of thermoelectric figure of merit. In [2] it is shown that in going from single-crystal to fine-dispersed germanium with the average grain radius $2.0 \div 2.5 \mu\text{m}$ (of which samples with porosity 70 % were made), the ratio of electric conductivity to thermal conductivity increased by a factor of 100 as compared to single crystal, and thermoelectric figure of merit – only by a factor of 4 – 6, which, in the authors' opinion is attributable to incomplete restoration of negative thermoEMF after annealing. In [3], formulae were obtained for the determination of the electric and thermal conductivity of a dispersed medium comprising spherical particles of thermoelectric material, but electron and phonon scattering on the boundaries of spheres and contacts between them was not considered.

Paper [4] is a theoretical study of the thermal conductivity of the bulk nanostructured bismuth telluride samples which, nevertheless, does not take into account that phonon scattering on the boundaries of individual nanoparticles occurs at all phonon frequencies, rather than at "selected" ones.

In patent [5] for the efficient phonon drag it is proposed to use small-area contacts between relatively large parts of thermoelectric material. In so doing, said contacts must have dimensions of the order of several nanometers.

There were also considered the possibilities of creating such thermoelectric materials that would be "phonon glasses", remaining in this case "electron crystals" due to the fact that lattice thermal conductivity with a large concentration of structural defects is reduced more than the electric conductivity owing to the peculiarity of electron density of states [6]. The researchers' attention is also focused on the whiskers of organic conductors of the type TTF-TCNQ and the like [7, 8]. It is considered that a high degeneracy level of free charge carriers gas is attainable in these crystals, owing to which lattice thermal conductivity cannot affect considerably the thermoelectric figure of merit of material, and the latter can be regarded as the integral characteristic of free charge carriers subsystem in material [9], that is, the lower limit of thermal conductivity in these crystals has already been achieved, and the only opportunity of thermoelectric figure of merit improvement is the Lorentz number increase.

In the manufacture of thermoelectric modules of conventional material powders by hot pressing or extrusion methods, a question arises as to the optimal in terms of thermoelectric figure of merit size of powder grains and contacts between them. According to [10], particles of source powder can be adequately considered spherical. In the course of pressing they can acquire the shape of hemispheres

with a circular contact between them. The shape-forming element of such structure can be approximated by two equal-radius hemispheres contacting in a circle. Research on the generalized conductivities of such shape-forming element should be a preliminary to a research on the above mentioned characteristics of structure as a whole. It is this that motivates the relevance of the problem solved in this work.

Our purpose in this work is to calculate changes in the lattice thermal conductivity of shape-forming element of extruded thermoelectric material structure due to phonon scattering on the boundaries of contact between two osculating hemispheres, and estimate the radius of contact necessary for 30 – 40 % reduction of lattice thermal conductivity of shape-forming element.

Consideration of the problem of phonon scattering on the boundaries of shape-forming element in the approximation of constant relaxation time

As will be shown below, for consideration of this problem it is reasonable to involve a model of unit sphere placed in a heat flux. This will enable a more transparent physical interpretation of quantitative estimates. With a constant phonon relaxation time, the following expression for the resulting phonon mean free path in a limited sample is valid [11]:

$$l_{tp} = \frac{l_p L}{l_p + L}. \quad (1)$$

In this formula, l_p is phonon mean free path in material caused by all scattering mechanisms, except for the boundaries of contact spot or sample as a whole; L is effective phonon mean free path due to sample boundaries. As long as the effective mean free paths in a sample due to the boundaries are not equal for all the phonons, the thermal conductivity of material at boundary scattering is:

$$\chi_l^{ef} = \frac{1}{3} \rho v c_V l_p \left\langle \frac{L}{L + l_p} \right\rangle. \quad (2)$$

In this formula, ρ is material density, v is sound velocity in it, c_V is specific heat of material with a constant volume. The angular brackets mean averaging of respective expression over possible effective lengths L of phonon mean free path in a sample, including the shortest ones, because theirs is the major contribution to general possibility of phonon scattering [11]. In the case of a circular contact which is small as compared to hemisphere diameters, it can be considered that phonon drag takes place only in its vicinity. Moreover, all points of contact boundary are equivalent by virtue of its symmetry. Hence, formula (2) implies the following ratio between thermal conductivity of shape-forming element and that of the bulk sample:

$$\chi_l^{ef} / \chi_l = \pi^{-1} \int_0^{2\pi} x \frac{k \sqrt{1+x^2 - 2x \cos \varphi}}{1+k \sqrt{1+x^2 - 2x \cos \varphi}} d\varphi dx. \quad (3)$$

In this formula, $k = r/l_p$, l_p is phonon mean free path. As it must be, at $k = 0$ formula (3) gives zero, and at $k \rightarrow \infty$ – thermal conductivity of a bulk sample. The results of these calculations are shown in Fig. 1.

From the results of calculations it follows that for thermal conductivity reduction, for instance, by 30 – 40 %, the contact radius must not exceed $(1.3 \div 2.5) l_p$. Taking into account that according to

[12] the phonon mean free path corresponding to a greater thermal conductivity value is 4.16 nm, we obtain that contact radius must not exceed (5 ÷ 10) nm. The mean free path corresponding to the lower thermal conductivity value is, however, 1.4 nm. Therefore, for the same reduction of the lower thermal conductivity value the contact radius must not exceed (1.8 ÷ 3.3) nm. By analogy, this problem can be solved for a unit sphere. The respective formula is given by:

$$\chi_l^{ef} / \chi_l = 1.5 \int_0^{1/2\pi} \int_0^x x^2 \frac{k \sqrt{1+x^2 - 2xy}}{1 + k \sqrt{1+x^2 - 2xy}} dy dx. \quad (4)$$

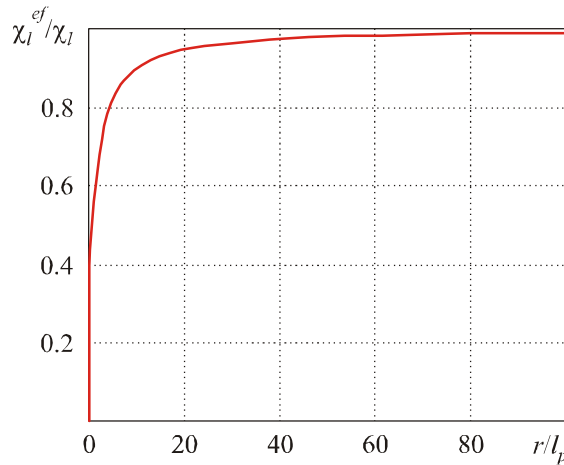


Fig. 1. Dependence of thermal conductivity of a system of two hemispheres contacting in a circle on the contact radius.

Double integral in this formula is caused by averaging the expression for thermal conductivity over the effective phonon mean free paths inside the sphere. In this formula, $k = R/l_p$, where R is sphere radius. The corresponding plot is presented in Fig. 2

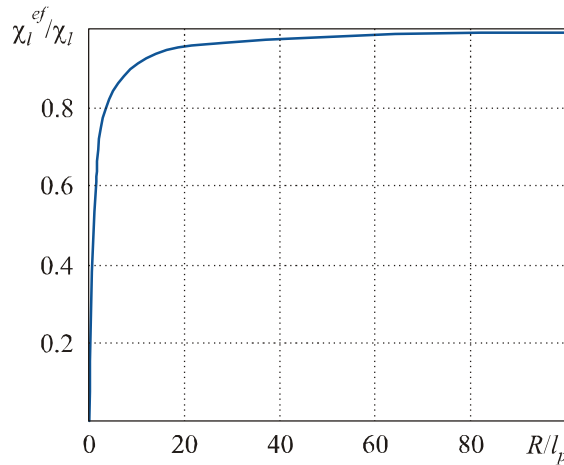


Fig. 2. Sphere radius dependence of a relative decrease in lattice thermal conductivity due to phonon drag size effect.

It is seen that for the above discussed thermal conductivity reduction the sphere radius should not exceed (1.2 ÷ 2.2) l_p . For a greater thermal conductivity value it makes (5.1 ÷ 9.3) nm, and for the lower – (1.6 ÷ 2.9) nm.

Problem consideration with regard to frequency dependence of phonon relaxation time

All previous calculations have been valid in the approximation of constant phonon relaxation time. Next, we consider the problem with regard to frequency dependence of phonon relaxation time.

If we normalize phonon relaxation time to the time of normal processes, then, taking into account [11], components of thermal conductivity tensor of the bulk sample of such layered material as bismuth telluride can be written as:

$$\chi_{l\parallel,\perp} = \frac{3\hbar M v_{\parallel,\perp}^4 k_B}{32\gamma^2 a_{\parallel,\perp}^3 (k_B T_D)^3 \pi^3} \int_0^1 \frac{x^4 \exp(x/\theta)}{\left[\exp(x/\theta) - 1\right]^2} \left(\frac{1}{Q_{l\parallel,\perp}(x)} + \frac{2}{Q_{t\parallel,\perp}(x)} \right) dx. \quad (5)$$

In these formulae, χ_l is lattice thermal conductivity; M is average atom mass in bismuth telluride; v is sound velocity in it; k_B is the Boltzmann constant; γ is the Gruneisen parameter; T_D is the Debye temperature of material; $\theta = T/T_D$, $Q_l(x)$ and $Q_t(x)$ are frequency polynomials introduced by one of the authors (P.V. Gorsky) that are to a power not higher than the fourth and caused by scattering mechanisms for the longitudinal and transverse phonons, indexes \perp and \parallel refer to thermal conductivity and sound velocity normal and parallel to the layers.

At room temperatures and higher the thermal conductivity of thermoelectric material is mainly determined by Umklapp processes (U -processes). Therefore, polynomials $Q_l(x)$ and $Q_t(x)$ are determined as:

$$Q_{l\parallel,\perp}(x) = Q_{t\parallel,\perp}(x) = \mu_{\parallel,\perp} x. \quad (6)$$

Coefficient μ in the analytical form was calculated by Leibfried and Shleman [11] for a cubic lattice. However, according to experimental data [11], the value μ is not universal. Therefore, we will “retrieve” μ_\parallel and μ_\perp coefficients from the real values of components of thermal conductivity tensor of bismuth telluride [12], on condition of their coincidence with the theoretical values (5) and (6). At $\chi_{l\perp} = 0.58 \text{ W/m}\cdot\text{K}$, $\chi_{l\parallel} = 1.45 \text{ W/m}\cdot\text{K}$, $M = 158.8 \text{ a.m.u.}$, $a_\perp = 3 \cdot 10^{-9} \text{ m}$, $v_\perp = 1867 \text{ m/s}$, $a_\parallel = 7 \cdot 10^{-10} \text{ m}$, $v_\parallel = 2952 \text{ m/s}$, $T_D = 155 \text{ K}$ and $T = 300 \text{ K}$ we obtain $\mu_\parallel = 0.131$, $\mu_\perp = 6.657 \cdot 10^{-4}$.

Based on these coefficients, it is easy to calculate a relative reduction of thermal conductivity due to scattering on the boundaries of circular contact and sphere. By analogy with formula (3) in the case of a circular contact:

$$\begin{aligned} \chi_{l\parallel,\perp}^{ef} / \chi_{l\parallel,\perp} &= \pi^{-1} \int_0^1 \int_0^{1/2\pi} \frac{zx^4 \exp(x/\theta)}{\left[\exp(x/\theta) - 1\right]^2} \left(\frac{k_{\parallel,\perp}^* \sqrt{z^2 - 2z \cos \varphi + 1}}{1 + k_{\parallel,\perp}^* Q_{l\parallel,\perp}(x) \sqrt{z^2 - 2z \cos \varphi + 1}} + \right. \\ &\quad \left. + \frac{2k_{\parallel,\perp}^* \sqrt{z^2 - 2z \cos \varphi + 1}}{1 + k_{\parallel,\perp}^* Q_{t\parallel,\perp}(x) \sqrt{z^2 - 2z \cos \varphi + 1}} \right) d\varphi dz dx \left\{ \int_0^1 \frac{x^4 \exp(x/\theta)}{\left[\exp(x/\theta) - 1\right]^2} \left(\frac{1}{Q_{l\parallel,\perp}(x)} + \frac{2}{Q_{t\parallel,\perp}(x)} \right) dx \right\}^{-1}. \end{aligned} \quad (7)$$

$$\text{In so doing, } k_{\parallel,\perp}^* = \frac{r_{\parallel,\perp} \gamma^2}{a_{\parallel,\perp}} \left(\frac{k_B T_D a_{\parallel,\perp}}{\hbar v_{\parallel,\perp}} \right)^4 \left(\frac{k_B T_D}{M v_{\parallel,\perp}^2} \right).$$

The afore-mentioned figures of thermal conductivity reduction for its greater value are obtained at $k^* = 17.37 \div 33.02$. With the above defined problem parameters we get $r_\parallel = (3.5 \div 6.7) \cdot 10^{-9} \text{ m}$. The same figures of thermal conductivity reduction for its lower value are obtained at $k^* = 3419 \div 6498$.

Therefore, $r_{\perp} = (0.6 \div 1.2) \cdot 10^{-9}$ m. Such radii of contacts between particles of diameter $60 \div 80$ μm are hardly feasible.

In the case of a sphere, by analogy with formula (4) we have:

$$\frac{\chi_{l||,\perp}^{ef}}{\chi_{l||,\perp}} = 1.5 \int_0^1 \int_{-1}^1 \int_{-1}^1 \frac{z^2 x^4 \exp(x/\theta)}{\left[\exp(x/\theta) - 1\right]^2} \left(\frac{k_{||,\perp}^* \sqrt{z^2 - 2zy + 1}}{1 + k_{||,\perp}^* Q_{l||,\perp}(x) \sqrt{z^2 - 2zy + 1}} + \frac{2k_{||,\perp}^* \sqrt{z^2 - 2zy + 1}}{1 + k_{||,\perp}^* Q_{l||,\perp}(x) \sqrt{z^2 - 2zy + 1}} \right) dy dz dx \left\{ \int_0^1 \frac{x^4 \exp(x/\theta)}{\left[\exp(x/\theta) - 1\right]^2} \left(\frac{1}{Q_{l||,\perp}(x)} + \frac{2}{Q_{t||,\perp}(x)} \right) dx \right\}^{-1}. \quad (8)$$

$$\text{where } k_{||,\perp}^* = \frac{R_{||,\perp} \gamma^2}{a_{||,\perp}} \left(\frac{k_B T_D a_{||,\perp}}{\hbar v_{||,\perp}} \right)^4 \left(\frac{k_B T_D}{M v_{||,\perp}^2} \right).$$

Hence, in case of a sphere, to obtain the above reduction of greater thermal conductivity value, there must be $k^* = 15.57 \div 29.07$, whence $R_{||} = (3.2 \div 5.9) \cdot 10^{-9}$ m. To obtain the same reduction of lower thermal conductivity value, there must be $k^* = 3420 \div 6500$, whence $R_{\perp} = (0.6 \div 1.2) \cdot 10^{-9}$ m. Such particle dimensions are realizable only in nanostructured thermoelectric materials. Thus, the approach that takes into account only U -processes, cannot explain yet a small change in thermoelectric figure of merit in going from a single crystal to extruded thermoelectric material.

Therefore, it is worthwhile to consider phonon scattering on the boundaries of a circular contact and sphere with regard to not only U -processes, but normal processes as well. For this purpose, frequency polynomials $Q_l(x)$ and $Q_t(x)$ may be written as follows:

$$Q_{l||,\perp}(x) = x^4 + \mu_{||,\perp} x, \quad (9)$$

$$Q_{t||,\perp}(x) = (\mu_{||,\perp} + 3.125\theta^3)x. \quad (10)$$

Hence we get $\mu_{||} = 4.142 \cdot 10^{-5}$, $\mu_{\perp} = 5.917 \cdot 10^{-12}$. In this case, to obtain the above reduction of greater thermal conductivity value with phonon scattering on the boundaries of a circular contact, there must be $k^* = (1.52 \div 4.37) \cdot 10^5$. Thus contact radius $r_{||} = 31 \div 89$ μm. To obtain the same reduction of lower thermal conductivity value, there must be $k^* = (1.839 \div 5.454) \cdot 10^{14}$, whence $r_{\perp} = 32 \div 97$ m. Quite similarly, in the case of phonon scattering on the boundaries of a sphere, to obtain the above reduction of greater thermal conductivity value, there must be $k^* = (1.37 \div 3.90) \cdot 10^5$, whence $R_{||} = 28 \div 80$ μm. For the same reduction of lower thermal conductivity value, there must be $k^* = (1.66 \div 4.88) \cdot 10^{14}$, whence $R_{\perp} = 29 \div 87$ m.

From the absurd, on the face of it, results for r_{\perp} and R_{\perp} parameters it follows that thermal conductivity anisotropy of macroscopic (e.g. meter long) samples cut from Bi_2Te_3 single crystal must be essentially dependent on their size, which is not the case. So, such an approach needs to be modified. Its main disadvantage introducing an excessive error lies in a forced replacement of real crystal lattice of material by a simple cubic lattice with one atom in the unit cell. However, in this case it is clear that neither $a_{||}$ nor a_{\perp} can serve as cube edges, since $M/a_{||}^3$ and M/a_{\perp}^3 quantities yield evidently understated material density values.

In conclusion, we consider an approach based on the substitution of a real Bi_2Te_3 crystal lattice by a simple cubic lattice of the same density. According to this approach, the value of dimensionless

parameter $k_{\parallel,\perp}^*$ for the case of a circular contact should be redefined as:

$$k_{\parallel,\perp}^* = \frac{r_{\parallel,\perp}\gamma^2}{\rho} \left(\frac{k_B T_D}{\hbar v_{\parallel,\perp}} \right)^4 \left(\frac{k_B T_D}{v_{\parallel,\perp}^2} \right), \quad (11)$$

and for the case of a sphere as:

$$k_{\parallel,\perp}^* = \frac{R_{\parallel,\perp}\gamma^2}{\rho} \left(\frac{k_B T_D}{\hbar v_{\parallel,\perp}} \right)^4 \left(\frac{k_B T_D}{v_{\parallel,\perp}^2} \right). \quad (12)$$

As to formula (5), it must be re-written as:

$$\chi_{l\parallel,\perp} = \frac{3\hbar\rho v_{\parallel,\perp}^4 k_B}{32\gamma^2 (k_B T_D^2) \theta^3 \pi} \int_0^1 \frac{x^4 \exp(x/\theta)}{\left[\exp(x/\theta) - 1 \right]^2} \left(\frac{1}{Q_{l\parallel,\perp}(x)} + \frac{2}{Q_{t\parallel,\perp}(x)} \right) dx. \quad (13)$$

Just as before, with regard to formulae (9) and (10), we obtain $\mu_{\parallel} = 0.022$, $\mu_{\perp} = 2.177 \cdot 10^{-3}$. According to this approach, for the reduction of either thermal conductivity values by 30 – 40 % in the case of phonon scattering on the circular contact boundaries, k_{\parallel}^* must be $69.6 \div 167.7$ and $k_{\perp} - 1008 \div 2691$. Therefore, contact radius must be $0.4 \div 1.1 \mu\text{m}$. In the case of phonon scattering on the sphere boundaries, k_{\parallel}^* must be $62.5 \div 149.1$ and $k_{\perp} - 908 \div 2400$. Therefore, the sphere radius is $0.35 \div 1 \mu\text{m}$.

Contacts of said dimensions can occur between particles of diameter $40 \div 80 \mu\text{m}$ at extrusion, which can account for the absence of a considerable decrease in thermoelectric figure of merit in going from a single crystal to extruded material.

Conclusions and recommendations

- Based on the model of a shape-forming element of thermoelectric material structure in the form of two hemispheres contacting in a circle, it is shown that one of possible mechanisms of thermoelectric material lattice conductivity reduction in going from a single crystal to extruded material can be additional phonon scattering on the boundaries of contacts or spherical particles themselves.
- In the approximation of constant phonon relaxation time it is shown that for the reduction of lattice thermal conductivity of a shape-forming element by 30 – 40 % as compared to that of the bulk material the radius of contact between the particles should not exceed $1.3 \div 2.5$ of the mean free path of phonon in material. With the use of a drag on the boundaries of spherical particles themselves, their radius should not exceed $1.2 \div 2.2$ of the mean free path of phonon in material.
- With a substitution of a real crystal lattice of bismuth telluride by a model simple cubic lattice with unchanged material density and account of both U - and normal processes, the above discussed reduction of both components of thermal conductivity tensor is obtained with contact or particle radii within $0.3 \div 1 \mu\text{m}$. As long as such contacts may be created between particles in the process of extrusion, it is exactly phonon scattering on their boundaries that can account for a slight change in thermoelectric figure of merit in going from a single crystal to extruded material.

The authors express gratitude to academician L.I. Anatychuk for the statement of the problem and important critical remarks.

References

1. N.S. Lidorenko, V.A. Andriyako, L.D. Dudkin, E.L. Nagayev, O.M. Narva, The Effect of Tunneling on the Efficiency of Thermoelectric Devices, *Doklady Akademii Nauk SSSR* **186**, 1295 (1969).
2. L.S. Stilbance, A.D. Terekhov and E.M. Sher, Some Issues of Transport Phenomena in Heterogeneous Systems. In: "Thermoelectric Materials and Films. Materials of All-Union Conference on the Deformation and Size Effects in Thermoelectric Materials and Films, Technology and Application of Films" (Leningrad, 1976), p. 199.
3. A.D. Terekhov, E.M. Sher, The Structure of Disperse Medium and the Effective Values of Thermal and Electric Conductivities, *Materials of All-Union Conference on the Deformation and Size Effects in Thermoelectric Materials and Films, Technology and Application of Films* (Leningrad, 1976), p. 211.
4. L.P. Bulat, I.A. Drabkin, V.V. Karataev, V.B. Osvensky and D.A. Pshenai-Severin, The Effect of Boundary Scattering on the Thermal Conductivity of Nanostructured $Bi_xSb_{2-x}Te_3$ Semiconductor Material, *Fizika Tverdogo Tela* **52**, 1712 (2010).
5. M. Green, Semiconductor Devices, *Patent of USA No 3524771*. Patented Aug.19, 1970, Int.Cl.H011 7/00, H01v 1/28.
6. A.V. Dmitriyev, I.P. Zvyagin, Current Development Trends in Physics of Thermoelectric Materials, *Uspekhi Fizicheskikh Nauk* **180**, 821.
7. A. Casian, V. Dusciac, I. Coropceanu, Huge Carrier Mobilities Expected in Quasi-One-Dimensional Organic Crystals, *Phys. Rev. B* **66**, 165404, 1-5 (2002).
8. A.I. Casian, I.I. Balmush and V.G. Dusciac, The Lorentz Number Reduction as a New Trend of ZT Increase in Quasi-One-Dimensional Organic Crystals, *J.Thermoelectricity* **3**, 19 (2011).
9. V. Dusciac, Thermoelectric Capabilities of Quasi-One-Dimensional Organic Semiconductors, *J. Thermoelectricity* **4**, 5 (2004).
10. A. Misnar, *Thermal Conductivity of Solids, Liquids, Gases and Their Compositions* (Moscow: Mir, 1968), 464p.
11. P.G. Klemens, Lattice Thermal Conductivity. – In: *Solid State Physics. Advances in Research and Applications*. Vol.7, pp. 1-98 (New York: Academic Press. Inc. Publishers, 1958), 526 p.
12. B.M. Goltsman, V.A. Kudinov and I.A. Smirnov, *Semiconductor Thermoelectric Materials Based on Bi_2Te_3* (Moscow: Nauka, 1972), 320p.

Submitted 23.01.2013.

E.M. Godzhayev, G.S. Dzhafarova, S.I. Safarova

Azerbaijan Technical University, 25, Huseyn Javid Ave., Baku,
AZ 1000, Republic Azerbaijan

**BAND STRUCTURE OF $TlInTe_2$ AND THERMOELECTRIC FIGURE
OF MERIT OF SOLID SOLUTIONS ON ITS BASIS**

In this work, using pseudopotential methods, the band structure of ternary compound $TlInTe_2$ is calculated, the origin of valence band and conduction band is identified, and, on the basis of temperature dependences of the electrical conductivity, Seebeck coefficient and thermal conductivity, the thermoelectric figure of merit of solid solution of the type $TlIn_{1-x}Ln_xTe_2$, where Ln is Ce, Nd, Pr, Sm, Eu, is calculated in the temperature range of 300 – 700 K.

Key words: $TlIn_{1-x}A_x^{III}Te_2$ solid solutions, band structure, thermoelectric figure of merit, group-theoretic analysis.

Introduction

State-of-the-art technology widely employs thermoelectric materials with high thermoelectric figure of merit. It is known that thermoelectric figure of merit of semiconductor materials is proportional to the ratio between current carrier mobility and crystal lattice thermal conductivity.

The thermoelectric figure of merit reaches maximum under certain concentration of carriers. To increase the thermoelectric figure of merit, it is necessary to find materials with maximum ratio between current carrier mobility and thermal conductivity, to create in these materials the concentration of carriers assuring optimal thermoelectromotive force, to develop methods for further increase of the ratio between current carrier mobility and lattice thermal conductivity.

These problems are solved as follows. A different substance, crystallized in the same syngony, is introduced into material crystal lattice. In such systems solid substitution solutions are formed. In this case distortions prove to be rather efficient for the dissipation of thermal vibrations, the wavelength of which at ordinary temperatures is little more than lattice constant, and, as a result, lattice thermal conductivity is considerably reduced, and mobility is reduced only slightly. On the other hand, the most efficient thermoelectric materials are based on multi-component semiconductor compounds or solid solutions comprising heavy elements with a complex or defective crystalline and a complex electronic structure. These requirements are met by solid solutions of the type $TlIn_{1-x}A_x^{III}Te_2$, obtained with a partial substitution of indium atoms by third group atoms, including lanthanides in $TlInTe_2$ lattice. The data can be found in the literature that $TlIn_{1-x}Ga_xTe_2$ solid solutions possess high thermoelectric figures of merit [1]. However, information on the research of thermoelectric figure of merit of solid solutions of the type $TlIn_{1-x}Ln_xTe_2$ is not available. In this connection, the purpose of this work is to study the thermoelectric properties of solid solutions of the type $TlIn_{1-x}Ln_xTe_2$, where Ln is Ce, Pr, Nd, Sm, Eu.

The electrical conductivity (σ), Seebeck coefficient (α) and thermal conductivity (χ) were measured using a compensation method, the errors of measuring σ , α , χ were 5, 7 and 4 %, respectively.

The alloys were synthesized by alloying the initial components taken in stoichiometric ratio, in

evacuated to 0.0133 Pa and sealed quartz ampoules. For synthesis of $TlIn_{1-x}Ln_xTe_2$ alloys as the initial substances there were used Tl – 99.99 mas.%, In – 99.99 mas.%, Pr -comprising rare-earth element – 0.5, Ca -0.01, Cu -0.04, Fe -0.03, Ce -comprising rare-earth element – 0.6, Ca -0.01, Cu -0.02, Fe -0.01, Nd -comprising rare-earth element – 0.31, Ca -0.01, Cu -0.01, Tl -0.017, Sm -comprising rare-earth element – 0.05, Fe -0.01, Cu -0.01, Eu -comprising rare-earth element – 0.03, Cu -0.016 and tellurium A-1. The temperature of the heater comprising quartz ampoules with the substance was raised to 750 to 900 K at the rate of 20 to 30 K/h depending on the composition. At these temperatures the samples were held for 2 – 3 hours and then heated to 1150 to 1250 K and held for another 4 – 5 hours. After that the samples were cooled to room temperature at the rate of 10 K/hour.

The ternary compound $TlInTe_2$ belongs to chain semiconductors of the type $TlSe$, is crystallized in the structure with bulk-centered tetragonal lattice with D_{4h}^{18} ($I4 / mcm$) symmetry group.

From considerations of a chemical bond, the formula of $TlInTe_2$ compound is written as $Tl^+(In^+Te_2)^-$. In this compound the ions In^{3+} and their nearest tetrahedral environment of four Tl_2^+ ions form negatively charged chains $-Tl_2^{2-} - In^{3+} - Te_2^{2-} -$ along the tetragonal \bar{c} axis. Univalent ions Tl^+ are localized between the four chains, having in this case an octahedral environment of eight ions Te^{2-} . $TlInTe_2$ is crystallized in tetrahedral syngony with the lattice parameters $a = 8.482 \text{ \AA}$, $c = 7.792 \text{ \AA}$. The band structure of $TlInTe_2$ was calculated by pseudopotential methods [2-4]. Maximum kinetic energy of plane waves was 20 rydbergs. The lattice parameters were $a = 8.494 \text{ \AA}$, $c = 7.181 \text{ \AA}$, the chalcogen parameter $x = 0.181$.

About 2700 plane waves were used in the expansion of wave function. The results of calculation of $TlInTe_2$ band structure are given in the Figure 1. The obtained data suggests the following conclusions.

1. The top of valence band is at high-symmetry point $T(0, 2\pi/a, 0)$ on the surface of Brillouin zone and corresponds to irreducible representation of T_3 , and the bottom of conduction band is on the line $D(\pi/a, \pi/a, k)$, also located on the surface of Brillouin zone between the points $P(\pi/a, \pi/a, \pi/c)$ and $N(\pi/a, \pi/a, 0)$, corresponds to irreducible representation of D . The energy gap width 0.66 eV, obtained from calculations, fits the experimental data well [5-9].
2. The lowest-energy direct transition is done approximately at point T between the states T_3 and T_4 . According to selection rules, $T_3 - T_4$ transition is forbidden in a dipole approximation. The bottom of conduction band at point T is a saddle point. The minimum lies a short distance from point $T(0, 0, 2\pi/c)$, which is an equivalent of T beyond the Brillouin zone, namely at point $A(0, 0, \pi/c)$ $[1+(c/a)]^2$ at the boundary of Brillouin zone along A_1 line and corresponds to irreducible representation of A_2 .
3. The third largest minimum of conduction band is also located on line A at point $A(0, 0, \pi/c)$ and corresponds to irreducible representation of A_4 .
4. According to composition and nature the valence bands can be divided into three groups. According to group-theoretic analysis, the lowest group consisting of four zones nearly –11 eV owes its origin to $5s$ states of Te . The middle group of four zones in the area of – 3.5 to –6 eV mainly comes from $6s$ states of Tl atoms and $5s$ states of In atoms. The upper group, structurally most complicated, consisting of 10 overlapping zones in the area from 0 to –3.5 eV, is mainly formed by $5p$ states of Te atoms, $5p$ states of In atoms. It should be noted that in the vicinity of valence band top the states of univalent ion Tl^+ begin to appear, whose main contribution is observed at point T . The main contribution to formation of the two lower conduction bands is made by a trivalent In^{3+} ion taking part in the formation of ion-covalent bond with Te^{2-} ions.

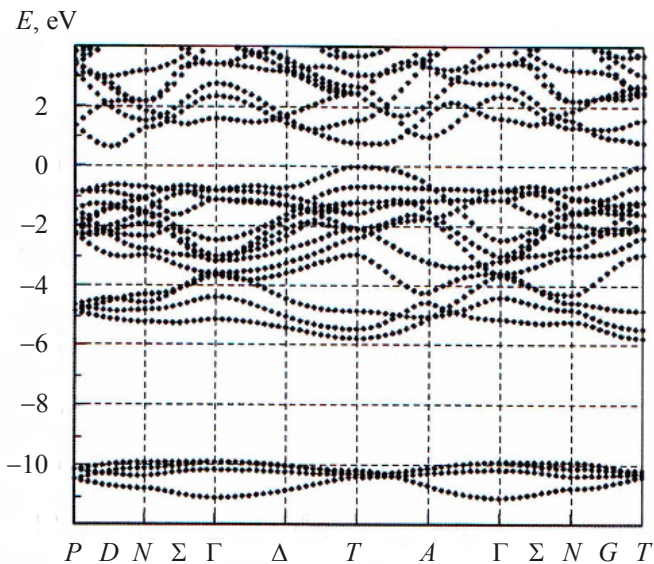


Fig. 1. Band structure of $TlInTe_2$ compound.

These results show that the band structure of $TlInTe_2$ is complex. In works [10-12] based on differential-thermal, microstructural, X-ray phase analyses it was established that in $TlInTe_2$ - $TlLnTe_2$ systems there is a solubility region based on $TlInTe_2$. In works [5-7] the electrophysical and thermal properties of solid solutions of the type $TlIn_{1-x}Ln_xTe_2$ were studied. These crystals satisfy the requirements of efficient thermoelectric materials, i.e. they are multi-component, comprise heavy elements and possess complex crystalline and band structures.

Investigations of the temperature dependences of the electrical conductivity, Seebeck coefficient and thermal conductivity of $TlIn_{1-x}Ln_xTe_2$ alloys were conducted in the temperature range of 300 to 700 K.

Experimental data shows that in solid solutions based on $TlInTe_2$ with increasing content of lanthanides in the alloys, the electrical conductivity grows by two orders of magnitude and then thermal conductivity is reduced. Therefore, it could be expected that in $TlInTe_2$ - $TlLnTe_2$ systems in certain compositions and in certain temperature range the thermoelectric figure of merit reaches the value which is of practical significance.

We have analyzed the thermoelectric peculiarities of $TlInTe_2$ - $TlLnTe_2$ solid solutions in the temperature range of 300 to 700 K. The results of calculation of the thermoelectric figure of merit of $TlInTe_2$ - $TlLnTe_2$, Ln -Ce, Pr, Nd, Sm, Eu alloys are given in the Table. As it follows from the Table, for all investigated alloys it is typical that as the content of lanthanides increases, the thermoelectric figure of merit grows. Increase in Z is also observed with temperature growth, and at 700 K the value of Z proves to be especially high. For $TlIn_{1-x}Eu_xTe_2$ solid solutions at 700 K Z is on the order of $2 - 2.5 \cdot 10^{-3}$ K⁻¹. Probably, the increase in Z is due to the fact that with a constant ratio between mobility and crystal lattice thermal conductivity in compounds with a complex structure the effective mass of charge carriers increases, and with a rise in carrier concentration or temperature, the Fermi level gets into a subband of heavy carriers. Then the important role is played not only by the energy gap width, but also by the energy gap between the subbands. This fact can be satisfied in $TlIn_{1-x}Ln_xTe_2$ crystals, since in $TlInTe_2$ the upper part of valence band is mainly formed of 5p states of tellurium and indium atoms. With a partial substitution of indium atoms by lanthanide atoms, both 6s² and 5d¹ lanthanide electrons take part in the formation of the upper part of valence band. Accordingly, there is a reduction of the energy gap and increase in free carrier concentration thermoelectric figure of merit of $TlIn_{1-x}Ln_xTe_2$ crystals.

Table

Thermoelectric parameters of $TlIn_{1-x}Ln_xTe_2$ system alloys

Compositions	300 K				500 K				700 K			
	$\alpha \cdot 10^6$, V/K	σ , S/m	χ , W/m·K	$Z \cdot 10^{-3}$, K^{-1}	$\alpha \cdot 10^6$, V/K	σ , S/m	χ , W/m·K	$Z \cdot 10^{-3}$, K^{-1}	$\alpha \cdot 10^6$, V/K	σ , S/m	χ , W/m·K	$Z \cdot 10^{-3}$, K^{-1}
$TlIn_{0.97}Ce_{0.03}Te_2$	800	1214	0.973	0.80	766	1116	0.96	0.65	750	1220	0.807	0.85
$TlIn_{0.95}Ce_{0.05}Te_2$	780	1360	0.87	0.95	684	1360	0.85	0.75	670	1403	0.70	0.90
$TlIn_{0.93}Ce_{0.07}Te_2$	720	1480	0.74	1.04	592	1782	0.79	0.79	583	1516	0.69	1.75
$TlIn_{0.97}Pr_{0.03}Te_2$	790	1290	0.77	1.05	760	1230	0.91	0.78	732	1310	0.78	0.89
$TlIn_{0.95}Pr_{0.05}Te_2$	770	1360	0.84	1.25	780	1600	0.82	1.04	708	1510	0.76	1.0
$TlIn_{0.93}Pr_{0.07}Te_2$	760	1580	0.82	1.11	682	1860	0.76	1.14	650	1920	0.71	1.14
$TlIn_{0.97}Nd_{0.03}Te_2$	700	1390	0.86	0.79	700	1590	0.90	0.87	680	1800	0.71	1.712
$TlIn_{0.95}Nd_{0.05}Te_2$	710	1580	0.84	0.95	690	1790	0.80	1.06	660	2600	0.65	1.74
$TlIn_{0.93}Nd_{0.07}Te_2$	680	1774	0.82	1.01	670	1980	0.74	1.2	590	2930	0.60	1.69
$TlIn_{0.97}Sm_{0.03}Te_2$	740	1400	0.92	0.84	720	1520	0.87	0.90	700	2200	0.68	1.58
$TlIn_{0.95}Sm_{0.05}Te_2$	710	1620	0.80	1.02	680	1760	0.86	0.95	640	2700	0.64	1.73
$TlIn_{0.93}Sm_{0.07}Te_2$	680	1910	0.76	1.19	640	1890	0.82	0.95	610	3000	0.62	1.8
$TlIn_{0.97}Eu_{0.03}Te_2$	743	1490	0.91	1.63	716	1610	0.85	0.97	790	2460	0.66	1.89
$TlIn_{0.95}Eu_{0.05}Te_2$	710	1689	0.76	1.14	684	2092	0.8	1.22	690	2900	0.63	2.19
$TlIn_{0.93}Eu_{0.07}Te_2$	680	2100	0.65	1.50	666	2864	0.7	1.81	660	3300	0.59	2.44

The obtained results testify that thermoelectric figure of merit of $TlIn_{1-x}Ln_xTe_2$ solid solutions can be increased and controlled with a variation of their composition. Research works in this direction should be continued.

Conclusion

In this work, the band structure of ternary compound $TlInTe_2$ was calculated using pseudopotential methods, the origin of valence band and conduction band of this phase was identified, and the results of research on thermoelectric properties of $TlIn_{1-x}Ln_xTe_2$ alloys obtained by substitution of trivalent indium atoms by *Pr*, *Nd*, *Ce*, *Sm* and *Eu* atoms in $TlInTe_2$ lattice in the temperature range of 300 to 700 K were stated. It was established that in certain temperature range these alloys possess high values of thermoelectric figure of merit and can be used in thermoelectric converters.

References

1. E.M. Godzhayev, M.M. Zarbaliyev, S.A. Aliyev, Electrophysical Properties of $TlInTe_2-TlGaTe_2$ system solid solutions, *Izvestia AN SSSR, Neorganicheskiye Materialy* **19**(1), 159-161 (1983).
2. F.D. Murnghan, The Compressibility of Media Under Extreme Pressures, *Proceedings of the National Academy of Sciences* **30**, 244-247 (1944).
3. G.B. Bachelet, D.R. Haman, V. Shlüter, Pseudopotentials That Work: From *H* to *Pu*, *Physical Review B* **26**(8), 4199-4228 (1982)
4. V. Heyne, M.L. Cohen, D. Wair, *Theory of Pseudopotentials* (Moscow: Mir, 1973), p. 557.
5. E.M. Godzhayev, K.D. Orudzhev, Electrophysical and X-ray Studies of $TlInX_2-TlLnX_2$ System Alloys, Where *X-Se, Te, Ln-Nd, Pr*, *Izvestia AN SSSR, Neorganicheskiye Materialy* **16**(3), 429-433 (1980).
6. E.M. Godzhayev, M.M. Zarbaliyev, Study on Electrophysical Properties of Substitutional Solid Solutions in $TlInTe_2-TlPrTe_2$ System, *Izvestia AN SSSR, Neorganicheskiye Materialy* **16**(4), 1296-1298 (1980).
7. E.M. Godzhayev, M.M. Zarbaliyev and V.A. Gadzhiyev, Electrical Conductivity of $TlInTe_2$ Single Crystal in Strong Electrophysical Fields, *Izvestia AN SSSR, Neorganicheskiye Materialy* **16**(11), 1929-1931 (1980).
8. E.M. Godzhayev, R.A. Kerimova and G.G. Binnatli, Thermophysical Properties of $TlInTe_2$, *Inzhenerno-Fizicheskii Zhurnal* **76**(2), 92-97 (2003).
9. E.M. Godzhayev, A.M. Nazarov, E.A. Allakhayrov, K.D. Gulmamedov, Kh.S. Khalilova and E.M. Mamedov, Acoustophotovoltaic Effect in $TlInSe_2$, $TlInTe_2$ and $TlGaTe_2$ Single Crystals, *Neorganicheskiye Materialy* **43**(10), 1184-1189 (2007).
10. E.M. Godzhayev, K.D. Orudzhev, V.A. Mamedov, Study on $TlNdSe_2-TlInSe_2$ and $TlInTe_2-TlNdTe_2$ Systems, *Izvestia AN SSSR, Neorganicheskiye Materialy* **17**(8), 1388-1391 (1981).
11. E.M. Godzhayev, M.M. Zarbaliyev and V.A. Mamedov, Interaction in $TlInTe_2-TlEuTe_2$ System, *Izvestia AN SSSR, Neorganicheskiye Materialy*, **17** (10), 1767-1769 (1981).
12. E.M. Godzhayev, V.A. Mamedov, Sh.M. Guseynova, Diagram of State and Study on Electrophysical Properties of $TlInTe_2-TlSmTe_2$ System Alloys, *Izvestiya AN SSSR, Neorganicheskiye Materialy* **19**(11), 1813-1815 (1983).

Submitted 05.04.2012.

**L.D. Ivanova¹, L.I. Petrova¹, Yu.V. Granatkina¹, V.G. Leontyev¹, A.S. Ivanov²,
S.A. Varlamov², Yu.P. Prilepo², A.M. Sychev², A.G. Chuiko², I.V. Bashkov²**

¹Federal State Budget Institution of Science A.A. Baikov Institute for Metallurgy and Materials
Science of the Russian Academy of Sciences, 49, Leninskiy Ave., Moscow, 119991, Russia;

²Open Joint-Stock Society “NPO “RIF” Corporation”, 17/2, Dorozhnaya Str.,
Voronezh, 394062, Russia

**MELT SPINNING AS A PROMISING METHOD FOR PREPARATION
OF BISMUTH AND ANTIMONY TELLURIDE
SOLID SOLUTION MATERIALS**

This work is concerned with fabrication and study of pressed fine-crystalline materials based on p-type Bi_{0.5}Sb_{1.5}Te₃ solid solution of melt spun powder. The effect of melt spinning conditions (temperature and disc rotation rate, purity of inert gas used in the chamber) on the dimensions and morphology of powders, the structure of hot-pressed samples and their thermoelectric properties has been studied. Mechanical properties of samples obtained by different methods were studied during compression and bending tests. Thermoelectric properties of materials, namely thermoelectric coefficient, electrical conductivity and thermal conductivity were measured at room temperature and in the range of 100 to 700 K. For samples pressed of melt spun powder the maximum value of thermoelectric figure of merit ZT was ~ 1.3, whereas for materials prepared by other methods ZT does not exceed 1.1. It became possible due to considerable reduction of lattice component of thermal conductivity and increase of thermoelectric coefficient of samples obtained by melt spinning method.

Key words: bismuth and antimony telluride solid solutions, melt spinning, scanning electron microscopy, mechanical properties, thermoelectric properties.

Introduction

Thermoelectric power converters are widely used in a variety of science and technology fields. Particularly topical is the problem of thermoelectric device efficiency improvement. Apart from traditional methods for improving thermoelectric material efficiency, such as doping and a search for novel materials, of large interest is a research on the effect of structure of known thermoelectric materials on their thermoelectric properties, where considerable increase of thermoelectric figure of merit ZT is possible due to their nanotexturing. The physics behind such ZT increase are changes in the energy spectrum of charge carriers and phonons in nanostructured materials. A number of researchers [1-5] think that ZT increase of nanostructured materials can be achieved due to the following mechanisms: additional phonon scattering at the grain boundaries, tunnelling of carriers between nanostructured elements and energy filtration of carriers on potential barriers between nanograins. Additional phonon scattering at the grain boundaries with a slight reduction of charge carrier mobility occurs in the case when grain size is less than the mean free path of electrons, which means less than 10 to 20 nm. According to theoretical estimates, the probability of tunneling thermoelectric material electrons becomes rather large with the gaps between grains of the order of several nanometers. In so doing, phonons cannot tunnel through vacuum gap and no longer participate in thermal conductivity processes.

In the nanostructured materials the structure of electron bands can change and energy filtration of carriers may occur, when high-energy charge carriers will overcome the boundary between nanograins, practically without being scattered. Reduced probability of scattering at the nanograin boundaries with increasing energy of carriers leads to thermoEMF increase. Theory predicts the increase in ZT of nanosized thermoelectric material up to 3.5, provided all three mechanisms of figure of merit increase are realized [1-5]. To this date, the bulk thermoelectric materials with grain size 10 to 20 nm and vacuum gaps between grains 1 to 2 nm have not been obtained yet. There are experimental works reporting on fine-dispersed materials with $ZT = 1.2 - 1.4$ [6-9].

Materials based on solid solution of $Bi_2Te_3-Sb_2Te_3$ system are used to manufacture *p*-type legs for various purpose thermoelectric coolers and generators. This work employs a method of manufacturing fine-crystalline pressed samples from the above solid solution of powder prepared by melt spinning. This method has been elaborated and used to obtain quickly quenched powders and thin stripes of amorphous, composite and magnetic metal alloys [10]. Thermoelectric materials based on solid solutions of antimony and bismuth chalcogenides were first obtained by spinning method in Sukhumi Physics and Technical Institute, which was reported in 1988 in Uzhgorod at VII All-Union Conference "Chemistry and Technical Application of Chalcogenides" [11-13]. Papers have appeared recently which show the promising character of using this method to obtain nano-sized powders [14-17] of the above indicated materials. A combination of melt spinning and arc plasma powder sintering methods was used to obtain materials of bismuth and antimony chalcogenide solid solutions of the *n*-type with thermoelectric figure of merit $ZT \sim 1.0$ [14] and *p*-type with $ZT \sim 1.5$ [16, 17].

Experimental procedure

Samples of bismuth and antimony telluride solid solution were obtained by hot pressing from powder prepared by melt spinning technique. This technique lies in obtaining fine particles of alloys by superfast cooling the melt on the surface of rotating cold disc. A pre-alloyed ingot was heated to temperature 30 – 50 K exceeding material melting point. A flush of melt of diameter 1 – 1.5 mm was poured on the surface of water-cooled disc rotating at the rate of 900 to 1500 rpm, which assured cooling rate $\sim 10^6$ K/s. The process took place in argon atmosphere at excess pressure 0.2 MPa. From the obtained powders briquettes were prepared by cold pressing which were subsequently subject to hot pressing in the air or in vacuum at temperature 350 °C and pressure 5 MPa. The samples were annealed in different media: inert gas atmosphere, hydrogen current and air from 4 to 24 hours at 280, 300 and 350 °C.

The morphology and size of particles of powder obtained by melt spinning and the structure of cleavages of hot-pressed samples was studied on scanning electron microscope (SEM) (LEO 1420). The X-ray diffraction study of powders was conducted on DRON-UM diffractometer ($Cu K\alpha$ -radiation) with a graphite monochromator. Qualitative and quantitative X-ray phase analysis of powders obtained by melt spinning was conducted with the use of XRAYAN program and the PDF (The Power Diffraction File) international database. Mechanical properties (strength limits, deformation ratio, elongation) of samples having identical dimensions and shape, obtained by different methods, were studied under compressive and bending strains at room temperature on INSTRON-5800 setup at strain rate $v_{strain} \sim 1$ mm/min. Thermoelectric properties of samples: thermoelectric coefficient α , electric conductivity σ and thermal conductivity κ were measured at room temperature and in the range of 100 to 700 K. The lattice component of thermal conductivity was determined as $\kappa_p = \kappa - \kappa_{el}$, where $\kappa_{el} = A\sigma T$ (A is the Lorentz number, T is the ambient temperature). The thermoelectric figure of merit of materials was calculated from the formula $Z = \alpha^2\sigma/\kappa$.

Discussion of results

The powders of bismuth and antimony telluride solid solution were obtained under different conditions of melt spinning. While the powders prepared according to traditional technology of ingot grinding in the ball mill are characterized by considerable oxidability in the air, no oxides were observed on the surface of particles obtained by melt spinning method. Powder compositions were analyzed using *X*-ray phase analysis. It was established that powders retain their crystalline structure, and their compositions in the main components meet the compositions of the initial charge. The *X*-ray diffraction pattern of one of the powders and its indexing results are given in Fig. 1.

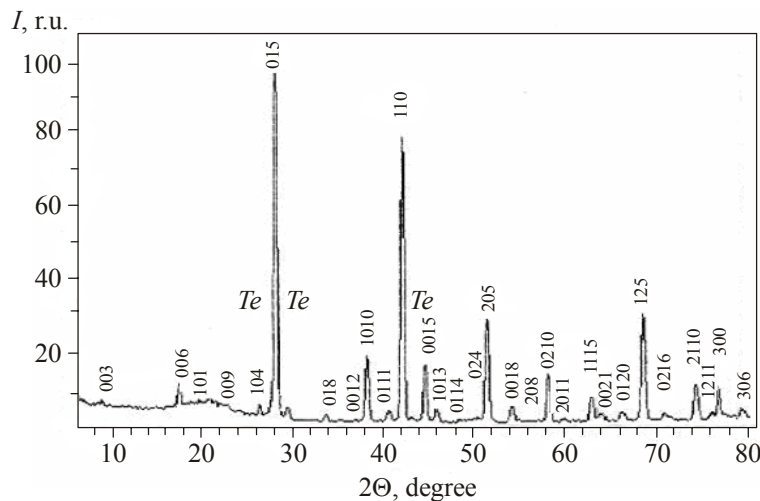


Fig. 1. *X*-ray diffraction pattern of powder obtained by melt spinning of $\text{Bi}_{0.5}\text{Sb}_{1.5}\text{Te}_3$ solid solution.

Analysis of this *X*-ray pattern and comparison of the results obtained to the PDF international database have shown that the main portion of peaks in the intensity, reflection angles and interplanar spaces coincides with the respective characteristics of $\text{Bi}_{0.5}\text{Sb}_{1.5}\text{Te}_3$ solid solution having the following parameters of hexagonal lattice: $a = 0.42852_{(1)}$ nm and $c = 3.04916_{(13)}$ nm. Moreover, there were lines on the *X*-ray pattern that can be referred to tellurium spectrum, the amount of which is estimated as $\sim 3\%$ of the total volume. Thus, it was established that powder under study has $\text{Bi}_{0.5}\text{Sb}_{1.5}\text{Te}_3$ composition and comprises Te excess that was introduced into the initial ingot.

SEM-images of powders obtained by melt spinning and grinding in the ball mill, as well as of cleavages of hot-pressed samples are represented in Fig. 2.

Powder obtained by melt spinning had rather coarse particles shaped as plates of size from units to hundreds of microns (Fig. 2 *a, b, c*). However, on the cleavage of sample after hot pressing of this powder the size of grains is considerably smaller than the size of particles of the initial powder, their maximum dimensions did not exceed tens of microns (Fig. 2 *d, e*), though it is known that at hot pressing the grains in the samples are enlarged due to recrystallization. Investigation of powder particles with a large magnification (Fig. 2 *b, c*) has shown that powder plates consist of thin flakes located with their flat side perpendicular to cooled disc surface. The thickness of scales is from units to hundreds of nanometers, their length is several microns. The size of flakes depends on the value of crystallization gradient (the temperature of disc where the melt finds itself). On hot pressing, powder particles disintegrate into small flakes of which sample grains are formed. In so doing, grains in the structure of samples retain their plate-like shape (Fig. 2 *d, e*). Powder obtained by grinding in the ball mill comprises both large particles to several hundreds of microns, and small particles, of less than micron in size, having round edges (Fig. 2 *f, g*). The samples pressed of such powders (Fig. 2 *h, i*)

retain a layered structure typical of these materials, but in the bulk the distribution of grains according to size is more heterogeneous as compared to samples pressed of powder obtained by melt spinning.

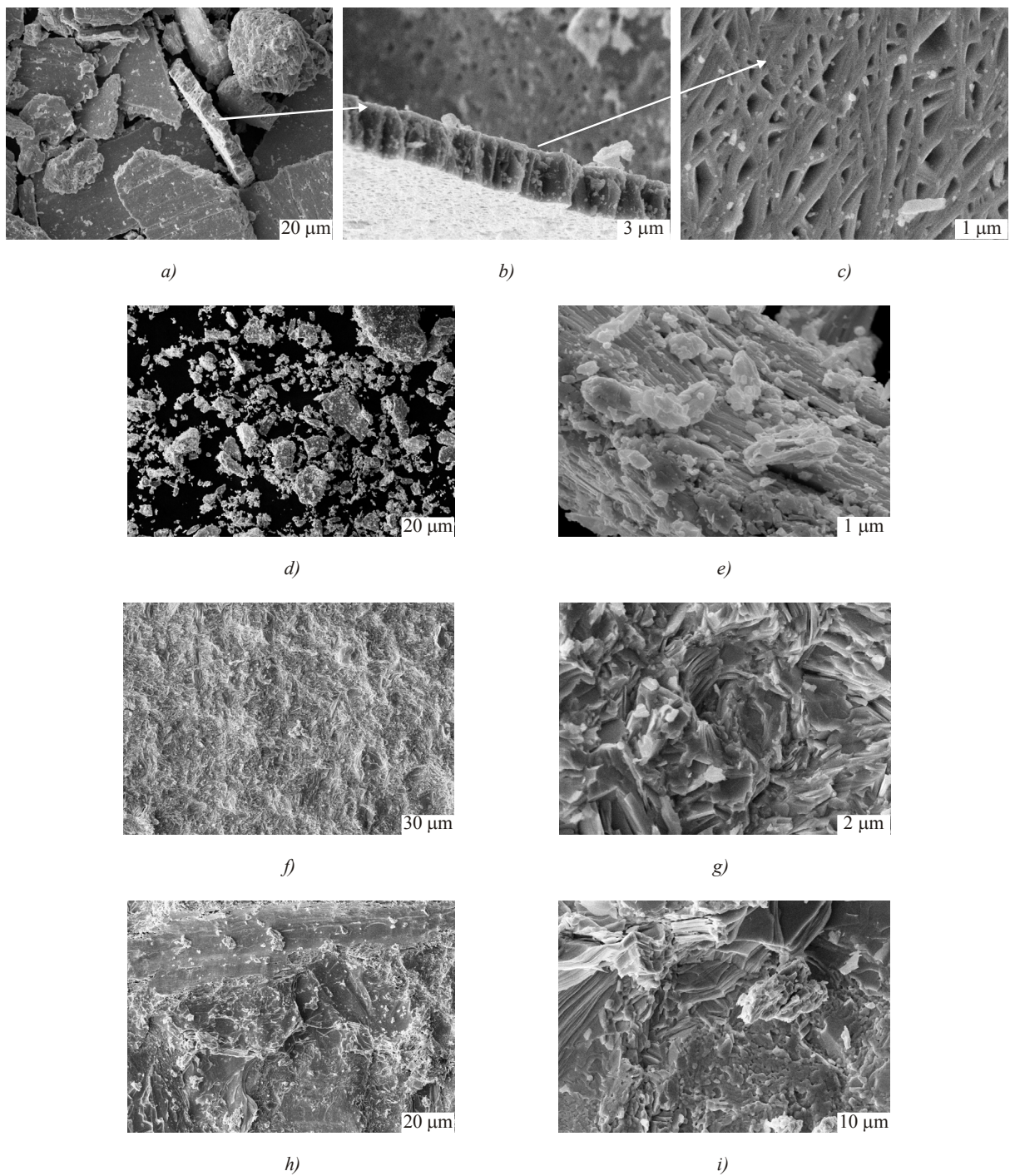


Fig. 2. SEM-images of powders obtained by $\text{Bi}_{0.5}\text{Sb}_{1.5}\text{Te}_3$ melt spinning (a, b, c) and ingot grinding in the ball mill (f, g), as well as of cleavages of hot-pressed samples from powders obtained by melt spinning (d, e) and grinding in the mill (h, i).

Fig. 3 shows the diagrams of strain due to compressive (Fig. 3 a) and bending loads (Fig. 3 b) of materials of bismuth and antimony telluride solid solutions prepared by different methods.

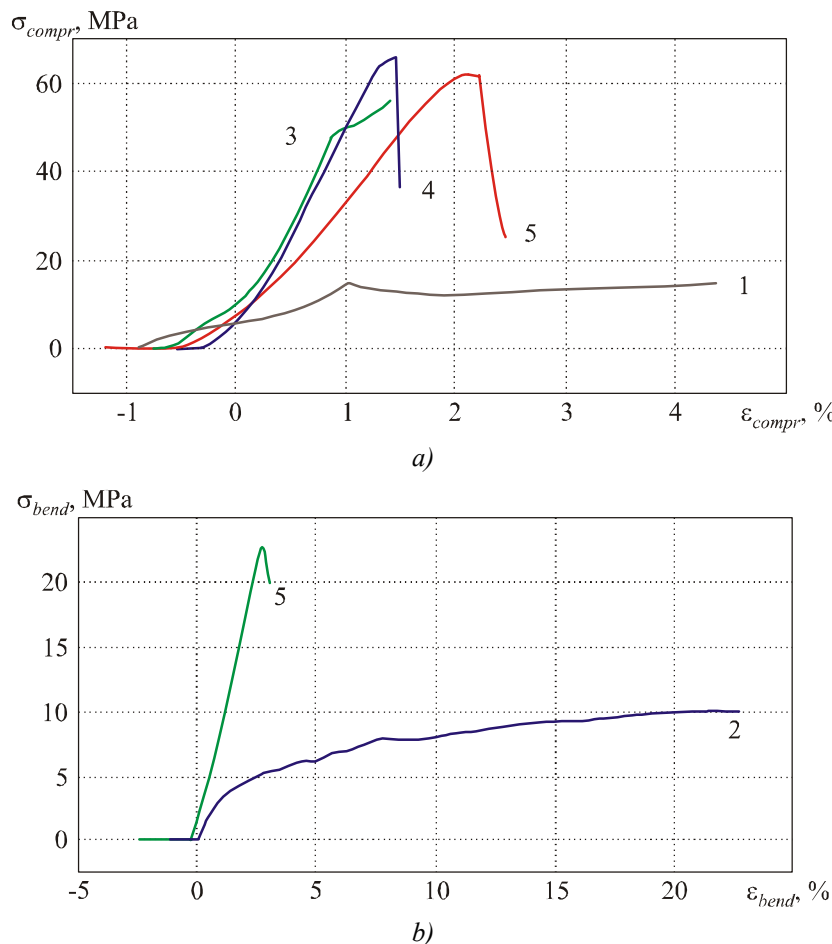


Fig. 3. Dependences of strain on compressive (a) and bending load (b) of samples obtained by different methods (curve numbers correspond to the numbers of samples in Table 2), deformed at strain rate $v_{strain} = 1 \text{ mm/min}$.

Table 1 gives strength limits ($\sigma_B^{compr}, \sigma_B^{bend}$) and strains ($\varepsilon_B^{compr}, \varepsilon_B^{bend}$) of samples obtained from the strain diagrams.

Table 1
 Maximum permissible strains ($\varepsilon_B^{compr}, \varepsilon_B^{bend}$) and strength limits ($\sigma_B^{compr}, \sigma_B^{bend}$) during compression and bending tests of samples obtained by different methods

№	Fabrication method	Compression		Bending	
		$\varepsilon_B^{compr}, \%$	$\sigma_B^{compr}, \text{MPa}$	$\varepsilon_B^{bend}, \%$	$\sigma_B^{bend}, \text{MPa}$
1	Czochralski method, Se doping	4.7	15		
2	Zone melting			22.7	10
3	Extrusion	1.4	48		
4	Hot pressing (ingot ground in the mill)	1.5	67		
5	Hot pressing (powder after melt spinning)	2.5	62	2.7	23

It has been established that hot-pressed samples of powder obtained by melt spinning of these solid solutions have rather high strength limits at compressive and bending strains. Brittle failure of such

samples takes place at strain 2.5 – 2.7 %. The strength limits made 62 MPa on compression and 23 MPa on bending. Samples obtained by Czochralski method and zone melting had the lowest compression strength (sample № 1) and bending strength (sample № 2), however, they are more ductile, and failure occurs due to shift of layers along cleavage planes. In such samples cracks appeared rather early which grew in number with further load increase, but, unlike pressed samples, these samples did not fail.

Research on thermoelectric properties (thermoelectric coefficient, electrical conductivity and thermal conductivity) of hot pressed samples of powder obtained by $Bi_{0.5}Sb_{1.5}Te_3$ melt spinning yielded the optimal conditions and modes for production of powders and bulk samples with high thermoelectric figure of merit. The results of research at room temperature on thermoelectric properties of samples depending on thermal treatment modes, powder particle dimensions and the rotation rate of disc where the melt comes are given in Tables 2, 3 and in Fig. 4.

The necessity of thermal treatment of samples was established. Annealing of samples can be conducted in the inert atmosphere, in hydrogen atmosphere (at 350 °C) or in the air (at 280 °C). It increases their thermoelectric figure of merit. The unannealed samples had different concentration of charge carriers: the values of thermoelectric coefficient of samples were ~ 230 $\mu\text{V/K}$ (№ 1 and № 2), ~ 220 $\mu\text{V/K}$ (№ 3) and 200 $\mu\text{V/K}$ (№ 4 and № 5) (Table 2).

Table 2

Thermoelectric properties: α , σ , κ and Z at room temperature of materials depending on conditions of melt spinning and thermal treatment of pressed samples

№	Particle size, mm	Disc rotation rate, rpm	Annealing			α , $\mu\text{V/K}$	σ , S/cm	$\kappa \times 10^3$, $\text{W/cm}\cdot\text{K}$	$Z \times 10^3$, K^{-1}
			T , °C	atm	time, h				
1	0.5 – 0.064	900	–	–	–	234	509	10.9	2.6
			350	H_2	4	220	764	10.8	3.4
2	0.5 – 0.064	900	–	–	–	232	523	10.2	2.5
			350	Ar	4	218	762	11.0	3.3
3	< 0.064	900	–	–	–	222	556	11.0	2.5
			350	H_2	4	221	600	9.6	3.0
4	without size grading	1500	–	–	–	204	657	11.0	2.5
			350	H_2	4	219	768	11.2	3.3
5	without size grading	1500	–	–	–	203	681	11.0	2.5
			280	Air	14	216	654	9.8	3.1

On annealing, the value of α of all these samples made ~ 220 $\mu\text{V/K}$. In so doing, σ increased and thermal conductivity was almost unchanged. Possibly, due to thermal treatment, charge carrier concentration became equalized and the nonequilibrium structure became ordered. As a result of annealing for 4 hours at 350 °C or 14 hours at 280 °C in the air (Fig. 4) an increase in Z by 10 – 20 % was obtained. A change in disc rotation rate (from 900 to 1500 rpm) hardly increased Z of these samples at room temperature.

To determine the effect of particle size of melt-spun powder on Z of materials made of this powder (Table 3, № 6 and № 7) as compared to materials made of powder ground in the mill (Table 3, № 8 and № 9), these samples were studied on annealing for 24 hours at 600 K in argon atmosphere. At room temperature the thermoelectric figure of merit of samples № 6 and 7 made $(3.5 \pm 0.2) \times 10^{-3} \text{ K}^{-1}$ which is considerably higher compared to samples № 8 and № 9, for which $Z = (2.8 \pm 0.2) \times 10^{-3} \text{ K}^{-1}$.

Table 3

Thermoelectric properties: α , σ , κ , κ_p and Z at room temperature of materials annealed for 24 hours at 300 °C in argon atmosphere, depending on the particle size of powder obtained by melt spinning (№ 6, № 7) and ingot grinding in the ball mill (№ 8, № 9)

№	Disc rotation rate, rpm	Particle size, mm	A , $\mu\text{V/K}$	σ , S/cm	$\kappa \times 10^3$, $\text{W/cm}\cdot\text{K}$	$\kappa_p \times 10^3$, $\text{W/cm}\cdot\text{K}$	$Z \times 10^3$, K^{-1}
6	1500	0.5 – 0.064	226	626	9.1	6.2	3.5
7	1500	< 0.064	240	580	9.0	6.3	3.5
8	–	0.5 – 0.064	203	800	11.2	7.4	2.9
9	–	0.5 – 0.064	194	1030	14.6	9.6	2.6

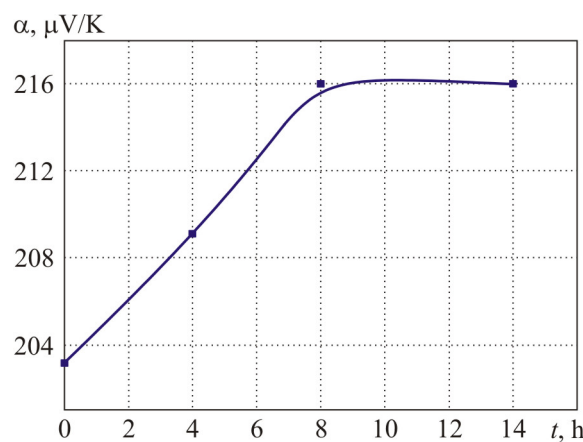


Fig. 4. Dependence of thermoelectric coefficient on annealing time at 280 °C in the air of samples made of melt spun powder.

Thermoelectric characteristics α , σ , κ , κ_p and Z at room temperature of bismuth and antimony telluride solid solution samples with close values of charge carrier concentration (α value), obtained by different methods, are given in Table 4.

Table 4

Thermoelectric properties: α , σ , κ , κ_p and Z at room temperature of materials depending on fabrication methods

№	Method of samples fabrication	α , $\mu\text{V/K}$	σ , S/cm	$\kappa \times 10^3$, $\text{W/cm}\cdot\text{K}$	$\kappa_p \times 10^3$, $\text{W/cm}\cdot\text{K}$	$Z \times 10^3$, K^{-1}
1	Czochralski method, Se doping	200	1060	13.5	8.5	3.1
2	Zone melting	200	1200	16.0	10.2	3.0
3	Extrusion	208	960	12.9	8.2	3.2
4	Hot pressing, ingot ground in the mill	200	700	10.2	6.8	2.75
5	Hot pressing, powder after melt spinning	212	780	10.0	6.3	3.5
6	Hot pressing, powder after melt spinning	230	587	9.4	6.7	3.3

In the hot-pressed samples of powders obtained by ingot grinding in the ball mill and melt spinning there was a reduction of both total and lattice component of thermal conductivity as compared to other samples. Besides, samples made of melt-spun powder had higher thermoelectric coefficient owing to which their Z is higher compared to samples obtained by other methods. A hot-pressed sample with $\alpha = 212 \mu\text{V/K}$ made of melt-spun powder has $Z \sim 30\%$ higher than Z of a sample having the same composition and obtained by ingot grinding in the ball mill and 15% higher than Z of a sample having the same charge carrier concentration and obtained by extrusion.

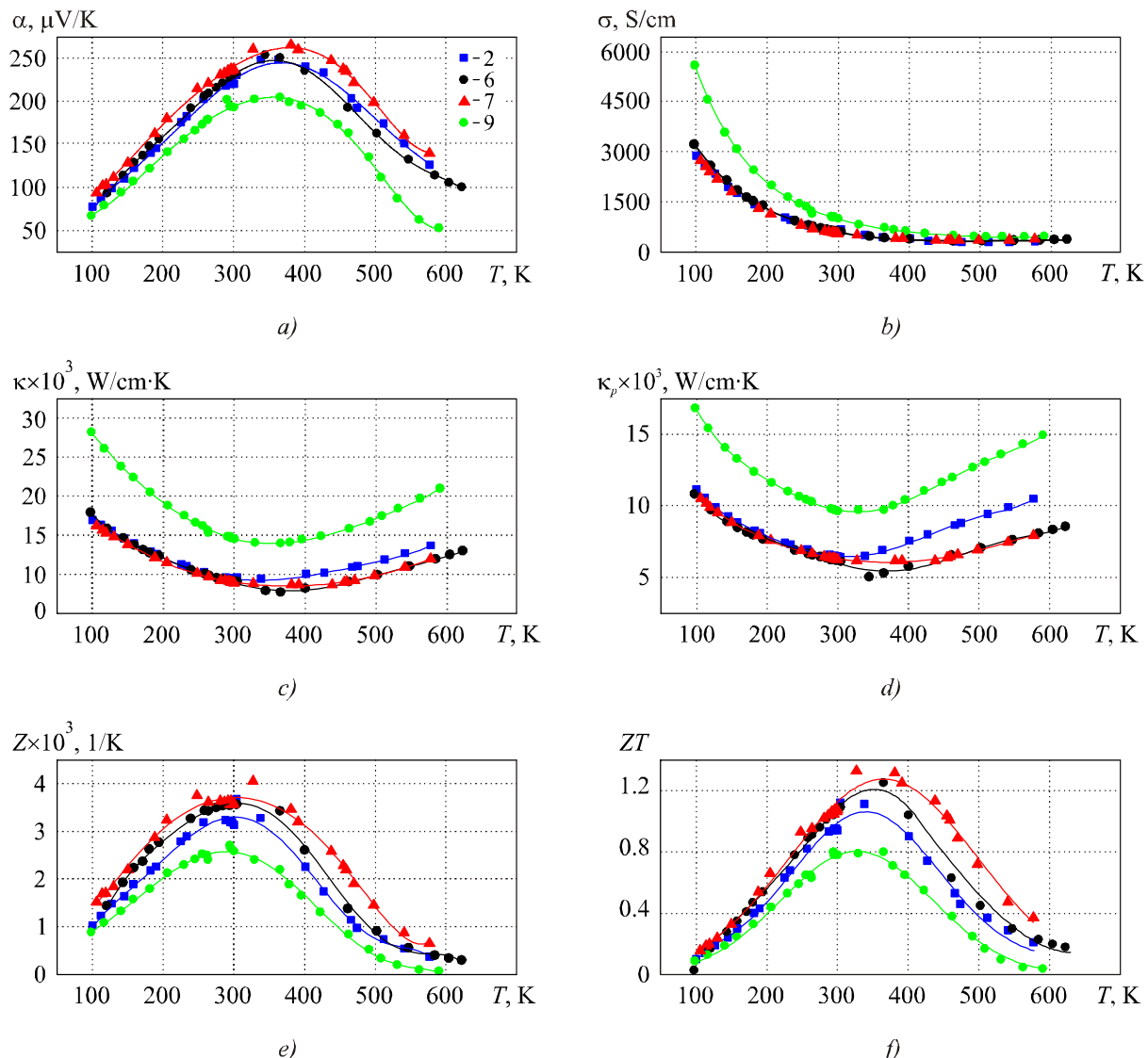


Fig. 5. Temperature dependences of thermoelectric coefficient (a), electric conductivity (b), total (c) and lattice thermal conductivity (d), thermoelectric figure of merit (e) and ZT (f) of samples made of melt-spun powders (№ 2, № 6, № 7) and ground in the ball mill (№ 9) (curve numbers correspond to numbers of samples in Tables 2 and 3).

Temperature dependences of thermoelectric properties (α , σ , κ , Z and ZT) in the range of 100 to 700 K of hot-pressed samples made of powders obtained by bismuth and antimony telluride melt spinning under different spinning conditions (№ 2, № 6, № 7), and of powders ground in the ball mill (№ 9) are represented in Fig. 5. The powders were prepared using ingot of the same solid solution

composition. The samples were annealed for 24 hours at 300 °C in argon atmosphere. Materials of various-size powders obtained by melt spinning (№ 6 and № 7, Table 2), had maximum $ZT = 1.32$ and 1.2. For the hot-pressed sample (№ 9, Table 3), obtained of powder ground in the ball mill, maximum ZT value did not exceed 0.8. The thermoelectric figure of merit of samples made of melt-spun powder increased mainly due to low lattice thermal conductivity and higher thermoelectric coefficient value, which resulted in ZT increase by ~ 30 %.

Conclusions

The effect of melt spinning modes on the size and morphology of particles of *p*-type $Bi_{0.5}Sb_{1.5}Te_3$ solid solution powders was studied. Thermoelectric and mechanical properties of the above solid solution materials prepared by different methods were investigated. Optimal conditions were found to obtain samples with the use of melt spinning method with thermoelectric figure of merit $Z = (3.5 \pm 0.2) \times 10^{-3} K^{-1}$ at room temperature and $ZT \sim 1.3$. As compared to conventionally used materials prepared by directional crystallization or extrusion methods, in the hot-pressed samples based on bismuth and antimony telluride solid solution made of melt-spun powder the lattice component of thermal conductivity is essentially reduced and thermoelectric coefficient is increased, which results in material thermoelectric figure of merit increase by ~ 15 %.

The work was performed under the financial support of Russian Foundation for Basic Research (project №11-08-01109-a).

References

1. P.J. Lin-Chung and T.I. Reinecke, Thermoelectric Figure of Merit of Composite Superlattice Systems, *Physical Review B* **51**(19), 13244-13247 (1995).
2. L.D. Hicks, T.C. Harman and M.S. Dresselhaus, Use of Quantum-Well Superlattices to Obtain a High Figure of Merit from Nonconventional Thermoelectric Materials, *Appl. Phys. Lett.* **63**(23), 3230-3232 (1993).
3. L.D. Hicks, M.S. Dresselhaus, Effect of Quantum-well Structure on Thermoelectric Figure of Merit, *Physical Review B* **47**(19), 2727-12731 (1993).
4. R.G. Yang and G. Chen, Thermal Conductivity Modeling of Periodic Two-Dimensional Nanocomposites, *Phys. Rev. B* **69**, 195316/1-10 (2004).
5. L.P. Bulat, D.A. Pshenai-Severin, V.V. Karataev, V.B. Osvensky, Yu.N. Parkhomenko, I.A. Drabkin, G.I. Pivovarov, V.T. Bublik and N.Yu. Tabachkova, On the Limit of Thermoelectric Figure of Merit in the Bulk Nanocrystalline Structures Based on Bismuth Telluride, *Thermoelectrics and Their Application: Reports to XII Interstate Workshop* (Saint-Petersburg: A.F.Ioffe Physics and Technical Institute of RAS, 2010, p.41).
6. Yi Ma, Q. Hao, B. Poudel, Y. Lan, B. Yu, D. Wang, G. Chen, Z. Ren, Enhanced Thermoelectric Figure-of-Merit in *p*-Type Nanostructured Bismuth Antimony Tellurium Alloys Made from Elemental Chunks, *Nano Letters* **8**, 2580/1-4 (2008).
7. B. Poudel, Q. Hao, Yi Ma, Y.C. Lan, A. Minnich, Yu Bo, X. Yan, D. Wang, A. Muto, D. Vashaee, X.Y. Chen, Y.M. Lui, M.S. Dresselhaus, G.G. Chen, Z. Ren, High-Thermoelectric Performance of Nanostructured Bismuth Antimony Telluride Bulk Alloys, *Science* **320**(5876), 634-638 (2008).
8. L.P. Bulat, V.T. Bublik, I.A. Drabkin, V.V. Karataev, V.B. Osvensky, G.I. Pivovarov, D.A. Pshenai-Severin, E.V. Tatyanyin, N.Yu. Tabachkova, Bulk Nanostructured Thermoelectrics

- Based on Bismuth Telluride, *J.Thermoelectricity* **3**, 70-75 (2009).
- 9. M.S. Dresselhaus, G. Chen, M.Y. Tang, R.G. Yang, H. Lee, D.Z. Wang, Z.F. Ren, J.P. Fleurial, P. Gogna, New Directions For Low-Dimensional Thermoelectric Materials, *Adv.Mater.* **19**, 1043-1053 (2007).
 - 10. A.I. Gusev, *Nanomaterials, Nanostructures, Nanotechnologies*. 2-nd edition (Moscow: Nauka, 2007), p. 416.
 - 11. O.Sh. Gogishvili, G.G. Kononov, S.P. Krivoruchko, I.P. Lavrinenko and I.I. Ovsyanko, Structure of $(Bi, Sb)_2Te_3$ Alloy Obtained by Liquid State Quenching, *VII All-Union Conference "Chemistry and Technical Application of Chalcogenides"* (Uzhgorod, 1988), p.367.
 - 12. O.Sh. Gogishvili, S.P. Lalykin, S.P. Krivoruchko, E.V. Krasnenkov, K.I. Puruchidi, E.S. Tsanava, Production of Alloys Based on Bismuth and Antimony Chalcogenides by Superfast Cooling of Melts, *VII All-Union Conference "Chemistry and Technical Application of Chalcogenides"* (Uzhgorod, 1988), p. 368.
 - 13. O.Sh. Gogishvili, S.P. Krivoruchko, I.I. Ovsyanko, G.N. Samoilenco, K.I. Puruchidi and E.S. Tsanava, Properties of Hot-Pressed Samples of $Bi_{0.52}Sb_{1.48}Te_3$ Alloy Obtained by High-Speed Quenching, *VII All-Union Conference "Chemistry and Technical Application of Chalcogenides"* (Uzhgorod, 1988), p. 372.
 - 14. S. Wang, W. Xie, H. Lie, X. Tang, Enhanced Performances of Melt Spun $Bi_2(Te, Se)_3$ for *n*-type Thermoelectric Legs, *Intermetallics* **19**, 1024-1031 (2011).
 - 15. W. Xie, X. Tang, Y. Yan, Q. Zhang, T. Tritt, Unique Nanostructures and Enhanced Thermoelectric Performance of Melt-Spun $BiSbTe$ Alloys, *J. Appl. Phys.* **94**, 102111/1-3 (2009).
 - 16. W. Xie, X. Tang, Y. Yan, Q. Zhang and T. Tritt, High Thermoelectric Performance $BiSbTe$ Alloy with Unique Low-Dimensional Structure, *J. Appl. Phys.* **105**, 113713/1-8 (2009).
 - 17. W. Xie, J. He, H. Kang, X. Tang., S. Zhu, M. Laver, S. Wang, J. Copley, C. Brown, Q. Zhang and T. Tritt, Identifying the Specific Nanostructures Responsible for the High Thermoelectric Performance of $(Bi, Sb)_2Te_3$ Nanocomposites, *Nano Lett.* **10**, 3283-3289 (2010).

Submitted 25.06.2012.

**S. Yamaguchi^{1,2}, Y. Ivanov¹, A. Sagara³, M. Emoto³, Y. Okamoto⁴, H. Nakatsugawa⁵,
H. Kitagawa⁶, M. Hamabe¹, F. Watanabe¹, J. Sun¹, T. Kawahara^{1,2}**

¹CASER, Chubu University, Aichi, 487-8501, Japan;

²Department of Electrical Engineering, Chubu University, Aichi, 487-8501, Japan;

³National Institute of Fusion Science, Gifu, 509-5292, Japan;

⁴National Defense Academy, Yokosuka, 239-8686, Japan;

⁵Yokohama National University, Yokohama, 240-8501, Japan;

⁶Shimane University, Matsue, 690-8504, Japan

A PROPOSAL OF THERMOELECTRIC DIVERTOR BY USING SILICON CARBIDE IN NUCLEAR FUSION EXPERIMENT

Fusion reactor needs a divertor plate to reduce a plasma surface interaction in order to realize long confinement time of high temperature plasmas. The plate is attached on the vacuum vessel, and it should be cooled. The function of the divertor is to control the plasma particle flow, and it is set with the pumping system. The heat flux to the divertor plate is quite high as the order of 10 MW/m² in fusion reactor, and the high-energy particles and the radiation from the plasma are bombarded on the surface of the plate. The heat flux on the divertor plate is the same as the inside of the rocket engine, but the heat flux of the rocket engine does not include high-energy particles. In order to remove the heat flux from the divertor plate, the reverse side of the plate is cooled by the water flow, and the plate should be thin to realize the low thermal resistance. Therefore, the temperature difference of the plate is higher than 1500 K. Carbon and tungsten are used in the present experiment as materials for the divertor plate because they possess high thermal conductivity and high melting point temperature. One of authors proposed the thermoelectric divertor to generate electric power in 2002, however, the Seebeck coefficients of these materials are not high and the output power of the thermoelectric divertor is not high. Here, we propose to use silicon carbide (SiC) as a new material for the thermoelectric divertor again because its thermal conductivity is higher than tungsten, the Seebeck coefficient of SiC is the order of 100 μ V/K, and it does not melt and its sublimation temperature is 2700 K. In the paper we also propose thermionic emission combined with the thermoelectric conversion system. We discuss the structure of the divertor plate and its performance about the heat removal and electric power generation.

Key words: thermoelectric cooling, energy conversion, nuclear fusion, high temperature materials.

Introduction

Fusion reactor needs the divertor plate [1, 2] to reduce the plasma surface interaction in order to realize the good confinement of high temperature plasmas. The plate is attached on the vacuum vessel, and the vacuum pumping system and the cooling system are connected with the divertor plate in order to control the particle influx and pumping, and the temperature of the plate [3, 4]. Since the energy confinement time of plasma is longer for larger plasma depending on the experimental scaling law [5, 6, 7], the heat flux to the divertor plate is high extremely, and its order is the order of 10 MW/m² in fusion reactor [8], and the high energy particles of plasma are bombarded on the plate, too. The heat flux on the divertor plate is the same as on the inner wall of the rocket engine, the heat removal is important to operate fusion experiment and reactors. The material of the divertor plate is carbon and

high melting point metals, such as tungsten and molybdenum, and their composite materials [9]. These materials should have high thermal conductivity because of the removal of high heat flux. They should conjugate to the copper plate, and the conjugation technology is also important. Usually the water and helium gas flows cool the copper plate. Therefore, large temperature difference appears between the plasma side of the plate and the copper plate, and it is higher than 1500 K.

This structure and the operation conditions are good for thermoelectric power generation because of high temperature difference, and one of authors proposed the thermoelectric divertor (TED) to generate electric power in 1996 [10] and 2002 [11], and also proposed the thermionic divertor (TID) and its structure in 1996 [12]. However, since the Seebeck coefficients of these materials (carbon and metals) are not high and their figures of merits are extremely low, the output power of the TED is not high. Here, in order to improve the performance of the TED, we propose to use silicon carbide (*SiC*) as a new material for the TED. Thermal conductivity of *SiC* is higher than those of tungsten, molybdenum and the carbon, and moreover the Seebeck coefficient of *SiC* is the order of 100 $\mu\text{V/K}$ [13, 14, 15], therefore we can expect high output voltage of the TED. It does not melt and its sublimation temperature is ~ 3000 K, therefore it is high temperature material. If we install the TED in the fusion reactor, we can also consider the concept of TID with the TED at the same time in order to enhance the electric power output. In the paper, we propose and discuss the new structure of the divertor plate, and estimate its performance about the heat removal, electric power generation, and the perspective of the future experiment in the present device.

Proposal of *SiC* Thermoelectric Divertor

In order to generate high temperature plasma, the plasma-wall interaction should be reduced, and the limiter had been used in tokamaks in 1960's and 1970's. However, the limiter material is going into plasma as the impurities because the surface temperature of the limiter may exceed 2500 K. The radiation loss of the impurity is high, and finally the energy confinement time is limited and not long for fusion reactor. The divertor configuration was developed in magnetic confinement devices, such as the tokamak and the helical system in order to reduce the impurity contaminations in the plasma. This can be called the magnetic limiter, and the magnetic field of the main plasma is not touched to the wall and the limiter directly. Therefore, the high temperature plasmas are realized in the divertor configuration in many experimental devices, and it is the standard magnetic configuration in the present time.

Fig. 1 shows the concept of TED in fusion experiments. This is based on the Fig. 1 (b) in ref. [4]. Some of the parts in the figure are changed, such as the cooling channel in the first wall of the divertor. *X* point means the poloidal magnetic field is zero, and the upper parts of the *X* point is the main plasma, and this is called the divertor configuration. The dotted lines mean the magnetic surfaces, and those are composed of the magnetic field lines. The plasma particle flows along the magnetic field line mainly, and the wall where the magnetic field line is crossing must be cooled to keep it. The radiation from the plasma is strong, and the first wall must be cooled. The charged particles of the plasma are neutralized at the wall, and they can be pumped out from the vacuum vessel. This is an important process to control the density of plasma. The thermoelectric modules (TE modules) are added on the original figure and they are connected to the wall of the vacuum vessel where the particle fluxes bombard, as shown in Fig. 1.

The TE module is composed of *n*-type and *p*-type *SiC* semiconductor, and they are connected with the high temperature metallic material such as tungsten in high temperature side. The low temperature side of the semiconductor is connected with the copper and the copper parts are cooled by

the water. This configuration is the same as the divertor plate fundamentally. The plasma side of the TE module is hot because of high heat flux of the plasma particle and the radiation, and the other side is cold. Therefore, the TE module has large temperature difference, and can generate electric power.

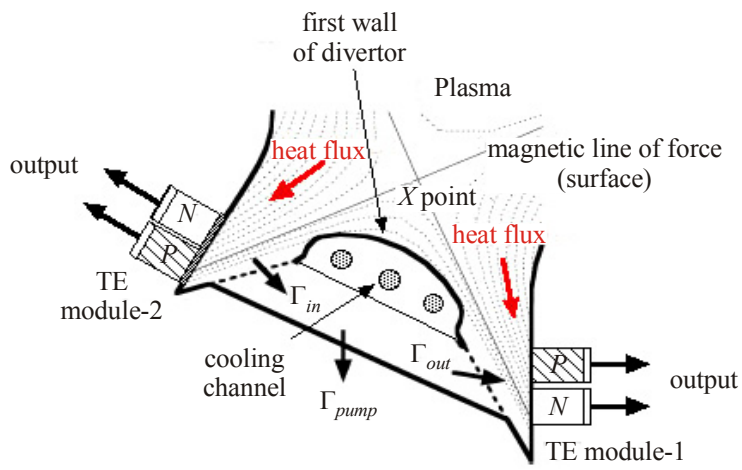


Fig. 1. Setup of the thermoelectric divertor (TED), and the magnetic configuration of plasma.

The functions of the TED should be as

- 1) to remove the heat at the wall of the vacuum vessel,
- 2) to pump out the particles from the plasma for controlling the plasma density,
- 3) to generate electric power.

The first two functions are the same as the original divertor's, but the last one is a new addition. Therefore, the material of TED has high thermal conductivity and strong for the bombardment of high-energy particle from plasma and the thermal shock (rapid temperature change), and in addition its Seebeck coefficient should be high and it is low electrical resistivity in order to generate electric power. The materials of the divertor are tungsten and molybdenum as the first wall because they are high melting points material and have high thermal conductivities. The carbon and the related materials are also used because it can be used in high temperature and their thermal conductivity is also high. However, their Seebeck coefficients are low, and therefore they are not good material from thermoelectric points of view. We cannot expect high electric power output from these materials.

We proposed the silicon carbide, SiC , to solve the problem. The thermal conductivity of SiC is higher than those of tungsten, molybdenum and carbon, and therefore it is good for cooling and we can keep the same structure of the present divertor. The Seebeck coefficient of SiC is also higher than those of tungsten, molybdenum and carbon, and therefore it is good for electric power generation as in Fig. 1. In the present time, we do not have enough data of SiC 's parameters at high temperature, but the known parameters are listed in Table 1. The tungsten is a good material to connect the p -type and n -type semiconductors in the high temperature side because it is strong for the bombardment of high-energy particle from plasma and it is used in the present experiment. SiC is a good material as n -type semiconductor even in high temperature, but it is hard to make p -type. Therefore, B_4C is a candidate of the p -type semiconductor at high temperature. Usually we can find p -type semiconductor in high temperature. However, since the thermal conductivity of B_4C is low, this is limited to use in divertor.

It is valuable to estimate the electric power generation by using SiC . The figure of merit of the SiC in Table 1 is expected to be $\sim 10^{-5} [K^{-1}]$, and it is not large as the present $BiTe$, but the temperature difference of the module is high as 1500 K, therefore the efficiency of the electric output power is not

low, and can be evaluated by the following equation, where α is the Seebeck coefficient, κ is the thermal conductivity, ρ is the electrical resistivity, T_H is the temperature of high temperature side of the element, T_C is the temperature of low temperature side of the element.

$$\varepsilon = \frac{T_H - T_C}{T_H} \frac{\sqrt{1 + \frac{Z(T_H + T_C)}{2}} - 1}{\sqrt{1 + \frac{Z(T_H + T_C)}{2}} + \frac{T_C}{T_H}}, \quad Z = \frac{\alpha^2}{\kappa\rho} \quad (1)$$

Table 1
Parameters of the high temperature materials

Material	MP(melting point) SP(sublimation point) [K]	Thermal conductivity [W/m·K]	Seebeck coeff. [μV/K]	Resistivity [Ωm]	comments
Tungsten	3695/MP	~ 170 ≤ 300 K	< 10	5.2×10^{-8} ≤ 300 K	for first wall
Carbon	3915/SP	100 ~ 300	< 10	$10^{-6} \sim 10^{-2}$	high thermal conductivity in diamond
B_4C [16]	2763/MP	30 ~ 42 ≤ 300 K	~ 120 ≤ 1000 K	~ 0.006 ≤ 1000 K	used in fission reactor
<i>SiC</i>	3003/SP	~ 490	> 400	< 0.0001	new proposal

The calculation result of the efficiency is shown in Fig. 2. The efficiency of the thermoelectric conversion is shown as the vertical axis, and the horizontal axis is the figure of merit Z [%]. If Z exceeds 10^{-5} K, the efficiency is higher than 1%. Therefore, the output power of the TED is several hundred kWatts for the ITER design, and the conversion efficiency may not be low because the temperature difference is larger as 1500 K. Moreover, the cooling of the divertor may be easy because of high thermal conductivity of *SiC*.

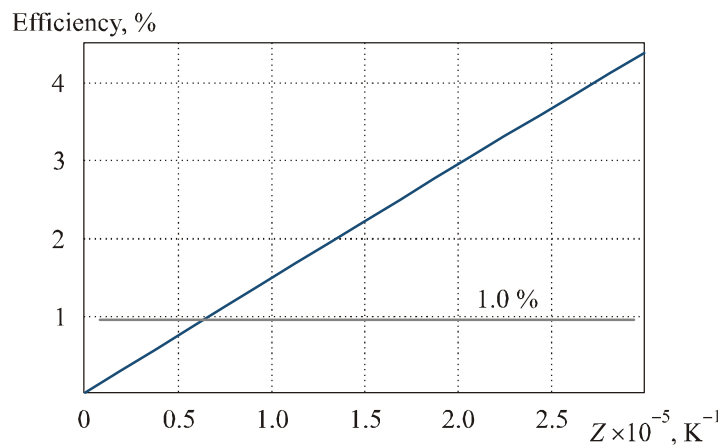


*Fig. 2. Efficiency of thermoelectric divertor (TED) by using silicon carbide (*SiC*)
for temperature difference of 1500 K.*

Discussions and Future Perspective

The concept of *SiC* TED will be good for the divertor plate, but unfortunately the experimental data is not enough at high temperature for *SiC* and the related materials in the present time. Therefore, it would be good subjects to study. The connection with the metallic material is also important, and the tungsten is used at the high temperature side and the copper should be connected as the electrode in the proposal of Fig. 1. In this meaning, we should develop the connecting technology, and it is not easy because the thermal expansions of these materials are not same usually. The plasma is one of electric conducting media, and the resistivity along the magnetic field line is low because the electron in the plasma can be moved easily along the field line. And it is high for the perpendicular direction of the magnetic field. Moreover, the electrical resistivity is low for high temperature plasma. Therefore, if we can set the TED along the magnetic field line, we may be able to omit the tungsten-plate connection to make the TED. But the magnetic field configuration is controlled by the currents of the magnet current and the plasma. However, when we look at the divertor configuration shown in Fig. 1 carefully, we can find many available settings for the TED.

The other idea is related with thermionic emission [12]. We bring the two electrodes into the vacuum vessel as shown in Fig. 3. One is *W*-plate 1, and the other is *W*-plate 2. These are connecting each other electrically by the magnetic field line and plasma. And we should control that the surface temperature of the *W*-plate 1 is set to be low and the *W*-plate 2's is high. The setting of temperature difference between two plates depends on the design of the plate and the control of plasma and the cooling system operation. The system can operate as the thermionic emission generator if we connect the electrode and the cables as shown in Fig. 3.

The radiation from high temperature plasma is strong, and therefore we can expect the photon enhanced thermionic emission in this case, and the solid angle of two plates for the plasma is not the same in Fig. 3, it means that we can realize the temperature difference of these two surface plates. And if the electrical connection between two plates is realized, we can install the thermoelectric part behind the plates. Because high temperature and/or high radiation flux plate can emit electron and low temperature plate adsorb the electron from plasma, the *p*-type semiconductor should be attached behind the high temperature plate, and the *n*-type semiconductor should be connected to the low temperature plate. Then, we can expect the power from both the thermoelectric and thermionic conversions from proposed schemes. It is also important idea to apply the usual system that is not fusion reactor.

Acknowledgement

The authors thank to Prof. Atsuo Iiyoshi, Chancellor of Chubu University for his continuous support of the research. The authors also thank to Prof. Lev Bulat, Head of Department of Electrical Engineering and Electronics, St. Petersburg State University of Refrigeration and Food Engineering,

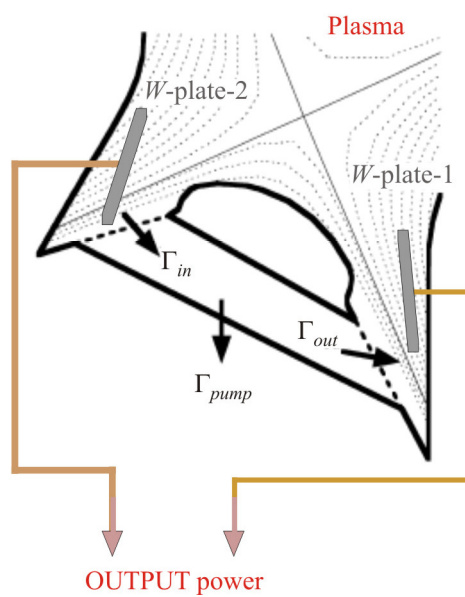


Fig. 3. Concept of thermoelectric and photon enhanced thermionic emission divertor for increasing the output power.

for his kind support, discussions and arrangement of the presentation in XIV Forum on Thermoelectricity in Moscow, Russia.

References

1. A.W. Leonard, W. Suttrop, T.H. Osborne, T.E. Evans, D.N. Hill, A. Herrmann, C.J. Lasnier, D.N. Thomas, J.G. Watkins, W.P. West, M. Weinlich, H. Zohm, Divertor Heat and Particle Flux due to ELMs in DIII-D and ASDEX-upgrade, *J. Nucl. Materials* **241-243**, 628-632 (1997).
2. A. Herrmann, T. Eich, S. Jachmich, M. Laux, P. Andrew, A. Bergmann, A. Loarte, G. Matthews, J. Neuhauser, ASDEX Upgrade team, Contributors to EFDA-JET Work Programme, Stationary and Transient Divertor Heat Flux Profiles and Extrapolation to ITER, *J. Nucl. Materials* **313-316**, 759-767 (2003).
3. M.S. Tillack, A.R. Raffray, X.R. Wang, S. Malang, S. Abdel-Khalik, M. Yoda and D. Youchison, Recent US Activities on Advanced He-cooled W-alloy Divertor Concepts for Fusion Power Plants, *Fusion Eng. Des.* **86**, 71-98 (2011).
4. A.S. Kukushkin, H.D. Pacher, G. Federici, G. Janeschitz, A. Loarte, G.W. Pacher, Divertor Issues on ITER and Extrapolation to Reactors, *Fusion Eng. Des.* **65**, 355-366 (2003).
5. A. Sagara, O. Motojima, K. Watanabe, S. Imagawa, H. Yamanishi, O. Mitarai, T. Satow, H. Tikaraishi, FFHR Group, Blanket and Divertor Design for Force Free Helical Reactor (FFHR), *Fusion Eng. Des.* **29**, 51-56 (1995).
6. D.N. Hill, A review of ELMs in Divertor Tokamaks, *J. Nucl. Materials* **241-243**, 182-198 (1997).
7. T. Tsunematsu, The Scaling Law of Energy Confinement Time for ITER, *Fusion Eng. Des.* **15**, 309-310 (1992).
8. P. Gavila, B. Riccardi, S. Constans, J.L. Jouvelot, I. Vastra Bobin, M. Missirlian, M. Richou, High Heat Flux Testing of Mock-ups for a Full Tungsten ITER Divertor, *Fusion Eng. Des.* **86**, 1652-1655 (2011).
9. E. Visca, F. Escourbiac, S. Libera, A. Mancini, G. Mazzone, M. Merola and A. Pizzuto, Testing of High Heat Flux Components Manufactured by ENEA for ITER Divertor, *Fusion Eng. Des.* **84**, 309-313 (2009).
10. S. Yamaguchi, Thermoelectric Energy Conversion in Fusion Reactor, *J. Plasma Fusion Res.* **72**, 1283-1291 (1996) (in Japanese).
11. S. Yamaguchi, Thermoelectric Conversion and its Application for Nuclear Fusion, *J. Plasma Fusion Res.* **78**, 19-35(2002) (in Japanese).
12. S. Yamaguchi, S. Ohyabu and O. Motojima, A Proposal for Divertor Cooling and Electric Power Generation in Plasma Fusion Device, Proc. 1996 Int. Conf. on Plasma Physics (ICPP96) (Nagoya, Japan, 1996), 1394-1397.
13. K. Koumoto, T. Seki, C.H. Pai and H. Yanagida, CVD Synthesis and Thermoelectric Properties of Boron Carbide, *J. Ceram. Soc. Jpn.* **100**, 853-857 (1992).
14. Y. Arita, K. Suzuki and T. Matsui, Development of High Temperature Calorimeter: Heat Capacity Measurement by Direct Heating Pulse Calorimetry, *J. Phys. Chem. Solids.* **66**, 231-234 (2005).
15. S. Fukuda, T. Kato, Y. Okamoto, H. Nakatsugawa, H. Kitagawa, S. Yamaguchi, Thermoelectric Properties of Single-Crystalline SiC and Dense Sintered SiC for Self-Cooling Devices, *Jpn. J. Appl. Phys.* **50**, 031301 (2011).
16. M. Bouchacourt, F. Thevenot, The Correlation Between the Thermoelectric Properties and Stoichiometry in the Boron Carbide Phase $B_4C-B_{10.5}C$, *J. Mater. Sci.* **20**, 1237-1247 (1985).

Submitted 14.12.2011.



L.I. Anatychuk

Institute of Thermoelectricity of NAS and MESYS
of Ukraine, 1, Nauky Str, Chernivtsi, 58029, Ukraine



R.R. Kobylianskyi

**COMPUTER DESIGN OF
THERMOELECTRIC HEAT METER
READINGS UNDER REAL-SERVICE
CONDITIONS**

This paper presents the results of computer investigations of thermal insulation effect on thermoelectric heat meter readings under real-service conditions. Three-dimensional physical, mathematical and computer models of biological tissue having on its surface thermoelectric heat meter with thermal insulation are constructed. It is established that the presence of medical thermal insulation on thermoelectric heat meter and biological tissue can change heat meter readings up to 35 %.

Key words: computer design, thermoelectric heat meter, medical thermal insulation.

Introduction

General characterization of the problem. It is known [1, 2] that inflammatory processes are attended by a change in heat release that can become a reliable indicator of various diseases. Any changes in human heat release can be readily determined by thermoelectric heat meters [3, 4] that are an efficient tool for local diagnostics of human organism, early detection of inflammatory processes, oncologic diseases, blood circulation anomalies and analysis of human state of health under extreme conditions [5-8]. The effect of such heat meters on the object under research was studied with the help of computer simulation in [9, 10].

In the investigation of human heat release of paramount importance is a manner of heat meter fastening to human body surface, heat meter spatial orientation, the presence of thermal insulation on heat meter (medical bandage, clothes, etc) that can essentially distort the temperature field of investigated human body area and affect thermoelectric heat meter readings.

The purpose of this work is to determine the effect of thermal insulation on thermoelectric heat meter readings under real-service conditions.

A physical model of biological tissue with thermoelectric heat meter and thermal insulation

According to a physical model (Fig. 1), an area of human biological tissue is a three-layered structure (epidermis 1, dermis 2, subcutis 3) and internal tissue 4 characterized by thermal conductivity κ_i , specific heat C_i , density ρ_i , blood perfusion rate ω_{bi} , blood density ρ_b , blood heat capacity C_b , human blood temperature T_b and specific heat release q_{met} due to metabolic processes (Table 1). The respective biological tissue layers 1 – 4 are considered as the bulk sources of heat q_i , where:

$$q_i = q_{met} + \rho_b \cdot C_b \cdot \omega_{bi} \cdot (T_b - T), \quad i=1\dots4. \quad (1)$$

The geometric dimensions of each such layer are a_i , b_i and l_i . The temperatures at the boundaries of respective biological tissue layers are T_1 , T_2 , T_3 and T_4 .

Thermoelectric heat meter 6 is a rectangular bar of the geometric dimensions a_6 , b_6 and l_6 , characterized by thermal conductivity κ . From the theory it is known [3, 4] that thermoelectromotive force (EMF) of thermoelectric gradient heat meter is determined as follows:

$$E = \alpha \cdot N \cdot \Delta T, \quad (2)$$

where α is the Seebeck coefficient, N is the number of thermoelectric material legs in heat meter, ΔT is temperature difference between the upper and lower surfaces of thermoelectric heat meter. As a rule, the number of thermoelectric material legs in heat meter is $N = 1500 - 2500$ pcs. Simulation of heat meter with such a number of elements is an intricate problem even for modern personal computers. At the same time, from formula (2) it is seen that the heat meter EMF values are mainly influenced by temperature difference ΔT between heat meter surfaces. Therefore, to reach the purpose set in this paper, it is quite sufficient to replace thermoelectric heat meter having a large number of elements by the bulk homogeneous sample of equivalent thermal conductivity κ . Then, on the basis of calculated ΔT , one can easily determine heat meter EMF value according to formula (2).

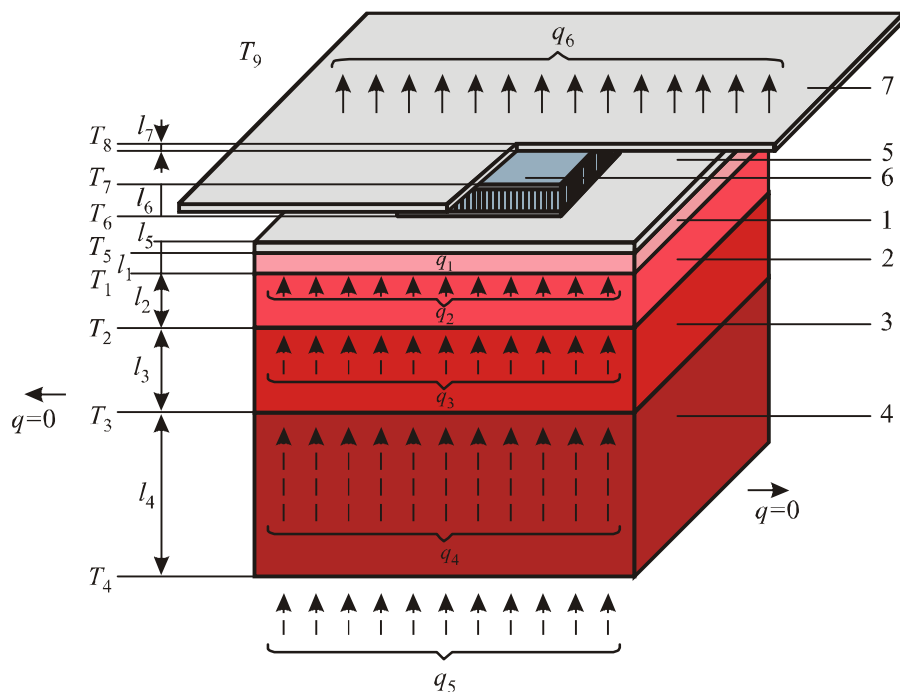


Fig. 1. A physical model of biological tissue with thermoelectric heat meter and thermal insulation 1 – epidermis, 2 – dermis, 3 – subcutis, 4 – internal tissue, 5, 7 – thermal insulation, 6 – thermoelectric heat meter.

As long as a physical model is an area of a four-layered biological tissue, with identical biochemical processes occurring in adjacent layers, it can be assumed that there is no heat overflow along biological tissue ($q = 0$).

The skin surface layer (epidermis 1) of temperature T_5 is in the state of heat exchange with thermal insulation 5 of the geometrical dimensions a_5 , b_5 and l_5 and contact surface temperature T_6 . Located on the surface of thermal insulation 5 is thermoelectric heat meter 6 of the geometric dimensions a_6 , b_6 , and l_6 and contact surface temperature T_7 . In the absence of thermal insulation 5, the heat exchange between skin surface and the environment of temperature T_9 is taken into account by heat exchange coefficient α_1 and emissivity coefficient ε_1 . Skin heat exchange due to perspiration is disregarded.

Additional thermal insulation 7 of the geometric dimensions a_7 , b_7 and l_7 is arranged on the

surface of thermoelectric heat meter 6. Free surface of thermal insulation 7 of temperature T_8 is in the state of heat exchange with the environment of temperature T_9 which is taken into account by heat exchange coefficient α_2 and emissivity coefficient ε_2 . Specific heat flux from the surface of thermal insulation 7 to the environment is q_6 , and specific heat flux from human internals – q_5 .

Table 1
Thermophysical properties of human biological tissue [11-15]

Biological tissue layers	Epidermis	Dermis	Subcutis	Internal tissue
Thickness, l (mm)	0.08	2	10	30
Specific heat, C ($J \cdot kg^{-1} \cdot K^{-1}$)	3590	3300	2500	4000
Thermal conductivity, κ ($W \cdot m^{-1} \cdot K^{-1}$)	0.24	0.45	0.19	0.5
Density, ρ ($kg \cdot m^{-3}$)	1200	1200	1000	1000
Metabolism, q_{met} ($W \cdot m^{-3}$)	368.1	368.1	368.3	368.3
Tissue blood perfusion rate, ω_b ($m^3 \cdot s^{-1} \cdot m^{-3}$)	0	0.00125	0.00125	0.00125
Blood density, ρ_b ($kg \cdot m^{-3}$)	1060	1060	1060	1060
Blood heat capacity, C_b ($J \cdot kg^{-1} \cdot K^{-1}$)	3770	3770	3770	3770

Mathematical description and a computer model

A general equation of heat exchange in biological tissue is as follows [11-15]:

$$\rho_i \cdot C_i \cdot \frac{\partial T}{\partial t} = \nabla(k_i \cdot \nabla T) + \rho_b \cdot C_b \cdot \omega_{bi} \cdot (T_b - T) + q_{met}, \quad (3)$$

where ρ_i is the density of corresponding biological tissue layer, C_i is specific heat of biological tissue layer, ρ_b is blood density, C_b is specific heat of blood, ω_{bi} is blood perfusion rate, T_b is human blood temperature, where $T_b = 310.15$ K, q_{met} is specific metabolic heat release.

The sum in the left-hand side of equation (3) is the rate of change in thermal energy comprised in the unit volume of biological tissue. Three summands in the right-hand side of this equation are the rate of change in thermal energy due to thermal conductivity, blood perfusion and metabolic heat, respectively.

To solve the problem formulated in this work, it is sufficient to consider a three-dimensional steady-state model. Then equation (3) will acquire the form of (4):

$$k_i \cdot \left(\frac{\partial^2 T}{\partial x^2} + \frac{\partial^2 T}{\partial y^2} + \frac{\partial^2 T}{\partial z^2} \right) + \rho_b \cdot C_b \cdot \omega_{bi} \cdot (T_b - T) + q_{met} = 0. \quad (4)$$

Steady-state equation of heat exchange in biological tissue (4) was solved with the respective boundary conditions (5 – 6):

$$\begin{cases} q \Big|_{x=0} = 0, & q \Big|_{y=0} = 0, \\ q \Big|_{x=a} = 0, & q \Big|_{y=a} = 0, \end{cases} \quad i = 1 \dots 4. \quad (5)$$

$$\begin{cases} T_4 \Big|_{z=0} = 310.15 \text{ K}, \\ q_6 \Big|_{z=b} = \alpha_1 \cdot (T_9 - T_8) + \alpha_2 \cdot (T_9 - T_8). \end{cases} \quad (6)$$

Here, q_i is heat flux density of the respective layer of biological tissue, T_4 is absolute temperature of the lower surface of internal tissue 4, T_8 is absolute temperature of thermal insulation surface 7, T_9 is ambient temperature, α_1 is effective heat exchange coefficient of skin surface, α_2 is effective heat exchange coefficient of heat meter and thermal insulation. Conditions of temperature equality and thermal balance are observed at the boundaries between the biological tissue layers.

To determine the effect of thermal insulation on thermoelectric heat meter readings, a three-dimensional computer model of biological tissue having on its top thermoelectric heat meter with thermal insulation was created. For this purpose, the Comsol Multiphysics software package was employed [16] enabling simulation of thermophysical processes in biological tissue with regard to blood circulation and metabolism.

The distribution of temperature and heat flux density in biological tissue and thermoelectric heat meter was calculated by finite element method (Fig. 2). According to this method, an object under study is split into a large number of finite elements, and in each of them the value of function is sought which satisfies given differential equations of second kind with the respective boundary conditions. The accuracy of solving the formulated problem depends on the level of splitting and is assured by using a large number of finite elements [16].

Computer simulation results

Calculations were performed for two models: in the first case the values of effective heat exchange coefficient α_2 were taken from the experimental measurements of heat exchange between the environment and heat meter surface without thermal insulation, and in the second case medical thermal insulation was taken into account.

Computer simulation was used to obtain the distributions of temperature and heat flux density lines in human biological tissue and thermoelectric heat meter (Figs. 3 to 5), as well as to construct the isothermal surfaces in biological tissue (Figs. 6 and 7) with regard to edge effects in a three-dimensional computer model.

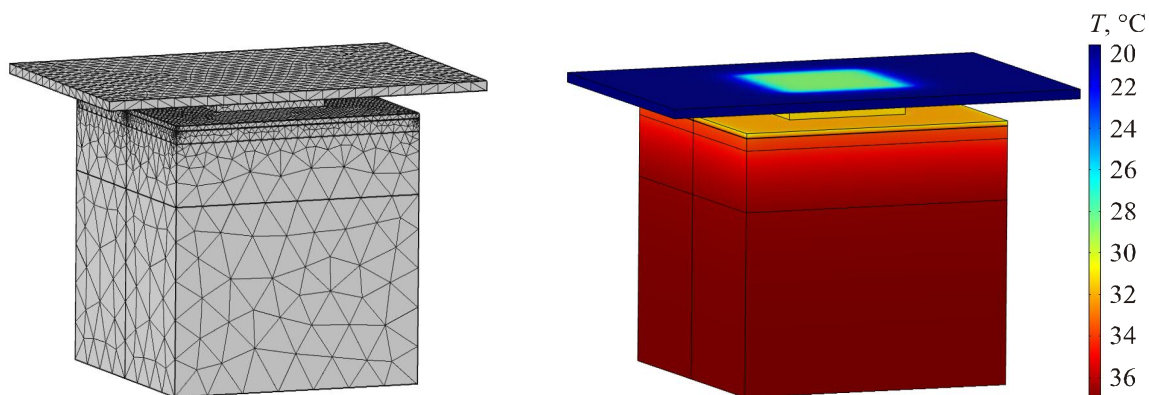


Fig. 3. Temperature distribution in biological tissue

Fig. 2. Finite element method mesh.

*having on its top thermoelectric heat meter
 with thermal insulation.*

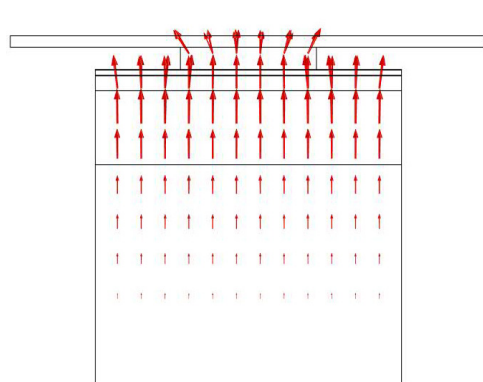


Fig. 4. Heat flux density distribution in biological tissue having on its top thermoelectric heat meter with thermal insulation.

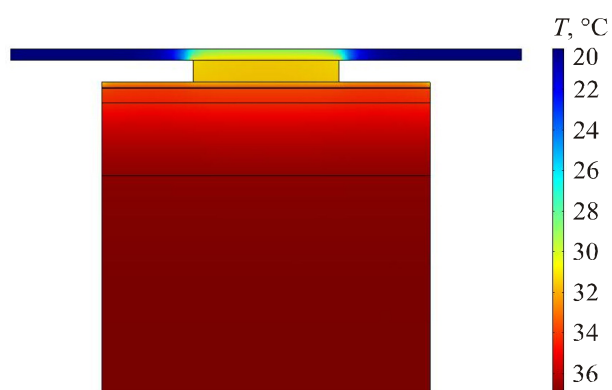


Fig. 5. Temperature distribution in the cut of biological tissue having on its top thermoelectric heat meter with thermal insulation

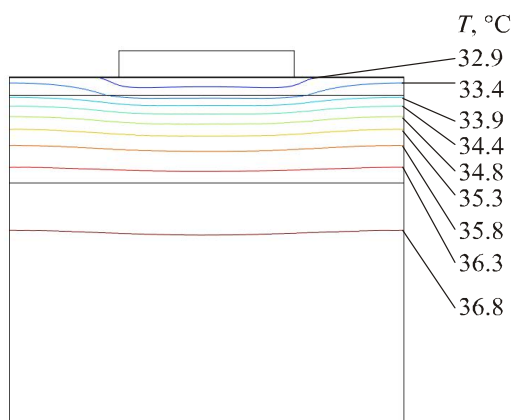


Fig. 6. Isothermal surfaces in biological tissue having on its top thermoelectric heat meter without thermal insulation.

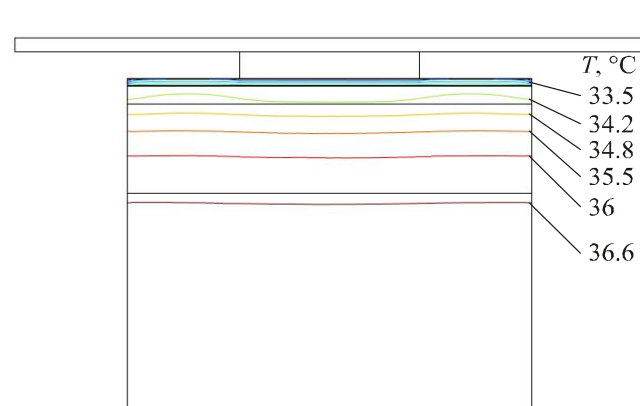


Fig. 7. Isothermal surfaces in biological tissue having on its top thermoelectric heat meter with thermal insulation.

To determine temperature difference between thermoelectric heat meter surfaces, the resulting temperature distributions on the upper and lower heat meter surfaces were averaged, since such distributions are uneven. As an example, temperature distributions along the line in the centre of the lower (Fig. 8) and upper (Fig. 9) surfaces of thermoelectric heat meter are shown.

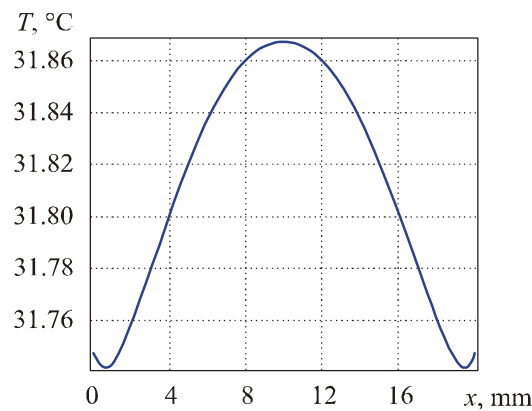


Fig. 8. Temperature distribution on the lower surface of thermoelectric heat meter with thermal insulation extending beyond the heat meter.

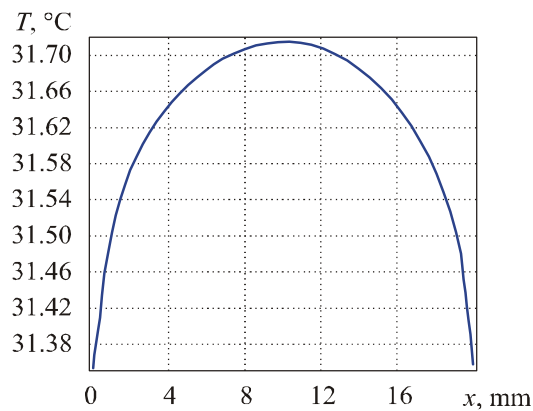


Fig. 9. Temperature distribution on the upper surface of thermoelectric heat meter with thermal insulation extending beyond the heat meter.

Fig. 10 depicts temperature distribution in biological tissue having on its top thermoelectric heat meter with thermal insulation. Fig. 11, accordingly, shows temperature distribution on the surface of external thermal insulation.

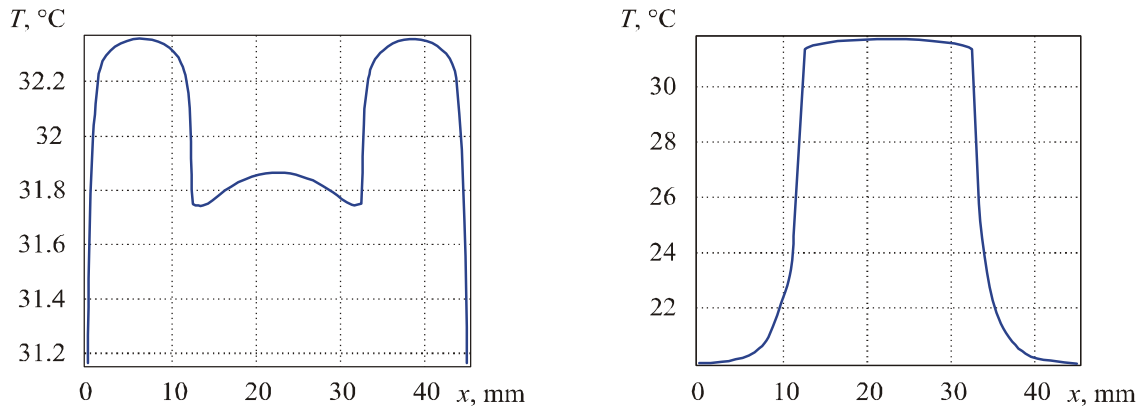


Fig. 10. Temperature distribution on the surface of biological tissue having on its top thermoelectric heat meter with thermal insulation.

Fig. 11. Temperature distribution on the surface of thermal insulation located on thermoelectric heat meter.

Computer simulation was used to determine the effect of thermal insulation on thermoelectric heat meter readings under real-service conditions. Dependence of temperature difference in thermoelectric heat meter on the thickness of heat meter thermal insulation (the number of external bandage layers N_{extern}) with a different thickness of thermal insulation between biological tissue and heat meter (the number of internal bandage layers N_{in}) was established for the case when thermal insulation does not extend beyond the heat meter (Fig. 12) and does so (Fig. 13).

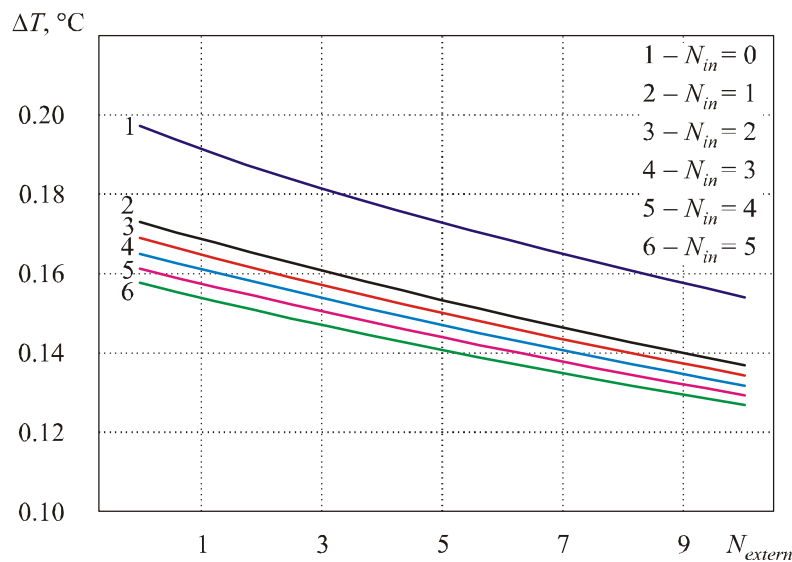


Fig. 12. Dependence of temperature difference in thermoelectric heat meter on the thickness of heat meter thermal insulation (the number of external bandage layers N_{extern}) with a different thickness of thermal insulation between biological tissue and heat meter (the number of internal bandage layers N_{in}) for the case when the external thermal insulation does not exceed beyond the heat meter upper surface.

From Fig. 12 it is seen that increasing the thickness of thermal insulation between biological tissue and thermoelectric heat meter, as well as increasing the thickness of external insulation on heat meter definitely results in decreasing temperature difference between heat meter surfaces. A reduction

in thermoelectric heat meter readings can reach 35 % as compared to the case when thermal insulation is absent. The irregularity of curves in Figs. 12 and 13 is due to the difference in heat exchange coefficients between the skin surface and thermoelectric heat meter surface.

For the case when the external thermal insulation extends beyond the heat meter upper surface, its effect on temperature difference changes for the opposite (Fig. 13).

Thus increasing the thickness of thermal insulation on the biological tissue results in the reduction of temperature difference between heat meter surfaces, however, increasing the thickness of heat meter insulation in this case results in the increase of the corresponding temperature difference. It is due to the fact that thermal insulation on thermoelectric heat meter serves as a peculiar heat exchanger. From Fig. 13 it is seen that the presence of external thermal insulation on thermoelectric heat meter can increase heat meter readings up to 30% as compared to the case when such insulation is absent.

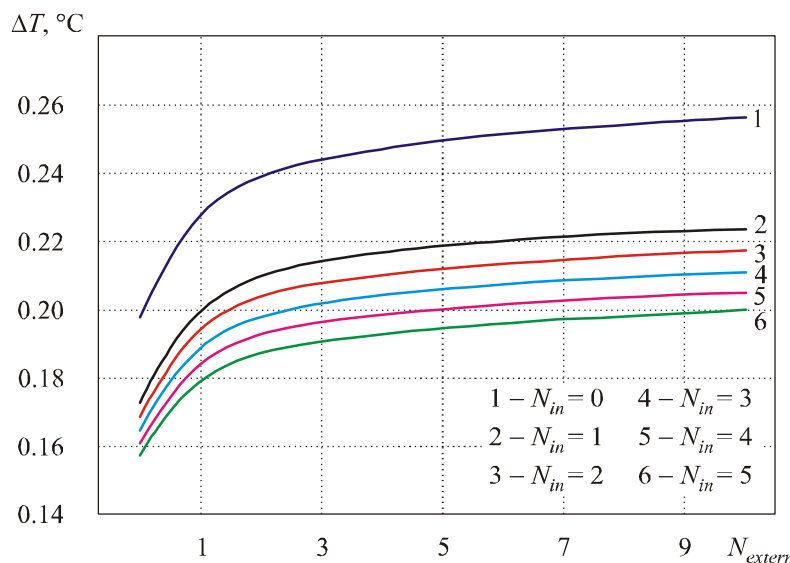


Fig. 13. Dependence of temperature difference in thermoelectric heat meter on the thickness of heat meter thermal insulation (the number of external bandage layers N_{extern}) with a different thickness of thermal insulation between biological tissue and heat meter (the number of internal bandage layers N_{in}) according to a physical model when the external thermal insulation extends beyond the heat meter.

Thus it is established that the presence of thermal insulation on the biological tissue and thermoelectric heat meter really has an effect on heat meter readings. Thermal insulation does not always cause a decrease in heat meter readings. In some cases it leads to their increase, since thermal insulation serves as a peculiar heat exchanger. This, in turn, should be taken into account in the measurement of human heat fluxes by creating identical conditions at repeated measurements.

Conclusions

1. With the aid of computer simulation the effect of thermal insulation on thermoelectric heat flux readings under real-service conditions is investigated. It is established that the presence of thermal insulation on thermoelectric heat meter does not always cause a decrease in its readings, and there are instances where it leads to their increase, since thermal insulation serves as a peculiar heat exchanger.
2. It is established that due to the presence of medical thermal insulation on thermoelectric heat meter and biological tissue, heat meter readings can change up to 35%. This fact should be taken into account in the measurement of human heat fluxes by creating identical conditions at repeated measurements.

References

1. R.B. Ladyka, D.N. Moskal, V.D. Didukh, Semiconductor Heat Meters in Arthropathy Diagnostics and Treatment, *Meditinskaya Tekhnika* **6**, 34-35 (1992).
2. R.B. Ladyka, O.N. Dakalyuk, L.P. Bulat and A.P. Myagkota, Use of Semiconductor Heat Meters in the Diagnostics and Treatment, *Meditinskaya Tekhnika* **6**, 36-37 (1996).
3. L.I. Anatychuk, *Thermoelements and Thermoelectric Devices: Handbook* (Kyiv: Naukova Dumka, 1979), p.766.
4. O.A. Geraschenko, *Foundations of Heat Flux Measurement* (Kyiv: Naukova Dumka, 1971), p.192.
5. L.I. Anatychuk, N.G. Lozinsky, P.D. Mykytyuk, Yu.Yu. Rozver, Thermoelectric Semiconductor Heat Meter, *Pribory i Tekhnika Eksperimenta* **5**, 236 (1983).
6. L.I. Anatychuk, L.P. Bulat, D.D. Gutsal and A.P. Myagkota, Thermoelectric Heat Meter, *Pribory i Tekhnika Eksperimenta* **4**, 248 (1989).
7. B.M. Demchuk, L.Ya. Kushneryk and I.M. Rublenyk, Thermoelectric Sensors for Orthopedics, *J.Thermoelectricity* **4**, 80-85 (2002).
8. A. Acheulov, L.Ya. Kushneryk, Thermoelectric Device for Medico-Biological Express-Diagnostics, *Tekhnologiya i Konstruirovaniye v Elektronnoi Apparature* **4**, 38-39 (2004).
9. L.I. Anatychuk, R.R. Kobylyanskii, Research into the Effect of Thermoelectric Heat Meter on Human Heat Release Measurement, *J.Thermoelectricity* **4**, 59-65 (2012).
10. L.I. Anatychuk, R.R. Kobylyanskii, 3D-Model for Determination of Thermoelectric Heat Meter Effect on the Accuracy of Human Heat Release Measurement, Scientific Bulletin of Chernivtsi University: Collected Scientific Works. Physics. Electronics, **2**, issue 1 (Chernivtsi: Chernivtsi National University, 2012), p. 15-20.
11. S.C. Jiang, N. Ma, H.J. Li and X.X. Zhang, Effects of Thermal Properties and Geometrical Dimensions on Skin Burn Injuries, *Burns* **28**, 713-717 (2002).
12. M.P. Cetingul, C.Herman, Identification of Skin Lesions from the Transient Thermal Response Using Infrared Imaging Technique, *IEEE*, 1219-1222 (2008).
13. M. Ciesielski, B. Mochnacki and R. Szopa, Numerical Modeling of Biological Tissue Heating. Admissible Thermal Dose, *Scientific Research of the Institute of Mathematics and Computer Science* **1**(10), 11-20 (2011).
14. Florin Filipoiu, Andrei Ioan Bogdan and Iulia Maria Carstea, Computer-Aided Analysis of the Heat Transfer in Skin Tissue, *Proceedings of the 3rd WSEAS Int. Conference on Finite Differences - Finite Elements - Finite Volumes - Boundary Elements*, 2010, p. 53-59.
15. Daniela Carstea, Ion Carstea and Iulia Maria Carstea, Interdisciplinarity in Computer-Aided Analysis of Thermal Therapies, *WSEAS Transactions on Systems and Control* **6**(4), 115-124 (2011).
16. COMSOL Multiphysics User's Guide, COMSOLAB, 2010, p.804.

Submitted 23.01.2013.

Yu.M. Lobunets



Yu.M. Lobunets

Institute of Thermoelectricity of NAS and MESYS of Ukraine,
1, Nauky Str., Chernivtsi, 58029, Ukraine

PERFORMANCE EVALUATION OF OTEC WITH THERMOELECTRIC POWER CONVERTER

The possibility of using thermoelectric generators in systems of ocean thermal energy conversion (OTEC) is considered. Performance evaluation of such configurations is made, the possibility of creating OTEC with acceptable technical and economic features is shown.

Key words: ocean thermal energy; thermoelectric generator; OTEC.

Introduction

The world ocean is a natural accumulator of solar energy whose heat content is estimated as 20 to 25 kWh/m³. A small part of energy stored in the ocean would have sufficed to cover all needs of mankind. However, this resource is hard to reach, since currently existing technologies of ocean thermal energy conversion have not reached yet the level sufficient for a large-scale application.

Though a number of implemented pilot projects have confirmed the possibility of obtaining quite acceptable technical and economic features of OTEC [1, 2], this technology has not received any commercial development effort. This is due to the necessity of heavy capital investments in OTEC projects – their sum is estimated as 1 milliard \$ for a plant of power 200 to 300 MW, which, naturally, is a serious constraint on the way to using the energy source under study. Nevertheless, research and activities related to OTEC keep up. They are primarily aimed at developing the most capital-intensive system components, namely heat exchangers, turbines, cold and hot water pipelines.

The experience of using modern systems of renewable energy sources conversion (photovoltaic converters, wind-powered engines) shows that their wide application became possible due to commercial use of low-power systems (of order 1 to 100 kW) and introduction of special feed-in tariffs assuring the profitability of running such systems. For ocean thermal energy converters the use of low-power generators is considered to be unacceptable, since economic feasibility of the system is affected considerably by scale factor, i.e. with power reduction below 10 MW, the relative capital investments in OTEC drastically increase (Fig. 1) [1]. It is due to peculiarities of employed energy conversion system based on steam-turbine cycle using a low-boiling heat carrier.

This paper is concerned with the possibility of using a thermoelectric converter in OTEC and analyzes the possibilities of application of such devices in the power range of order 0.1 MW.

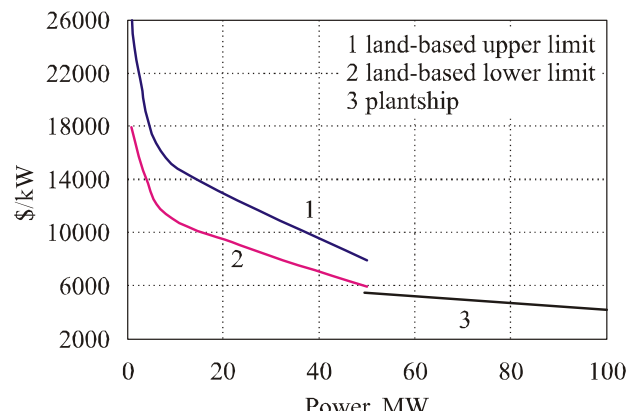


Fig. 1. Specific cost of OTEC versus power level.

OCEC configuration with a thermoelectric energy converter

Similar to a classical OTEC system, as a source of thermal energy the configuration under study employs warm water of ocean surface layers and as a heat sink – cold water of deep layers.

The major configuration components:

- thermoelectric generator with systems of supply and removal of heat;
- cold and hot water pipelines;
- pumps;
- OTEC direct current converter into alternating current of industrial parameters (mains inverter).

All configuration components, except for thermoelectric generator, are standard; their characteristics can be determined knowing the source data (power, heat carrier flow rates, hydraulic resistance of the system, etc).

Thermoelectric generator is a thermopile consisting of $n \times m$ standard modules equipped with systems of supply and removal of heat in the form of counter-current heat exchanger. The specific feature of this configuration is essential dependence of generator characteristics on the flow regime of heat carriers. A change in mass flow affects both the available and working temperature difference (i.e. the generator power and efficiency) and the thermal and hydraulic resistance of heat exchangers (i.e. the size and cost of device, as well as auxiliary energy expenditures). Therefore, in the analysis of OTEC characteristics it is necessary to use a mathematical model taking into account the interrelation of said parameters with regard to real design peculiarities.

To determine the generator characteristics, we will use a mathematical model of counter-current TEG in the form [3]:

$$\theta(J, Y) = C_1 + C_2 Y - 0.5 J^2 Y^2 / I_o, \quad (1)$$

where

$$C_1 = (a_2 Bi_c t_c - a_1) / (J - Bi_h + a_2 (J + Bi_c)), \quad (2)$$

$$C_2 = C_1 (J + Bi_c) - Bi_c t_c, \quad (3)$$

$$a_1 = J^2 / I_o - 0.5 J^2 (J - Bi_h) / I_o + Bi_h t_h, \quad (4)$$

$$a_2 = J - Bi_h - 1. \quad (5)$$

Here $\theta = T/t_o$ is dimensionless temperature of thermoelement; Y is dimensionless coordinate; $J = jeh/\lambda$ is dimensionless current density; e is thermoelectric coefficient; λ is thermal conductivity; α is heat transfer coefficient; $Bi = \alpha h/\lambda$ is the Biot criterion; $I_o = zt_o$ is the Ioffe criterion; $z = e^2 \sigma / \lambda$ is thermoelectric figure of merit of material; h is thermoelement height; $t_o = t_h$ is defining temperature; t_c is cold water temperature; t_h is hot water temperature.

Indexes “c” and “h” correspond to the cold and hot thermopile temperatures.

To specify current values of heat carrier temperatures t_c, t_h , we use a well-known expression for heat carrier temperature difference in a counter-current heat exchanger:

$$\Delta t = A(t_{ho} - t_{co}), \quad (6)$$

where t_{ho} and t_{co} are initial temperatures of heat carriers;

$$A = 1 / (1 + W / KS), \quad (7)$$

$W = G_o \cdot C_p$ is water equivalent of heat, kJ/s; $K = 1 / (1/\alpha_h + 1/\alpha_c + h/\lambda)$ is heat transfer coefficient, $W/m^2 \cdot K$; S is heat exchange surface, m^2 .

Considering a change in heat carrier temperatures within one module to be negligibly small, we obtain expressions for heat carrier temperatures:

$$t_c(x) = t_{co} + dt, \quad (8)$$

$$t_h(x) = t_{ho} - dt, \quad (9)$$

where

$$dt = \Delta t / n.$$

Solving the system of equations (1 – 9), one can find temperature distribution in a thermopile and, accordingly, thermoelectric generator power.

As mentioned above, parameters of thermoelectric generator are essentially dependent on heat carrier flow rate and the intensity of heat exchange on the surface of modules. A significant influence on the economic feasibility of OTEC is also exercised by heat exchanger's hydraulic resistance which dictates the auxiliary power expenditures. All these parameters are interrelated; the kind of these relations is mainly determined by heat exchanger construction.

For specification of the source data we use characteristics of standard 100 kW plate heat exchanger of the type Funke FP-10 (Fig. 2).

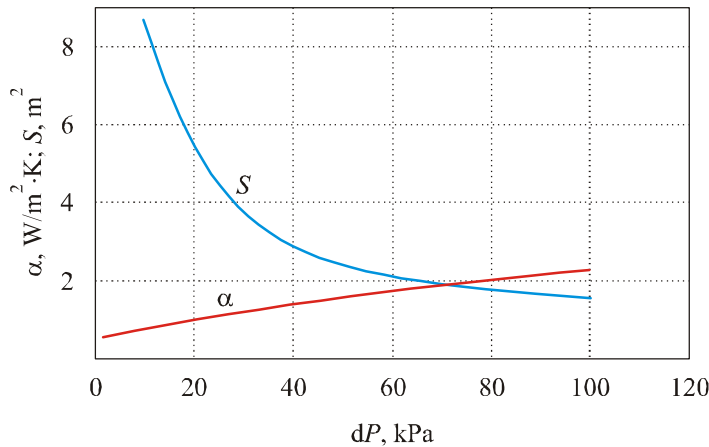


Fig. 2. The correlation between heat exchange intensity α , heat exchange area S , and hydraulic resistance dP of 100 kW heat exchanger (corresponds to 1 kW OTEC).

The data given in the figure is approximated by dependences of the type

$$S(G_o, dP) = (aG_o - b) dP^e, \quad (10)$$

$$\alpha(G_o, dP) = dG_o dP^e, \quad (11)$$

where G_o is heat carrier flow rate, kg/s.

As the source data, we also use the following:

- hot water temperature $t_{ho} = 27^\circ\text{C}$;
- cold water temperature $t_{co} = 5^\circ\text{C}$;
- thermoelectric module figure of merit $z = 0.003$;
- thermoelement height $h = 0.5 \text{ mm}$;
- module size $40 \times 40 \text{ mm}$;
- the cost of one module – 3 \$;
- specific cost of heat exchanger – 250 \$/m²;
- total length of pipelines 3000 m;
- the cost of pipeline – 10 \$/m;
- the cost of pumps – 75 \$/(kg/s);
- the cost of inverter – 150 \$/kW.

All prices are taken from manufacturers' catalogs [4].

The analysis of a mathematical model of OTEC has shown that in conditions under consideration the governing operating parameter affecting the cost of system in general is a hydraulic resistance of heat exchangers that can be varied over considerably wide limits with a specified heat exchanger power and heat carrier flow rate (in this case, in conformity with hydrothermal analogy concept, the thermal resistance also changes accordingly). The specific cost of a TEC optimized with respect to heat carrier flow rate for different values of heat exchanger hydraulic resistance is illustrated in Fig. 3.

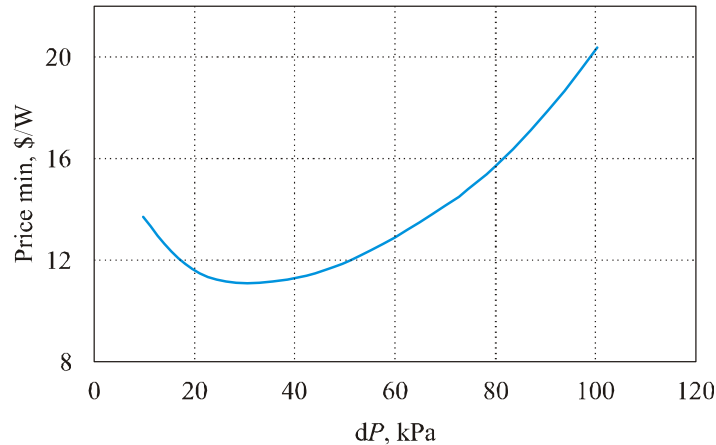


Fig. 3. Specific cost of TEC (\$/W net power) versus heat exchanger hydraulic resistance.

Fig. 4 represents dependences of relative net power (N_{net}/N_o), full power N_o , relative power of feed pumps (N_{pump}/N_o) and specific cost of OTEC (\$/W) on heat carrier flow rate (kg/s) for generator of net power 100 kW.

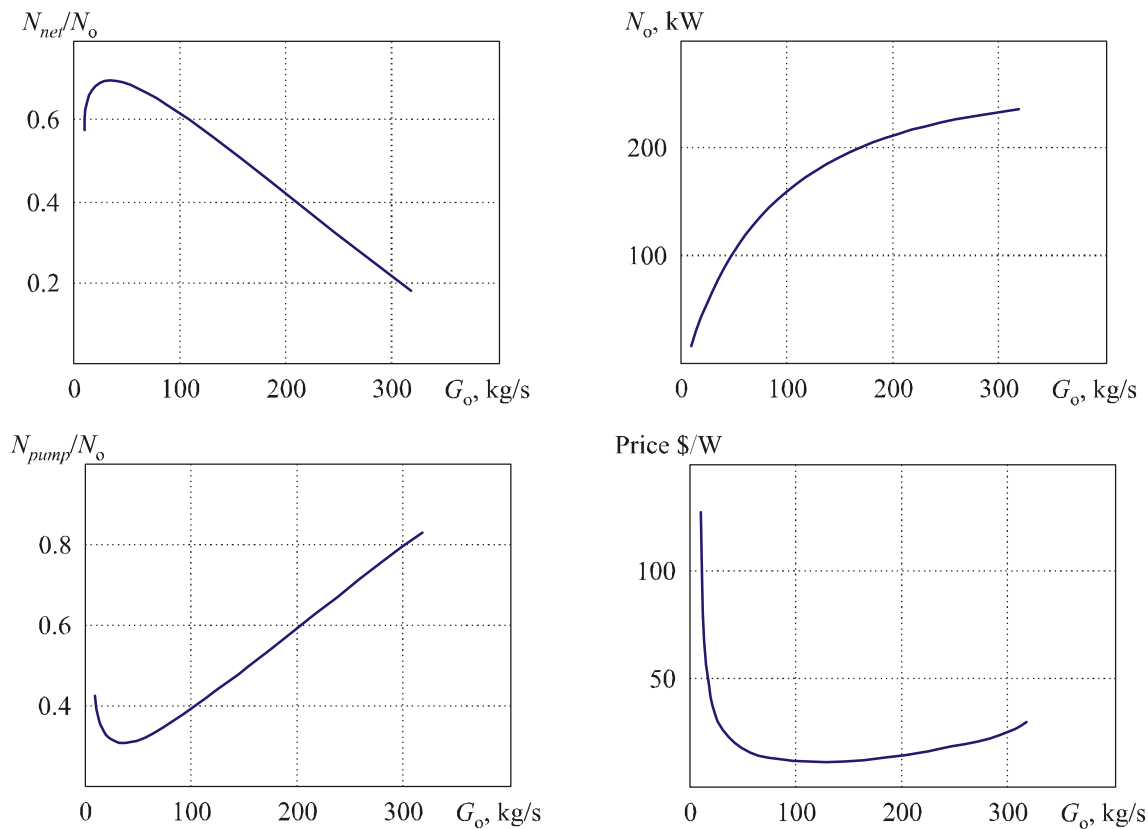


Fig. 4. Characteristics of 100 kW OTEC versus heat carrier flow rate (kg/s). N_o – full power; N_{net}/N_o – relative net power; N_{pump}/N_o – relative power of feed pumps; Price – specific cost of OTEC, \$/kW.

The resulting data helps to determine the basic technical and economic features of OTEC configuration under study, i.e. the cost of electric energy produced. For a 100 kW generator, with the above source data, the project cost is:

- generating part – 1 million 110 thousand \$;
- pipelines – 50 thousand \$;
- pumps – 20 thousand \$;
- invertor – 15 thousand \$;
- other expenditures (50 %) – 600 thousand \$;
- Total: 1 million 795 thousand \$.

With 100% load of OTEC the electric energy production is about 900 thousand kW·h/year, which for standard appreciation periods of 20 years yields the cost price of electric energy of order 0.1 \$/kW·h. With regard to maintenance costs, tax deduction and operating organization profit, this figure can increase by another 50% maximum, i.e. to 0.15 \$/kW·h.

For comparison, it can be noted that current feed-in tariff for systems of photovoltaic conversion of solar energy in power range under study is 0.3...0.6 \$/kW·h [4-6]. That is, the existing tariffs exceed by a factor of 2...4 the values obtained for OTEC, which confirms high competitive ability of OTEC configuration analyzed.

Conclusions

The analysis of thermoelectric system of ocean thermal energy conversion has shown the possibility in principle of creating OTEC in the power range of 100 kW with technical and economic features acceptable for a wide commercial use.

References

1. Luis A. Vega Ph.D, Economics of Ocean Thermal Energy Conversion (OTEC): An Update, *2010 Offshore Technology Conference* (Houston, Texas, USA, 3-6 May 2010).
2. G.C. Nihous and M.A. Syed, A Financing Strategy for Small OTEC Plants, *Energy Convers. Mgmt.* **38**(3), 201-211 (1997).
3. Yu.M. Lobunets, *Methods for Calculation and Design of Thermoelectric Power Converters* (Kyiv: Naukova Dumka, 1989), 175p.
4. <http://pv.energytrend.com/pricequotes>
5. <http://www.nerc.gov.ua/?id=4225>
6. <http://www.renewableenergyworld.com/rea/news/article/2012/06/japan-approves-feed-in-tariffs>

Submitted 04.01.2013.

V.R. Bilinsky-Slotylo, L.N. Vikhor, V.Ya. Mykhailovsky

Institute of Thermoelectricity of NAS and MESYS of Ukraine,
1, Nauky Str., Chernivtsi, 58029, Ukraine

**DESIGN OF THERMOELECTRIC GENERATOR
MODULES MADE OF *Mg* AND *Mn* SILICIDE
BASED MATERIALS**

The results of computer simulation of segmented thermoelectric modules, functionally graded materials based modules, as well as stage structures from Mg and Mn silicide-based materials are presented in this work. The optimal concentrations of doping impurities for the materials of segments and optimal inhomogeneity distributions in functionally graded materials (FGTM) based thermoelements have been defined. The optimal values of thermoelectric parameters have been estimated thus providing maximum efficiency for the two-stage generator modules within the temperature range of 323 – 773 K. It has also been demonstrated that in silicide-based modules manufactured from homogeneous silicide-based materials maximum efficiency equals $\eta \approx 6.5\%$, whereas in modules made of two-segmented thermoelements it is $\eta \approx 8.5\%$, and $\eta \approx 8.1\%$ for two-stage generator modules. The use of Bi_2Te_3 -based materials for cold segments or for cold stage of the module, can improve their efficiency up to $\sim 10\%$.

Key words: generator modules, heat recovery, energy converters, efficiency.

Introduction

A thermoelectric way of conversion of heat energy into electric one is widely used for waste heat of various industrial devices and combustion engines utilization [1, 2]. The temperature level of such sources can reach 800 – 900 K. Therefore the design and development of high-efficient, low-cost and environmentally friendly thermoelectric energy converters (generator modules) for heat recovery with the range of operating temperatures from 300 to 800 K is a topical task.

For generator modules such materials should be used whose figure of merit Z temperature dependence reaches its maximum in the interval of generator operating temperatures. Moreover, along with demands for high values of the figure of merit, important features for industrial applications are considered to be the low cost of the initial materials, mechanical strength and ecological safety. For generator modules with operational temperatures in the range from 300 to 800 K thermoelectric materials based on some metals (*Mg*, *Mn*, *Fe*) silicides [3-5], are the best option and among those the most promising seem doped solid solutions on the base of *MgSi* and *MnSi* of *n*-type and *p*-type, correspondingly. Such compositions are characterized by similar physicochemical, mechanical and cost criteria and can, therefore, be used as materials for fabrication of generator thermoelements of the medium temperature range.

The objective of the present research is the calculation of the optimal doping level for magnesium and manganese silicides and estimation of characteristics of generator modules fabricated from homogeneous, segmented, as well as functionally graded and stage structures on the base of the said materials.

Optimization of materials and modules made of homogeneous, segmented and functionally graded $MgSi$ and $MnSi$ based thermoelements

A number of scientific publications [6-17] give examples of technologies of fabrication of specimen and results of experimental research into thermoelectric properties of magnesium and manganese based silicides. The analysis of these results has shown that, considering high values of the figure of merit, the following materials can be effective for generator thermoelements:

for *n*-type conductivity legs:

– $Mg_2Si_{0.58}Sn_{0.42-x}Bi_x$ ($0.005 \leq x \leq 0.01$), obtained by melting of the initial components followed by hot pressing [6]. Maximum figure of merit ZT of such bismuth doped silicide reaches 0.62 at 675 K for the composition $x = 0.0075$.

– $Mg_2(Si_{0.3}Sn_{0.7})_{1-x}Sb_x$ ($0.02 \leq x \leq 0.03$), obtained by way of two-stage solid-state reaction in connection with spark plasma sintering [7]. Maximum figure of merit of this antimony doped silicide $ZT \approx 1.0$ at 640 K for the composition $x = 0.025$.

for *p*-type conductivity legs:

– $Mn(Al_xSi_{1-x})_{1.80}$ ($0 \leq x \leq 0.003$), obtained using induction melting of compressed powders of the initial components with further spark plasma sintering [8]. Maximum figure of merit of this aluminium doped manganese silicide $ZT \approx 0.65$ at 850 K for the composition $x = 0.0015$.

– $Mn(Si_{1-x}Ge_x)_{1.733}$ ($0.2 \leq x \leq 1.6$), obtained using induction melting with further hot compaction [9]. Maximum figure of merit of such germanium doped specimen $ZT \approx 0.6$ at 830 K for the composition $x = 0.8$.

Experimental dependences of thermoEMF α , electric conductivity σ and thermal conductivity κ of those materials on the temperature T and concentration x of corresponding impurities have been used to estimate optimal characteristics of generator modules in the maximum efficiency mode. The calculations have been carried out with computer methods designed on the base of the theory of optimal control [18-20]. Concentration-temperature dependences α , σ , κ have been approximated with the help of two-dimensional polynomial in the form of $\alpha^{n,p} = \alpha^{n,p}(x, T)$, $\sigma^{n,p} = \sigma^{n,p}(x, T)$, $\kappa^{n,p} = \kappa^{n,p}(x, T)$. Polynomial coefficients were entered into the computer programme as input data for thermoelectric modules design.

The results of calculations for optimal impurity concentrations in silicides for homogeneous two-segmented thermoelements and parameters of generator modules based on such materials in the maximum efficiency mode within the range of operating temperatures from 323 to 773 K are presented in Table 1. The estimation of parameters was performed for the modules with the dimensions 40×40 mm 2 , containing 32 thermoelements, with the height of legs $L = 5.6$ mm and cross section area 4×4 mm 2 . The values of contact resistances in calculations were accepted to be equal $5 \cdot 10^{-5}$ Ω·cm 2 .

Analysis of the results obtained shows that the efficiency of modules with two-segmented thermoelements exceeds the efficiency of modules from homogeneous materials by 1.3 to 1.5 times. The highest efficiency of about 8.5 % can be reached on the modules from two-segmented thermoelements fabricated from *n*-type conductivity $Mg_2(Si_{0.3}Sn_{0.7})_{1-x}Sb_x$ materials and *p*-type $Mn(Al_xSi_{1-x})_{1.80}$ materials. That is why these very compositions are appropriate for creation of functionally graded thermoelectric materials, those being created by way of inhomogeneous impurity distribution.

Fig. 1 demonstrates optimal antimony concentrations distributions x_n along the *n*-type conductivity $Mg_2(Si_{0.3}Sn_{0.7})_{1-x}Sb_x$ leg and aluminium concentration x_p along *p*-type $Mn(Al_xSi_{1-x})_{1.80}$ leg calculated by computer methods. The calculated maximum efficiency of the module fabricated from the said FGTMs is reached 8.5 % at the temperature difference from 323 to 773 K at the power of

19.9 W thus giving no significant advantages to a FGTM module over a similar one fabricated from two-segmented thermoelements.

Table 1

*Optimal impurity concentrations in Mg and Mn silicides and parameters
 of generator modules on their base at the temperature differences 323 – 773 K*

Materials of the legs	<i>n</i> -type $Mg_2Si_{0.58}Sn_{0.42-x}Bi_x$	<i>n</i> -type $Mg_2Si_{0.58}Sn_{0.42-x}Bi_x$	<i>n</i> -type $Mg_2(Si_{0.3}Sn_{0.7})_{1-x}Sb_x$	<i>n</i> -type $Mg_2(Si_{0.3}Sn_{0.7})_{1-x}Sb_x$
	<i>p</i> -type $Mn(Al_xSi_{1-x})_{1.80}$	<i>p</i> -type $Mn(Si_{1-x}Ge_x)_{1.733}$	<i>p</i> -type $Mn(Al_xSi_{1-x})_{1.80}$	<i>p</i> -type $Mn(Si_{1-x}Ge_x)_{1.733}$
Modules with homogeneous legs				
Optimal impurity concentration	x_n	0.008	0.008	0.025
	x_p	0.0021	0.8	0.00203
Power, W		8	7.3	15.8
Efficiency %		4.2	4.2	6.5
Modules with two-sectional legs				
Optimal impurity concentration	x_n^h	0.00825	0.008	0.027
	x_n^c	0.0074	0.00725	0.0255
	x_p^h	0.00204	0.92	0.0021
	x_p^c	0.0018	0.8	0.00165
Height of legs, mm	ℓ_n^h	2.8	2.8	3.2
	ℓ_n^c			2.4
	ℓ_p^h			2.4
	ℓ_p^c			3.2
Intersectional temperature, K	T_n	547	550	505
	T_p	545	539	582
Power, W		12.7	11.4	20.4
Efficiency %		6.3	6.1	8.5

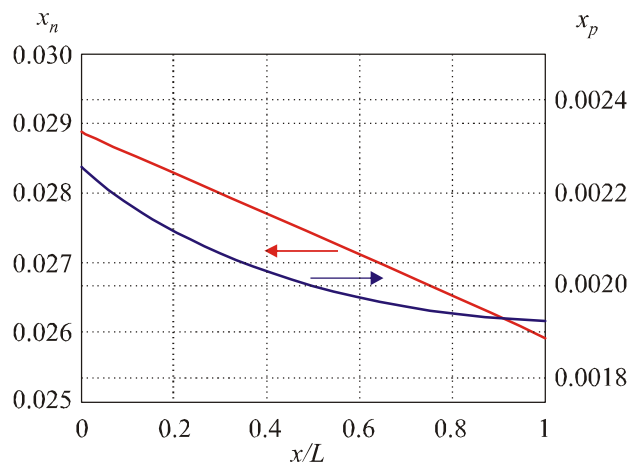


*Fig. 1. Antimony concentration optimal distribution x_n along the n-type leg
 from $Mg_2(Si_{0.3}Sn_{0.7})_{1-x}Sb_x$ and aluminium concentration x_p along the p-type leg from $Mn(Al_xSi_{1-x})_{1.80}$
 for generator modules. $x/L = 0$ corresponds to the cold side of the leg.*

Results of optimization of modules from *Bi-Te* and *Mg i Mn* silicides based materials

It is a well-known fact that in the temperature range from 300 to 450 K *Bi-Te* based compositions is the most efficient materials for thermoelectric generators. Thus reasonable models of generator modules with the range of operating temperatures from 323 to 773 K the following ones can be considered:

- modules with two-segmented legs where low-temperature sections are fabricated from *Bi-Te* based materials, whereas high-temperature ones from *Mg* and *Mn* based silicides;
- two-stage modules with a low-temperature *Bi-Te* based stage and a high-temperature one based on *Mg* and *Mn* silicides.

The results of calculations for parameters of modules from two-segmented legs are given in Table 2. There optimal values of characteristics (electric conductivity σ and thermoEMF α) of materials based on *n*- and *p*-type conductivity *Bi-Te* for low-temperature sections and impurity concentrations x_n , x_p in *Mg* and *Mn* silicides for high-temperature sections. Electric power and efficiency were calculated for the modules of two different designs. It has been found out that if *Bi-Te* based materials are used for cold sections instead of silicides the efficiency can be increased from 8.5 % to 9.6 % (Module No. 1). Optimizing the module design by search of optimal segments heights ratio optimal cross section areas of legs allows reaching the efficiency as high as 10 % (Module No. 2). Here wastes of thermoelectric materials are 2.5 times reduced for such module design.

Table 2
Parameters of generator modules from two-segmented legs fabricated from Bi-Te-based materials and Mg and Mn silicides under operating temperatures within the temperature difference of 323 – 773 K

Parameter			Parameter value		
			Module No. 1	Module No. 2	
Parameters of the materials of segments	cold	<i>n</i> -(Bi_2Te_3) _{0.90} (Sb_2Te_3) _{0.05} (Sb_2Se_3) _{0.05} , I_2 -doped [19]	$\sigma_n(300\text{ K}) = 1340\text{ }\Omega^{-1}\text{ cm}^{-1}$	$\alpha_n(300\text{ K}) = 187\text{ }\mu\text{V/K}$	
		<i>p</i> -(Bi_2Te_3) _{0.25} (Sb_2Te_3) _{0.72} (Sb_2Se_3) _{0.03} , Pb -doped [19]	$\sigma_p(300\text{ K}) = 1680\text{ }\Omega^{-1}\text{ cm}^{-1}$	$\alpha_p(300\text{ K}) = 164\text{ }\mu\text{V/K}$	
	hot	<i>n</i> - $Mg_2(Si_{0.3}-Sn_{0.7})_{1-x}Sb_x$ [7]	$x_n = 0.027$		
		<i>p</i> - $Mn(Al_xSi_{1-x})_{1.80}$ [8]	$x_p = 0.00195$		
Segments height, mm	cold	<i>n</i> -(Bi_2Te_3) _{0.90} (Sb_2Te_3) _{0.05} (Sb_2Se_3) _{0.05} , I_2 -doped [19]	$\ell_n = 2.4$	$\ell_n = 0.9$	
		<i>p</i> -(Bi_2Te_3) _{0.25} (Sb_2Te_3) _{0.72} (Sb_2Se_3) _{0.03} , Pb doped [19]	$\ell_p = 3.2$	$\ell_p = 0.9$	
	hot	<i>n</i> - $Mg_2(Si_{0.3}-Sn_{0.7})_{1-x}Sb_x$ [7]	$\ell_n = 3.2$	$\ell_n = 2.1$	
		<i>p</i> - $Mn(Al_xSi_{1-x})_{1.80}$ [8]	$\ell_p = 2.4$	$\ell_p = 2.1$	
Intersectional temperature, K		T_n	526	473	
		T_p	582	480	
Number of thermocouples			32	48	
Cross-section area of legs, mm ²			4×4	1.8×4.3	
Electric power P , W			22.9	30.8	
Efficiency η , %			9.6	10	

The results of calculation of two-stage modules of different designs provided the cold and the hot stages are connected in series under the electrical and thermal compatibility are given in Table 3. For both stages of the module No. 3 silicides based materials have been chosen. *Bi-Te* is suggested for the low-temperature stage in modules No. 4 and No. 5. Table 3 gives optimal values of parameters of *Bi-Te* based materials and optimal impurity concentrations in *Mg* and *Mn* silicides, as well as calculated values of modules power and efficiency for every stage. Efficiency and power dependences of modules No. 3 and No. 4 on the modules hot side temperature are shown in Fig. 2.

Table 3

Parameters of two-stage generator modules fabricated from Bi-Te-based materials and Mg and Mn silicides under operating temperatures within the temperature difference of 323 – 773 K

Parameter	Parameter value			
	Module No. 3	Module No. 4	Module No. 5	
Parameters of materials	Cold stage	<i>n</i> - $Mg_2(Si_{0.3}-Sn_{0.7})_{1-x}Sb_x$ [7] $x = 0.0255$	n -(<i>Bi₂Te₃</i>) _{0.90} (<i>Sb₂Te₃</i>) _{0.05} (<i>Sb₂Se₃</i>) _{0.05} , <i>I₂</i> -doped [19] $\sigma_n(300\text{ K}) = 1365 \Omega^{-1}\cdot\text{cm}^{-1}$ $\alpha_n(300\text{ K}) = 189 \mu\text{V/K}$	
		<i>p</i> - $Mn(Al_xSi_{1-x})_{1.80}$ [8] $x = 0.00165$	p -(<i>Bi₂Te₃</i>) _{0.25} (<i>Sb₂Te₃</i>) _{0.72} (<i>Sb₂Se₃</i>) _{0.03} , <i>Pb</i> -doped [19] $\sigma_p(300\text{ K}) = 1570 \Omega^{-1}\cdot\text{cm}^{-1}$ $\alpha_p(300\text{ K}) = 175 \mu\text{V/K}$	
	Hot stage	<i>n</i> - $Mg_2(Si_{0.3}-Sn_{0.7})_{1-x}Sb_x$ [7] $x = 0.027$	<i>n</i> - $Mg_2(Si_{0.3}Sn_{0.7})_{1-x}Sb_x$ [7] $x = 0.025$	
		<i>p</i> - $Mn(Al_xSi_{1-x})_{1.80}$ [8] $x = 0.0021$	<i>p</i> - $Mn(Al_xSi_{1-x})_{1.80}$ [8] $x = 0.00203$	
	Cold stage	3		
	Hot stage	3	3	5.6
Number of thermocouples	Cold stage	48		
	Hot stage	48	48	32
Cross-section area of legs, mm ²	Cold stage	1.8 × 4.3		
	Hot stage	1.8 × 4.3	1.8 × 4.3	4 × 4
Temperature between stages, K		518	501	489
Electric power <i>P</i> , W		10.2	11.9	8.9
Efficiency η , %		8.1	10.2	9.4

Application of *Bi-Te* based materials instead of silicides for the low-temperature stage and design optimization can ensure the efficiency of such modules as high as 10 %. It should be stated here that the waste of material for module No. 4 fabrication is 2.5 times less than that for module No. 5, whereas its efficiency and power are higher.

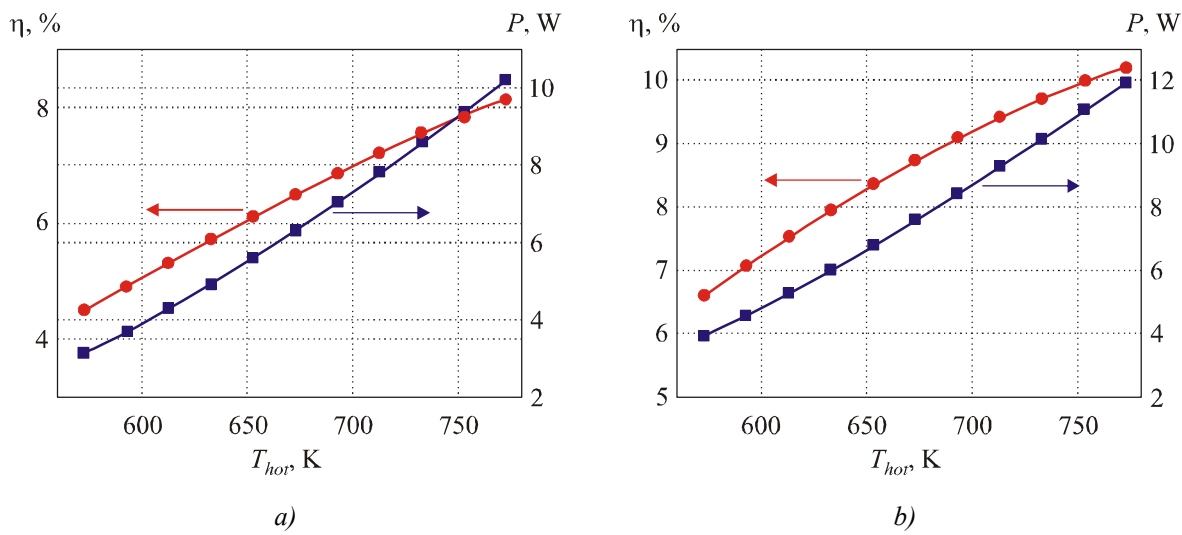


Fig. 2. Efficiency η and electric power P of two-stage modules No. 3 (a) and No. 4 (b)

as a function of module hot side surface temperature T_{hot} .

Module cold side surface temperature $T_c = 323$ K.

The data presented make it evident that, when similar materials are used for stages and segments, the efficiency of two-stage modules does not, actually, exceed the efficiency of modules fabricated from two-segmented legs.

Conclusions

With computer simulation methods implemented, both optimal composition and impurity concentrations in *Mg* and *Mn* silicides have been found that ensure maximum efficiency of the generator modules fabricated from such materials provided the operational temperature difference is from 323 to 773 K.

When two-segmented or FGTM legs are used for *Mg* and *Mn* silicides based modules instead of homogeneous materials, their efficiency can be increased by 1.3 to 1.5 times. Furthermore, if silicides in low-temperature sections of the legs is substituted by bismuth telluride, the efficiency can even reach 10 %.

Research into two-stage structures has shown that the use of *Bi-Te* based materials for the cold stage and magnesium and manganese silicides for the hot stage enables the heat energy conversion within the temperature range from 323 – 773 K with the efficiency of ~ 10 %.

Such values of the generator modules efficiency together with the relatively low cost of silicides allows expanding of both possibilities and spheres of practical application of thermoelectric converters of heat power into electric one.

References

1. T. Kajikawa. Current State of Thermoelectric Power Generation Technology in Japan, *J. Thermoelectricity* **2**, 21-31 (2007).
2. Kh.M. Saqr, M.Kh. Mansour, M.N. Musa. Thermal Design of Automobile Exhaust-Based Thermoelectric Generators: Objectives and Challenges, *J. Thermoelectricity* **1**, 59-66 (2008).
3. C.B. Vining. Thermoelectric properties of Silicides. *CRC Handbook of Thermoelectrics*, edited by D.M. Rowe, 1995, p. 277-285.

4. U. Birkholz, E. Gross, U. Stoehrer. Polycrystalline iron disilicide as a thermoelectric generator material. *CRC Handbook of Thermoelectrics*, edited by D.M. Rowe, 1995, p. 287-298.
5. M.I. Fedorov, V.K. Zaitsev. Silicides. *CRC Thermoelectrics Handbook. Macro to Nano*. Edited by D.M. Rowe, (2006), p. 31-1 – 31-14.
6. Zh. Du, T. Zhu, X. Zhao. Enhanced thermoelectric properties of $Mg_2Si_{0.58}Sn_{0.42}$ compounds by *Bi* doping, *Materials Letters*, **66** (1), (2012). p. 76-78.
7. W. Liu, Q. Zhang, X. Tang, H. Li, J. Sharpet. Thermoelectric Properties of *Sb*-doped $Mg_2Si_{0.3}Sn_{0.7}$, *Journal of Electronic Materials*, **40** (5), (2011), p. 1062-1066.
8. W. Luo, H. Li, F. Fu, W. Hao, X. Tang. Improved Thermoelectric Properties of *Al*-doped Higher Manganese Silicide Prepared by a Rapid Solidification Method, *Journal of Electronic Materials*, **40** (5), (2011), p. 1233-1237.
9. A.J. Zhou, T.J. Zhu, X.B. Zhao, S.H. Yang, T. Dasgupta, C. Stiewe, R. Hassdorf, E. Mueller. Improved Thermoelectric Performance of Higher Manganese Silicides with *Ge* Additions, *Journal of Electronic Materials*, **39** (9), (2010). p. 2002-2007.
10. M.J. Yang, L.M. Zhang, L.Q. Han, Q. Shen, C.B. Wang. Simple fabrication of Mg_2Si thermoelectric generator by spark plasma sintering, *Indian Journal of Engineering and Materials Sciences*, **16**, (2009), p. 277-280.
11. T. Sakamoto, T. Iida, A. Matsumoto, Ya. Honda, T. Nemoto, J. Sato, T. Nakajima, H. Taguchi, Y. Takanashi. Thermoelectric Characteristics of a Commercialized Mg_2Si Source Doped with *Al*, *Bi*, *Ag*, and *Cu*, *Journal of Electronic Materials*, **39** (9), (2010), p. 1708-1713.
12. T. Sakamoto, T. Iida, Sh. Kuroaki, K. Yano, H. Taguchi, K. Nishio, Y. Takanashi. Thermoelectric Behavior of *Sb*- and *Al*-doped *n*-Type Mg_2Si Device Under Large Temperature Differences, *Journal of Electronic Materials*, **40** (5), (2011), p. 629-634.
13. R. Song, Y. Liu, T. Aizawa. Solid State Synthesis and Thermoelectric Properties of *Mg-Si-Ge* System, *Journal of Materials Science & Technology*, **21** (5), (2005), p. 618-622.
14. Q. Zhang, J. He, T.J. Zhu et al. High Figures of Merit and Natural Nanostructures in $Mg_2Si_{0.4}Sn_{0.6}$ Based Thermoelectric Materials, *Applied Physics Letters*, **93**, (2008), 102109. 3 p.
15. J. Zhou, X. Li, G. Chen, R. Yang. Semiclassical Model for Thermoelectric Transport in Nanocomposites, *Physical Review B*, **82**, (2010), 115308. 16 p.
16. J. Tani, H. Kido. Thermoelectric Properties of *Al*-doped $Mg_2Si_{1-x}Sn_x$ ($x \leq 0.1$), *Journal of Alloys and Compounds*, **466**, (2008), p. 335-340.
17. Y.-J. Shi, Q.-M. Lu, X. Zhang, J.-X. Zhang. Microstructure and Thermoelectric Properties of Higher Manganese Silicides, *Journal of Inorganic Materials*, **26** (7), (2011), p. 691-695.
18. L.I. Anatychuk, L.N. Vikhor. *Thermoelectricity, Vol.IV, Functionally Graded Thermoelectric Materials* (Chernivtsi: Bukrek, 2012), 180 p.
19. L.N. Vikhor, L.I. Anatychuk. Generator modules of segmented thermoelements, *Energy Conversion and Management*, **50**, (2009), p. 2366-2372.
20. L.N. Vikhor. Computer-aided design of thermoelectric generator modules, *J. Thermoelectricity* **2**, (2005), p. 60-67.

Submitted 18.01.2013.

L.I. Anatychuk, R.V. Kuz, A.V. Prybyla

Institute of Thermoelectricity of NAS and MESYS of Ukraine,
1, Nauky Str., Chernivtsi, 58029, Ukraine;
Yu. Fedkovych Chernivtsi National University, 2, Kotsyubinsky Str.,
Chernivtsi, 58012, Ukraine

**THE EFFECT OF HEAT EXCHANGE SYSTEM
ON THE EFFICIENCY
OF THERMOELECTRIC AIR CONDITIONER**

Results of calculation of the efficiency of thermoelectric air conditioner with regard to the effect of heat exchange system are presented. Optimal operating conditions of heat exchange system for achieving the highest air conditioner efficiency are determined.

Key words: air conditioner, heat exchange, thermoelectricity.

Introduction

General characterization of the problem. Efficiency enhancement of thermoelectric air conditioners [1] in the majority of cases comes down to increase in the figure of merit [2] of thermoelectric materials. However, their efficiency to no small degree depends on the heat exchange devices and systems used to transfer thermal energy through thermoelectric power converters (the so-called heat pumps). Preliminary analysis shows that the real efficiency values of thermoelectric air conditioners are much lower than the expected ones even at the achieved values of material figure of merit. It is due to the fact that in the design and optimization of thermoelectric equipment use is mostly made of simplified physical models [3-6] that do not take into account the quality of heat exchange systems, the thermal and electric losses that may deteriorate considerably the energy characteristics of thermoelectric air conditioner. In Ref. [7], a procedure for calculation of thermoelectric air conditioner efficiency for generalized physical models of thermoelectric power converters is discussed.

The purpose of this work is to analyze the effect of real heat exchange system on the efficiency of thermoelectric air conditioner and to optimize its operation. For this purpose, multi-parameter computer optimization of thermoelectric air conditioner efficiency was carried out with regard to the experimentally determined characteristics of heat exchange system.

1. Physical model of thermoelectric air conditioner

A physical model of thermoelectric air conditioner is shown in Fig. 1. Closed space 1 is cooled by thermoelectric cooling modules 7. Heat abstraction system is composed of the cold and hot loops 5, 10. The cold loop comprises a liquid-air heat exchanger 3 with a fan 2, a liquid pump 4 and a liquid heat exchanger 6. The cold loop assures heat abstraction from cooling chamber 1 to thermoelectric modules. The hot loop comprises a liquid heat exchanger 8, a liquid pump 9 and a liquid-air heat exchanger 11 with a fan 12. The hot loop assures heat abstraction from thermoelectric modules to the

environment. The electric energy consumers in the physical model are thermoelectric modules of electric power W_m , fans of liquid-air heat exchangers of electric power W_{v1} and W_{v2} , and liquid pumps of electric power W_{n1} and W_{n2} for the cold and hot loops, respectively.

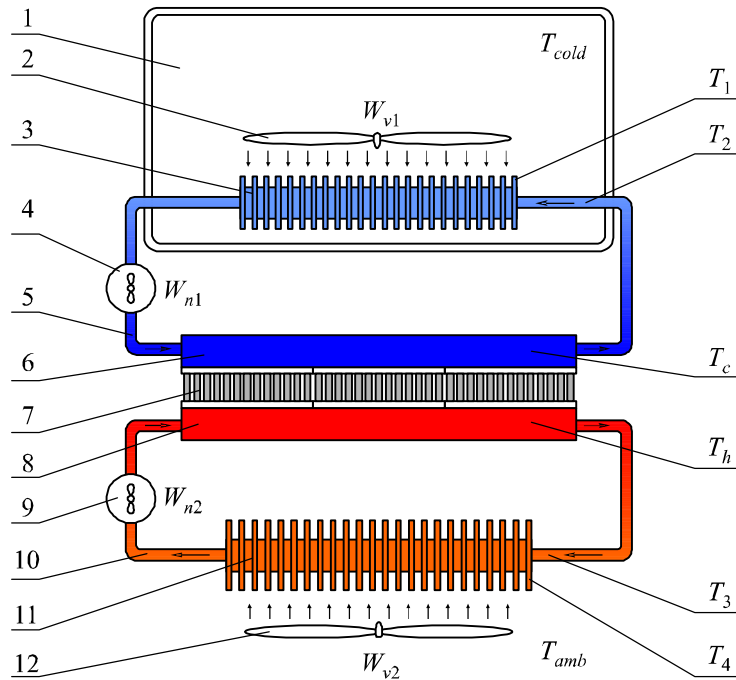


Fig. 1. Physical model of thermoelectric heat pump: 1 – cooling chamber; 2, 12 – fans; 3, 11 – liquid-air heat exchangers; 4, 9 – liquid pumps, 5, 10 – liquid loops; 6, 8 – liquid heat exchangers, 7 – thermoelectric cooling modules.

2. Thermoelectric air conditioner efficiency

The air conditioning system is characterized by such parameters as cooling capacity Q_0 , that is, the amount of heat abstracted from cooling chamber (it is a function of temperature difference on thermoelectric modules, heat leak-in through air-conditioner chamber insulation from the ambient and the quality of heat exchange system), as well as coefficient of performance ε which is a ratio between cooling capacity Q_0 and electric energy spent on supply of thermoelectric modules, fans and liquid pumps. It is obvious that the real-life coefficient of performance of thermoelectric air conditioner will be much different from the coefficient of performance of thermoelectric modules. In so doing, it will depend on the electric power values of all system consumers:

$$\varepsilon(W_{n1}, W_{n2}, W_{v1}, W_{v2}, W_m, N) = \frac{Q_0}{W_{n1} + W_{n2} + W_{v1} + W_{v2} + W_m} \quad (1)$$

where N is the number of thermoelectric modules.

Thus, to achieve maximum coefficient of performance of thermoelectric air conditioner, one should find the optimal operating conditions for each of heat exchange system components. For this purpose, in the present paper we employ the experimental dependences of parameters of heat exchange system components on their electric power consumption and seek the multi-parameter maximum of coefficient of performance using numerical methods.

2.1. Thermal and energy balance equations

The air conditioner thermal balance equations may be written as:

$$\begin{cases} Q_{r1} = Q_{TEB} \\ Q_{r2} = Q_{TEB} + W_0 \end{cases} \quad (2)$$

where Q_{r1} is heat which is absorbed on liquid-air heat exchanger of the cold loop. It defines air-conditioner cooling capacity Q_0 and corresponds to heat which is absorbed on the cold side of thermopile, Q_{r2} is heat which is dissipated on liquid-air heat exchanger of the hot loop. It corresponds to heat which is released on the hot side of thermopile, Q_{TEB} is thermopile cooling capacity, W_0 is thermopile supply power.

The balance of temperatures is given by:

$$T_{amb} = T_{cold} - \Delta T_{r1} - \Delta T_{t1} + \Delta T_{TEB} - \Delta T_{t2} - \Delta T_{r2} \quad (3)$$

where T_{amb} is ambient temperature, T_{cold} is designed temperature in the isolated chamber, $\Delta T_{r1} = T_{cold} - T_1$ is temperature drop on the liquid-air heat exchanger of the cold loop, $\Delta T_{t1} = T_2 - T_c$ is temperature drop on the liquid heat exchanger of the cold loop, $\Delta T_{TEB} = T_h - T_c$ is temperature drop on the thermopile, $\Delta T_{t2} = T_h - T_3$ is temperature drop on the liquid heat exchanger of the hot loop, $\Delta T_{r2} = T_3 - T_{amb}$ is temperature drop on the liquid-air heat exchanger of the hot loop.

Let us introduce the following functional dependences of air conditioner component characteristics.

$Q_m(W_m, \Delta T, T_h)$ is cooling capacity of thermoelectric modules as a function of the electric power of modules, temperature drop on the modules, and the hot side temperature of modules;

$G(W_n, N)$ liquid flow rate in the heat-exchange loop as a function of pump supply power and the number of thermoelectric modules;

$Q_r(W_n, W_v, \Delta T_r, N) = F_r(W_n, W_v, N) \cdot \Delta T_r$ is thermal power which is transferred by liquid-air heat exchanger as a function of liquid pump and fan supply powers and the difference in temperature between the air and liquid at the heat exchanger inlet;

$Q_t(\Delta T_t, W_n, N) = F_t(W_n, N) \cdot \Delta T_t$ is thermal power which is transferred by liquid heat exchanger as a function of temperature difference between thermoelectric module surface and liquid at the heat exchanger inlet, liquid pump and fan supply powers and temperature difference between the air and liquid at the heat exchanger inlet.

Based on this, the following relations will be obtained to find temperature drops listed in (3):

$$Q_{r1} = F_r(W_{n1}, W_{v1}, N) \cdot \Delta T_{r1} = Q_0 \quad (4)$$

$$Q_{r2} = F_r(W_{n2}, W_{v2}, N) \cdot \Delta T_{r2} = Q_0 + W_0 \quad (5)$$

$$Q_{t1} = F_t(W_{n1}, N) \cdot \Delta T_{t1} = Q_0 \quad (6)$$

$$Q_{t2} = F_t(W_{n2}, N) \cdot \Delta T_{t2} = Q_0 + W_0 \quad (7)$$

The air conditioner cooling capacity will be found from equation (8)

$$Q_0 = Q_{TEB}(W_0, \Delta T_{TEB}, T_h) \quad (8)$$

The expression for temperature drop on thermopile ΔT_{TEB} will be obtained by substituting (4) – (7) into (2):

$$\begin{aligned}\Delta T_{\text{TEB}} = & T_{\text{amb}} - T_{\text{cold}} + Q_0 \left(\frac{1}{F_r(W_{n_1}, W_{v1}, N)} + \frac{1}{F_t(W_{n1}, N)} \right) + \\ & + (Q_0 + W_0) \left(\frac{1}{F_r(W_{n_2}, W_{v2}, N)} + \frac{1}{F_t(W_{n2}, N)} \right).\end{aligned}\quad (9)$$

The expression for T_h will be obtained from the equation

$$T_h = T_{\text{amb}} + \Delta T_{r2} + \Delta T_{t2}. \quad (10)$$

Substituting (4) and (6) into (10), we obtain:

$$T_h = T_{\text{amb}} + (Q_0 + W_0) \left(\frac{1}{F_r(W_{n_2}, W_{v2}, N)} + \frac{1}{F_t(W_{n2}, N)} \right). \quad (11)$$

The expressions (8), (9) and (11) form a system of equations to find the air conditioner cooling capacity Q_0 which is solved with respect to Q_0 , ΔT_{TEB} , T_h for given T_{amb} , T_{cold} values and $F_r(W_n, W_v, N)$, $F_t(W_n, N)$ and $Q_{\text{TEB}}(W_0, \Delta T_{\text{TEB}}, T_h)$ functions.

The air conditioner coefficient of performance is found from (1). The objective function of optimization will be air conditioner coefficient of performance, and optimization parameters – the electric powers of air conditioner components.

2.2. Optimization methods

The above described awkward and complicated optimum criteria motivate the use of numerical methods of seeking the optimal value of objective function.

The objective function of thermoelectric air conditioner – coefficient of performance – is a nonlinear function that depends on the combination of parameters which, in turn, are expressed implicitly, using a plurality of empirical equalities. So, it is impossible to use the methods of search for the first and second-order extremes (due to the impossibility of finding the derivatives). A search for the optimal coefficient of performance value employed gradient-free zero-order method – a modified Hook-Jeeves method [8].

At each iteration step of the main program cycle, a system of nonlinear equations (8 – 11) is solved and cooling capacity is found. Coefficients of approximating polynomials that are used to determine the empirical relations between the physical parameters of optimization program are calculated.

3. Thermoelectric air conditioner optimization

3.1. Empirical functions of parameters of thermoelectric air conditioner components

Thermoelectric modules. Based on the experimental investigations of the dependence of cooling capacity of thermoelectric cooling module Altec-127 on the supply power and the hot and cold heat exchanger temperatures, in the numerical calculations the function of module heat capacity Q_m was approximated by the analytical dependences:

$$\begin{aligned}Q_m(W_m, \Delta T, T_h) = & \left[F_m(W_m) (1 - 0.0015 \Delta T) - (1.334 - 0.00233 T_h) \Delta T \right] \times \\ & \times (0.07217 + 0.00317 T_h),\end{aligned}\quad (12)$$

where

$$F_m = \left(8.45 \sqrt{W_m - 0.115} - 0.37 W_m + 3.25 \right). \quad (13)$$

Liquid pumps. Dependence of liquid flow rate in heat exchange loop on the pump power and the number of modules was found as follows:

$$G(W_n, N) = \frac{\Delta P_{\max}(W_n)}{r_g + NR_g^t}, \quad (14)$$

where $\Delta P_{\max}(W_n)$ is dependence of maximum pump pressure on its power, R_g^t is hydraulic resistance of liquid heat exchanger, r_g is hydraulic resistance of heat exchange loop without heat exchangers.

From the experiments with the liquid pump the following dependences were established:

$$\Delta P_{\max}(W_n) = 0.01283W_n \text{ (atm)}, \quad (15)$$

$$G(W_n, N) = \frac{0.01283W_n}{6.31 \cdot 10^{-4} + N \cdot 1.835 \cdot 10^{-3}} \text{ (ml/s)}. \quad (16)$$

Liquid-air heat exchangers. Experimental studies were used to establish the values of power that can be transferred from liquid to air depending on the difference in temperature between water at heat exchanger inlet and air, liquid losses in heat exchange loop and fan supply power $Q_r(\Delta T_r, G, W_v)$. Taking into account that $G = G(W_n, N)$, and $Q_r \sim \Delta T_r$, the value Q_r was obtained as follows:

$$Q_r(W_n, W_v, \Delta T, N) = F_r(W_n, W_v, N) \cdot \Delta T_r, \quad (17)$$

where $F_r(W_n, W_v, N)$ is experimental function which characterizes the heat exchanger.

For the heat exchanger under study function F_r was approximated as follows:

$$F_r(W_n, W_v, N) = \left[15.5783 + 0.3402G(W_n, N) - 0.0018G(W_n, N)^2 \right] \times \\ \times \left[0.15 + 0.14125W_v - 0.00437W_v^2 \right]. \quad (18)$$

Liquid heat exchangers. Dependence of liquid heat exchanger power $Q_t(\Delta T_t, G)$ on the difference in temperature between water at heat exchanger inlet and heat exchanger surface, and on water flow rate in the heat exchange loop was experimentally determined. Taking into account that $G = G(W_n, N)$ and $Q_t \sim \Delta T_t$ dependence Q_t will be sought as follows:

$$Q_t(\Delta T_t, W_n, N) = F_t(W_n, N) \cdot \Delta T_t, \quad (19)$$

where $F_t(W_n, N)$ is experimental function characterizing the heat exchanger. For the heat exchanger under study function F_t was approximated as:

$$F_t(W_n, N) = N \left[2.5349 + 0.08292G(W_n, N) - 3.02648 \cdot 10^{-4} G(W_n, N)^2 \right]. \quad (20)$$

3.2. Results of thermoelectric air conditioner optimization

As a result of thermoelectric air conditioner optimization, the operating conditions of air conditioner components were found whereby its coefficient of performance has a maximum.

Using the algorithms and program described in paragraph 2, the coefficient of performance of air conditioner ε_0 was calculated for the following input parameters of the problem:

ambient temperature $T_{amb} = 20, 25, 30, 35, 40 \text{ }^{\circ}\text{C}$,

reduction of temperature in the chamber $\Delta T = T_{amb} - T_{cold} = 10, 15, 20 \text{ }^{\circ}\text{C}$.

In Tables 1 – 3 are listed the results of calculation of maximum coefficient of performance ε_{\max} of air conditioner and its cooling capacity depending on the number of thermoelectric modules N .

Besides, in the Tables are listed the supply power values of air conditioner systems whereby coefficient of performance has a maximum.

Table 1

*Maximum coefficient of performance of air conditioner
at $T_{amb} = 20^{\circ}C$, $\Delta T = 10^{\circ}C$*

N	ε_{max}	Q_0 , W	W_0 , W	W_{n1} , W	W_{v1} , W	W_{n2} , W	W_{v2} , W
2	0.519	24.38	21	5	8	5	8
4	0.628	32.01	25	5	8	5	8
6	0.667	36.01	28	5	8	5	8
8	0.676	38.58	31	5	8	5	8.1
10	0.668	41.86	35	5	8.5	5	9.5
20	0.587	41.36	48	5	10	5	12

Table 2

*Maximum coefficient of performance of air conditioner
at $T_{amb} = 20^{\circ}C$, $\Delta T = 15^{\circ}C$*

N	ε_{max}	Q_0 , W	W_0 , W	W_{n1} , W	W_{v1} , W	W_{n2} , W	W_{v2} , W
2	0.422	22.34	27	5	8	5	8
4	0.475	29.92	35	5	8	5	8
6	0.481	32.68	42	5	8	5	8
8	0.468	36.94	50	5	8	7	11
10	0.448	40.06	58	5	9.5	9	12
20	0.331	40.99	87	5	11	21	12

Table 3

*Maximum coefficient of performance of air conditioner
at $T_{amb} = 20^{\circ}C$, $\Delta T = 20^{\circ}C$*

N	ε_{max}	Q_0 , W	W_0 , W	W_{n1} , W	W_{v1} , W	W_{n2} , W	W_{v2} , W
2	0.334	20.03	34	5	8	5	8
4	0.353	28.70	51	5	8	8	9.5
6	0.340	38.48	75	5	8	16	10
8	0.320	43.0	87	5	9	22	12
10	0.26	40.2	124	5.6	10.5	25	12
20	0.18	39.3	162	6	12	28	12

Fig. 2 gives a comparison of the coefficient of performance of thermoelectric modules and air conditioner under other optimal operating conditions of thermoelectric air conditioner components.

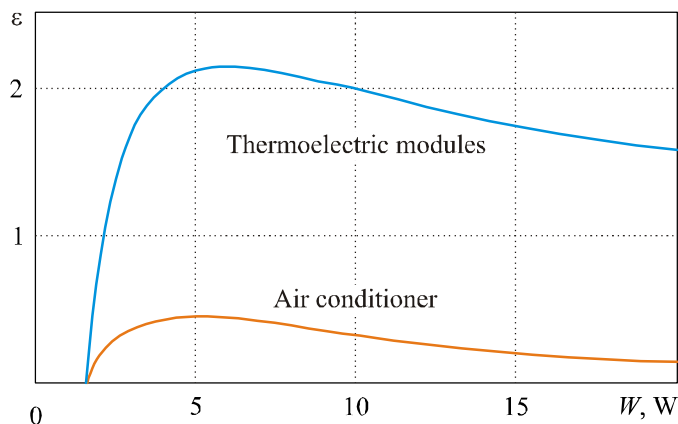


Fig. 2. Dependences of coefficient of performance of thermoelectric modules and thermoelectric air conditioner on the supply power of thermoelectric modules $T_{amb} = 20^{\circ}\text{C}$, $\Delta T = 15^{\circ}\text{C}$.

Conclusions

1. The physical and mathematical models, the algorithms and computer program of search for multi-parameter maximum of coefficient of performance of thermoelectric air conditioner have been developed.
2. For the specific designs of thermoelectric air conditioner, multi-parameter maxima of coefficient of performance have been found in the operating power ranges of thermopile, liquid pumps and air fans for specified cooling depth.
3. It has been established that even under the optimal operating conditions of air conditioner components the coefficient of performance of thermoelectric air conditioner differs by a factor of ~ 7 from that of thermoelectric modules. This testifies to the necessity of improving the components of heat exchange systems of thermoelectric air conditioner.

References

1. L.I. Anatychuk, *Thermoelectricity. Volume 1. Thermoelectric Power Converters* (Kyiv, Chernivtsi: Institute of Thermoelectricity, 2003), 376 p.
2. L.I. Anatychuk, Current Status and Some Prospects of Thermoelectricity, *J.Thermoelectricity* 2, 7-20 (2007).
3. L.I. Anatychuk, K. Misawa, N. Suzuki, Ya. Takai, Yu.Yu. Rozver, Thermoelectric Air Conditioner for Rooms, *J.Thermoelectricity* 1, 53-56 (2003).
4. Yu.Yu. Rozver, Thermoelectric Air Conditioner for Vehicles, *J.Thermoelectricity* 2, 70-72 (2003).
5. <http://www.fujitaka.com>
6. <http://www.hi-z.com>
7. L.I. Anatychuk, A.V. Prybyla, The Effect of Heat-Exchange Systems on the Efficiency of Thermoelectric Devices, *J.Thermoelectricity*, 3, 39-43 (2012)
8. V.M. Verzhbitsky, *Numerical Methods (Linear Algebra and Nonlinear Equations): Manual for Higher Education Institutions* (Moscow: “ONIX 21 Century” Publishing House, 2005), 432 p.

Submitted 19.12.2012.

V.S. Gischuk



V.S. Gischuk

Institute of Thermoelectricity NAS and MESYS
of Ukraine, 1, Nauky Str., Chernivtsi,
58029 Ukraine

**ELECTRONIC RECORDER WITH PROCESSING
SIGNALS FROM HEAT FLUX
THERMOELECTRIC SENSOR**

This paper presents the results of electronic recorder development with processing signals from thermoelectric sensor intended for contact measurement of human heat flux density and temperature. Its structural features, technical characteristics and functional block-diagram are shown.

Key words: electronic recorder, thermoelectric sensor, heat flux.

Introduction

General characterization of the problem. Thermoelectric sensors are becoming more common in various branches of medicine. A factor of importance in the investigation of human heat fluxes using such sensors is the accuracy and speed of recording signals from thermoelectric sensors.

Analysis of the literature. The need in high accuracy and speed of heat flux measurements leads to complication of electric circuits and enlargement of devices for recording signals from thermoelectric sensors. The existing devices of this type [1-4] have a relatively high measurement error, large dimensions and a low speed and are incapable of measurement time control. The main disadvantage of these devices is the absence of internal memory for storing measurement results and a demand for external power supply. Therefore, it is of current concern to develop a self-contained electronic recorder characterized by improved accuracy of measuring signals from heat flux thermoelectric sensor and high speed of processing and storing the measured data

The purpose of this work is to develop an electronic recorder with processing of signals from thermoelectric sensor that assures simultaneous measurement of human heat flux and temperature and recording their values in time.

Electronic recorder design and technical characteristics

At the Institute of Thermoelectricity NAS and MESYS of Ukraine an electronic recorder with processing signals from heat flux thermoelectric sensor has been developed (Fig. 1).

Device block-diagram (Fig. 2) consists of the following functional assemblies: thermoelectric sensor with a built-in thermocouple for measuring human heat flux and temperature, thermocouple signal amplifier with ambient temperature compensator, analog-to-digital converters for conversion of analog sensor signals into digital ones, digital signal processing unit for storing and graphic reproduction of data on the display.



Fig. 1. Electronic recorder with processing signals from heat flux thermoelectric sensor:
1 – electronic recorder; 2 – thermoelectric sensor.

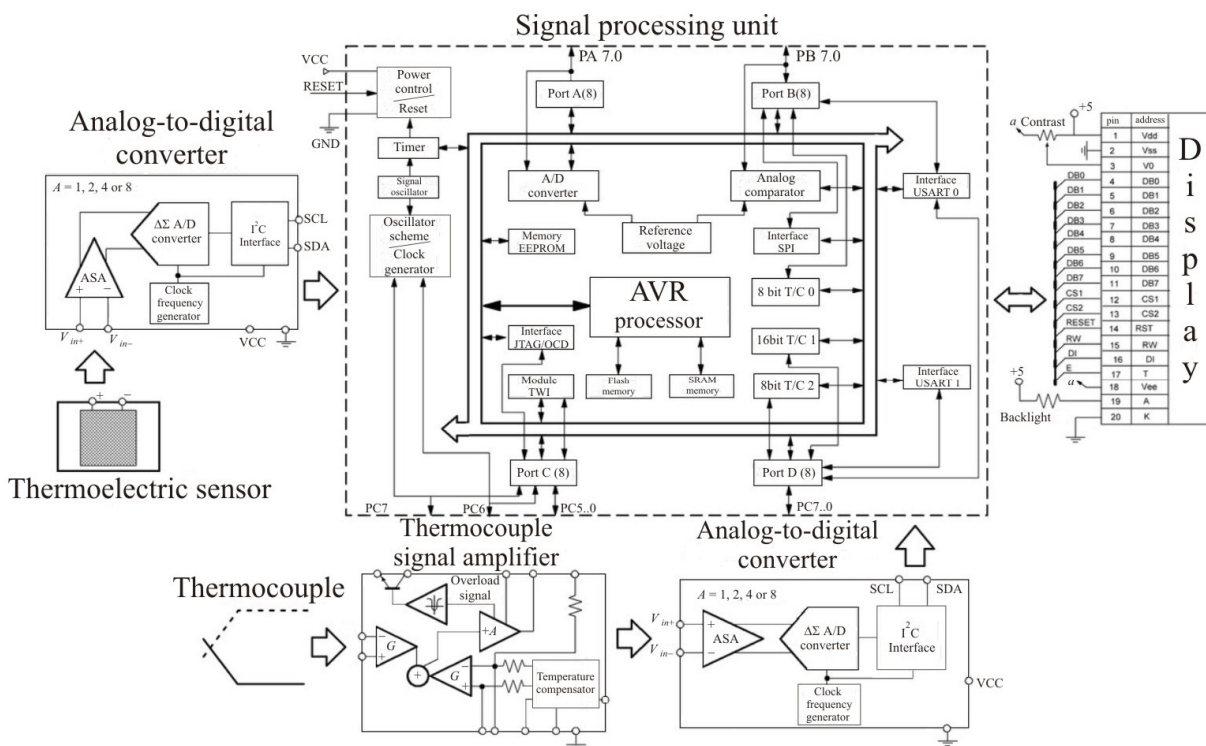


Fig. 2. Device block-diagram.

The main functional assembly of signal processing unit is a microcontroller [5] operating at a frequency up to 20 MHz which assures high processing rate of signals from thermoelectric heat flux sensor and comprises 32 Kb of internal memory. Personal computer is used to program the microcontroller which, in turn, controls the work of other functional assemblies of the block-diagram, information display and read-in

The left sidewall of the device has a socket for connection of heat flux thermoelectric sensor, a switch button and a socket for battery recharging. Thermoelectric sensor is connected to electronic recorder with the aid of a mini USB-connector. This allows replacing thermoelectric sensors in case of their failure and using sensors of varying configuration and geometry, which makes this device more convenient in operation.

Mounted on the front wall of the case is a liquid-crystal monochrome display with a resolution of 128×64 pixels. One pixel of display screen is matched by 5 mV of thermoelectric sensor

electromotive force. The display shows plotted values of the heat flux of respective human body area in millivolts (mV) and temperature values in centigrade ($^{\circ}\text{C}$). Thus, previous measurement data can be analyzed directly from the plot shown on the display.

Device power supply is from lithium-ion battery of capacity 1000 mA/h assuring 10 hours of uninterrupted device work. Device supply voltage is 3.3 V, current consumption is 100 mA, the accuracy of measuring human body temperature is $\pm 0.1\ ^{\circ}\text{C}$, the accuracy of measuring the thermoelectric sensor electromotive force is 2 – 3 mV. The overall dimensions of the electronic recorder are $90 \times 58 \times 24$ mm and the device weight is 0.15 kg.

Conclusions

1. An electronic recorder of signals has been developed that enables simultaneous determination of temperature and heat fluxes with recording their values in time over the course of 10 hours. The device assures visualization of signals in the form of time-dependent plots. Information transfer to personal computer for its subsequent processing according to the assigned algorithm is provided.
2. The device allows identifying the peculiarities of heat release on human skin surface for a correlation with human state.

The Author is sincerely grateful to academician L.I. Anatychuk for the proposed paper topic and the help during its execution.

References

1. L.I. Anatychuk, *Thermoelements and Thermoelectric Devices. Handbook* (Kyiv: Naukova Dumka, 1979), 766 p.
2. L.I. Anatychuk, N.G. Lozinsky, P.D. Mykytyuk, Yu.Yu. Rozver, Thermoelectric Semiconductor Heat Meter, *Pribory i Tekhnika Eksperimenta* **5**, 236 (1983).
3. A.A. Ascheulov, L.Ya. Kushneryk, Thermoelectric Device for Medico-Biological Express Diagnostics, *Tekhnologiya i Konstruirovaniye v Elektronnoi Apparature* **4**, 38-39 (2004).
4. L.K. Holtermann, Patent US 4198859, Heat flow probe, 1980.
5. A.V. Yevstifeyev, *ATMEL AVR Microcontrollers of Tiny and Mega Families, 5-th ed.* (Moscow: "Dodeka XXI" Publishing House, 2008), 430 p.

Submitted 28.12.2012.

NEWS

INTERNATIONAL THERMOELECTRIC ACADEMY

KIN-ICHI UEMURA

(Dedicated to the 90-th anniversary)



February 6, 2013 is the day of the 90th anniversary of Kin-ichi Uemura, academician of International Thermoelectric Academy, Doctor of Technical Sciences, a director of Institute for Thermoelectric Technologies Japan.

Kin-ichi Uemura was born in Saga prefecture Japan. He graduated as a Bachelor of Technical Sciences from Faculty of Engineering, Tokyo University (1946). The scientific interests of Kin-ichi Uemura cover a wide scope of relevant problems of modern thermoelectricity.

Since 1956 Uemura's professional activity has been inseparable related to thermoelectricity. He has studied the electrophysical properties of thermoelectric semiconductor materials, heat exchange processes, developed thermoelectric modules and devices on their basis in Thermoelectric Research Laboratory of Engineering Division, Komatsu Co. Ltd.

Kin-ichi Uemura has been in charge of scientific and development projects on thermoelectric cooling. Their subject matter: technology for production of superpure *Bi*, *Te*, *Sb* and other source materials; increase of thermoelectric figure of merit of materials based on bismuth telluride; methods for fabrication of thermoelectric modules for coolers and air-conditioners, including high-current ($I_{max} = \sim 30$ A) thermoelectric modules without ceramic substrates.

These studies formed the basis for his doctoral thesis brilliantly maintained in Tokyo University in 1961, and successful completion of the projects served the basis for creation in 1960 of a subsidiary company Komatsu Electronics Inc., the thermoelectric department of which was headed by Kin-ichi Uemura in 1960 – 1988, who was responsible for the thermoelectric activity of the company.

The scientist's high international prestige, his remarkable organizing talent, commercial success of his developments resulted in creation in 1990 of Institute for Thermoelectric Technologies Japan (ITTJ) of which Kin-ichi Uemura became a director.

Kin-ichi Uemura successfully combines scientific and production, administrative and social activities. He was organizer of the 12-th International Conference on Thermoelectrics (ICT93) and International Short Course on Thermoelectrics (SCT93) in Yokogama, Japan. In 1993 – 1996 he performed duties of a member of the Board of the International Thermoelectric Society. In 1994 Kin-ichi Uemura was elected academician and Vice-President of International Thermoelectric Academy (ITA). He is editorial board member and distributor of "Journal of Thermoelectricity". In 2002 Honorable Golden Prize of International Thermoelectric Academy was awarded to him for the fundamental contribution to development of thermoelectricity. Now Kin-ichi Uemura is at a well-deserved rest.

International Thermoelectric Academy, Institute of Thermoelectricity of the National Academy of Sciences and Ministry of Education and Science, Youth and Sports of Ukraine congratulate the esteemed Kin-ichi Uemura on his 90th jubilee, wishing him success in his multifarious activity, good health and longevity.



GIORGIO PASTORINO

(Dedicated to the 75-th anniversary)

Giorgio Pastorino, Italian scientist, corresponding member of International Thermoelectric Academy, president of company PELTECH srl, Bachelor in Mechanical Engineering, celebrates his 75-th anniversary.

The main lines of his research and developments are related to looking for the opportunities to realize a new concept of thermoelectric assemblies based on the “platform” concept.

“Platform” concept means:

- cost effective solutions;
- quick response to new requirements;
- certainty about performance.

Investigations performed by Giorgio Pastorino allowed finding an ingenious approach to the design of thermoelectric devices (a modular architecture made of a set of basic components with general interface definitions, using identical thermoelectric coupling methods, guided by the constraints of geometry and general assembly methods). Modular components, designed in a special way, are part of the platform’s basic set of parts, including the installed commercial components that are individually characterized with respect to constraints of platform structure. A proprietary mathematical model for predicting performance of any platform assembly has been developed and is maintained together with a database on the platform components’ parameters, properties and costs, thus permitting to conceive new solutions for any special basic operating characteristics with a precise and reliable prediction of parameters and manufacturing cost. Moreover, prototyping a new custom solution corresponds to sampling a new combination of well known elements with the generally known platform architecture, setting the premises for the shortest time-to-market for any solution.

The scientific and development pursuits of Giorgio Pastorino were highly commended at the International exhibition in Italy, 2006. He picked up Dame Design Award Metz (category “Winner”).

Giorgio Pastorino is one of the main organizers of International Workshop on July 14, 2005 in Como in honor of pioneer in thermoelectricity Alessandro Volta.

International Thermoelectric Academy, Institute of Thermoelectricity of the National Academy of Sciences and Ministry of Education and Science, Youth and Sports of Ukraine, “Journal of Thermoelectricity” Publishers congratulate the esteemed Giorgio Pastorino on his glorious jubilee, wishing him good health, creative success and happy longevity.

VOLODYMYR OLEKSIYOVYCH SEMENYUK

(Dedicated to the 75-th anniversary)

On February 3 this year Volodymyr Oleksiyovych Semenyuk, a well-known scientist in thermoelectricity, academician of International Thermoelectric Academy, celebrated his 75th birthday.

In 1960 he graduated from Odessa State Academy of Refrigeration. For many years the scientific and pedagogical activity of Volodymyr Oleksiyovych has been related to this academic and research institution.



The research interests of V.O. Semenyuk were formed immediately under the influence of the founder of scientific school in the field of power engineering and refrigeration technology, professor V.S. Martynovsky, the scientists in thermoelectricity A.F. Ioffe, L.S. Stilbance, E.K. Iordanishvili and others.

Volodymyr Oleksiyovych made a major contribution to study of nonequilibrium thermodynamics and physics of thermoelectric effects. He was the first to solve a variety of variational problems as applied to thermoelectricity which made the basis for creation of modern computer methods for design of thermoelectric instruments and devices.

The scientist has solved a series of important engineering problems of thermoelectricity, in particular, the problems of heat exchange in thermoelectric devices, efficiency increase of multi-stage coolers, the problems of using the bulk thermoelectric cooling elements with programmed inhomogeneous legs. He studied and successfully solved contact problems in thermoelectric coolers, which allowed creating efficient microminiaturization technologies of thermoelectric devices. The theory and practice of thermoelectric instrument making was developed, the parametric series of thermoelectric micromodules were created which defy competition on global markets. In the development of some thermoelectric projects V.O. Semenyuk successfully cooperated with many scientific centers in the USA and Western Europe.

V.O. Semenyuk is the author of over 100 scientific works, certificates of authorship and patents, notably a monograph (in co-authorship with academician L.I. Anatychuk) "Optimal Control over the Properties of Thermoelectric Materials and Devices". In 2006 and 2012 the results of his research in the theory and practice of thermoelectric instrument making were included as chapters into international handbooks "Thermoelectrics Handbook: Macro to Nano" and "Thermoelectrics and its Energy Harvesting"

Volodymyr Oleksiyovych gives special attention to training high-skilled scientific brainpower. He is an outstanding lector whose reports to scientific conferences and international forums arouse much interest and admiration among the attendees.

In recognition of the international level of his scientific achievements, V.O. Semenyuk was elected in 1995 full member of the International Thermoelectric Academy. V.O. Semenyuk is a member of the International and European Thermoelectric Societies, a member of American Institute of Aeronautics and Astronautics, a member of the Board of Directors of the European Thermoelectric Society.

International Thermoelectric Academy, Institute of Thermoelectricity of the National Academy of Sciences and Ministry of Education and Science, Youth and Sports of Ukraine, "Journal of Thermoelectricity" Publishers sincerely congratulate the esteemed Volodymyr Oleksiyovych on his glorious 75th jubilee, wishing him good health and happy longevity!



STEPAN VASYLYOVYCH MELNYCHUK

(Dedicated to the 65-th anniversary)

On January 14, 2013 the scientific community celebrated the 65th anniversary of Stepan Vasylyovych Melnychuk, Doctor of Science in Physics and Mathematics, professor, academician of International Thermoelectric Academy, Laureate of State Prize of Ukraine in Science and Technology, rector of Yuri Fedkovych Chernivtsi National University.

Stepan Vasylyovych Melnychuk was born in the village of Toporivtsi, Novoselytsia district, Chernivtsi region.

He graduated with distinction from Physics Faculty and the postgraduate course of Theoretical Physics Department of Chernivtsi National University.

Stepan Melnychuk started his career in 1973 in the capacity of an engineer, and then a junior research fellow of Chernivtsi Division of Institute of Semiconductors NAS Ukraine. Two years later he maintained his PhD Thesis ("Research on Impurity States in Excitonic Insulator").

Since 1976 he worked as a senior lecturer, and then associate professor of Theoretical Physics Department; having maintained DSc Thesis ("Localized States in Electron and Vibration Spectra of $A^{II}B^{VI}$ Semiconductors Doped with 3d-Elements") – as a professor of this department.

In 2001 S.V. Melnychuk was appointed a pro-rector of research, and in 2004 – the first pro-rector of Chernivtsi National University. In March 2005 poky Stepan Vasylyovych was elected rector of Yuri Fedkovych Chernivtsi National University.

Of high priority in the multifarious activity of the university leader is his fruitful research, pedagogical and public work. He is head of Computer Systems and Networks Department of Computer Sciences Faculty, delivers lecture courses to students, supervises the work of postgraduates. Under his guidance, 11 PhD Theses and 1 Doctoral Thesis have been maintained.

Professor S.V. Melnychuk is the author and co-author of over 160 scientific works, notably a monograph, a textbook and several manuals for students and two secondary school books.

The scope of professor's research interests covers the problems of mathematical simulation of physical characteristics of semiconductor materials and structures used for elements and devices of computer electronic, including infrared technique, which is reflected in the monograph (in co-authorship) "Cadmium Telluride: Impurity-Defect States and Detector Properties" (2000).

S.V. Melnychuk is Excellent Worker of National Education, Honoured Worker of Science and Technology of Ukraine.

Professor S.V. Melnychuk was honored with a distinguished title of Laureate of State Prize of Ukraine in Science and Technology (2007).

By Decree of the President of Ukraine for considerable personal contribution to development of national education, many years of fruitful scientific and pedagogical activity Stepan Vasylyovych Melnychuk was awarded with Third Class Order of Merit (2008).

International Thermoelectric Academy, Institute of Thermoelectricity of the National Academy of Sciences and Ministry of Education and Science, Youth and Sports of Ukraine, "Journal of Thermoelectricity" founders and its editorial board cordially congratulate the esteemed Stepan Vasylyovych on his glorious 65th jubilee, wishing him sound health and creative inspiration for may years to come!

TITO HUBER

(Dedicated to the 65-th anniversary)



2013 is a jubilee year for a well-known physical scientist, corresponding member of International Thermoelectric Academy, Doctor of Science, Professor of Howard University Tito Huber.

The scientific and pedagogical activity of Tito Huber is related to many educational and research institutions where he occupied different positions: Instructor, the National University of Comahue, Argentine (1973-1976), Research Assistant, Brown University (1976-1983), Assistant Professor of Physics, University of Puerto-Rico (1983-1991), Associate Professor of Physics, Polytechnic University, Brooklyn, New-York (1991-1998), Professor of Howard University (2000).

The main lines of research and developments of Prof. Tito Huber:

- thermoelectric microgenerators and microthermocouples;
- materials based on bismuth nanowires;
- nanocomposite synthesis;
- thermal resistance across interfaces;
- optical nanocomposites; experimental study of the optical properties of metal and semiconductor nanocomposites;
- nanocomposites synthesized by high pressure injection of porous dielectrics as optical materials;
- optical properties of scattered hydrogen: porous materials and inclusions;
- semiconductor nanowire composites for thermoelectricity;
- scanning force microscopy on the nanostructured conducting composites and polymer materials;
- synthesis, processing and characteristics of bismuth based wires;
- compact thermomagnetic cryocooler based on nanocomposites;
- nanotubes based on *GaN*: manufacture, characteristic and application.

For his successful work Professor Tito Huber was awarded a fellowship of the National Atomic Energy Commission (Argentine) and a NATO fellowship (1981).

International Thermoelectric Academy, Institute of Thermoelectricity of the National Academy of Sciences and Ministry of Education and Science, Youth and Sports of Ukraine, “Journal of Thermoelectricity” Publishers congratulate the esteemed Tito Huber on his jubilee, wishing him sound health and creative success in his work.



Kh.O. Khoshdurdyyev

Kh.O. Khoshdurdyyev

Turkmenkhimia State Concern, 11, A. Niyazov Ave.,
Ashgabat, 744036, Turkmenistan

THE EARTH'S THERMOELECTRICITY AS THE BASIS FOR POWER SUPPLIES OF MANKIND

Oil and other fossil fuels are formed of inorganic carbonates and water in the course of their electrochemical reduction by passing electric currents generated due to high temperature of the Earth's interior (thermal currents). Carbon dioxide formed during their combustion, absorbed by the Earth and converted into inorganic carbonates in its depths is the initial raw material of their formation, and due to the cyclic "formation-combustion" process, similar to water circulation in nature, the resource of fossil fuels is never-ending. Within this theory, clear definition is given of such global natural phenomena as non-photosynthetic process of oxygen release by the Earth through the oceans and absorption of carbon dioxide by the Earth through water surfaces.

Key words: thermal currents, electric reduction, fossil fuels.

Introduction

Fossil fuels account for almost all power supplies used by mankind, and without them it is difficult to imagine the today's level of human civilization. Nevertheless, oil ranks central due to its particularly valuable qualities. For some countries it is a vital necessity and to a large extent the basis for national policy. There is no product among the minerals that could be compared to oil in its significance. Annually, a huge amount of energy is consumed in the world which is equivalent in its energy effect to the use of over 11 milliard tons of oil. The share of oil, coal and natural gas is nearly 87 % of all energy resources consumed. And the first place is still occupied by oil which accounts for more than 1/3 of the entire world energy balance [1]. However, despite this, a conceptual scientific basis for a theory establishing the origin of oil in the Earth's crust which would be in good agreement with science, practice and logic does not exist today. Therefore, development of a scientific theory for this branch of science is a relevant scientific task which is also of a big practical value.

To have a chance for existence, any theory in the field of natural science, particularly related to energy and power engineering, should not contradict to the fundamental laws of natural science and logic. Moreover, it should be in full agreement with them. One of such laws is the first principle of thermodynamics, otherwise called "The law of conservation of energy" which means that energy can be neither created nor destroyed – it passes from one kind to another.

We will use this thesis as a foundation on which we will try to construct a theory of formation of oil and all other fossil fuels.

So, oil is energy material or, in other words, it carries energy. If it has energy, then it is only natural to ask: where did it take this energy from or, in terms of thermodynamics, what kind of energy has been converted into the energy of oil? In so doing, this energy, converted into oil, should be more than enough to cover the energy equivalent at least to 11 milliard tons of oil annually.

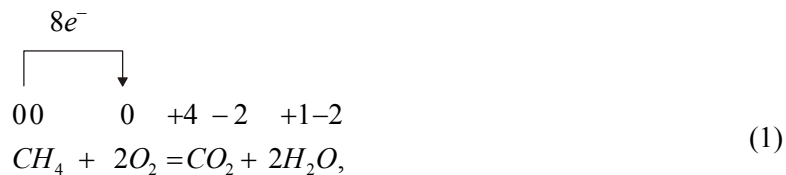
From the above information it logically follows that in the Earth's interior there should be a permanent source of energy whose energy passes into the energy of oil.

It is interesting what kind of a source it might be?

This question will serve a general line of seeking the ways for development of oil formation theory.

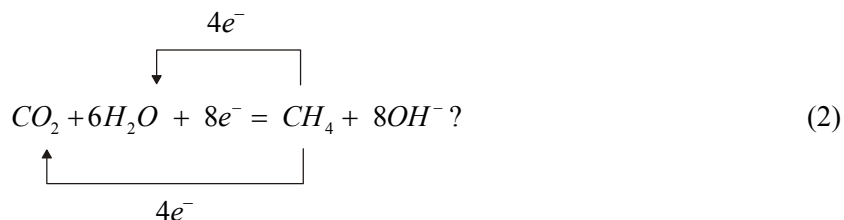
Hydrocarbon formation theory

The problem of creation of a new hydrocarbon formation theory will be formulated as a solution of the inverse problem of complete combustion of hydrocarbons in the presence of oxygen (the reason for this will become clear from the subsequent discussion).



The figures on the element symbols indicate their respective oxidation degrees.

As can be seen from equation (1), its respective reaction is oxidation-reduction, i.e. each methane molecule giving 8 electrons to two oxygen molecules is converted into one molecule of carbon dioxide and two molecules of water. It is natural to ask: could we obtain the initial reaction products (1) – $CH_4 + 2O_2$, if 8 electrons are passed into a mixture of final products ($CO_2 + 2H_2O$)? In other words, could reaction (1) proceed in the opposite direction:

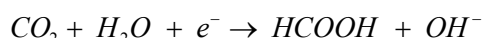


The origin of chemical processes in equation (2) means the reversibility of equation (1). It means the reversibility of processes described by these equations, which is in full agreement with the law of reversibility which is a fundamental law of nature and a principal conclusion from the universal thermodynamics [2, 3] elaborated by a Turkmen scientist, professor M. Mamedov.

Another natural question arises: is there any experimental data – as the basic truth criteria – as regards the electric reduction of carbonate compounds to lower carbon oxidation degrees? Yes, these processes successfully proceed in reactors-electrolyzers [4]. Besides, with carbon oxide reduction, a mixture of hydrocarbons - methane, ethane, ethylene – is formed on a cathode according to reaction:



or, with carbon dioxide reduction, formic acid is formed:



In so doing, processes of reduction of chemical substances are based both on direct and alternating electric current [5].

Thus, the intermediate conclusions:

1. The electrochemical theory of oil formation has sufficiently strong theoretical and experimental basis.
2. On passing electric current through oxidized carbon forms, the latter are reduced to less oxidized forms, sometimes completely to hydrocarbons.

For the electric reduction of carbonate compounds the following conditions should be observed in the electrolyzers: the presence of electrically conducting medium; the presence of electric current; the presence of carbonate material for the electric reduction.

If we show that in the Earth's crust there exist the same or close conditions for the above process, as in the electrolyzers, it will entitle us to admit the idea of the origin of similar processes in the Earth's crust.

According to classical geoelectricity, the electric current in the Earth is generated due to the action of solar plasma flux (the so-called "solar wind") on the magnetosphere [6, 7]. However, in our opinion, the main source of the Earth's electric current is high temperature of the Earth's centre (5000 °C) [8], owing to which a thermal current is formed which is directed from the Earth's centre to its entire surface.

The presence of a permanent magnetic field of the Earth [8] is a direct proof of the existence of direct electric current in it. Since thermal current is a direct current by nature, it should also create a direct field. If a direct magnetic field of the Earth is 99 % of the entire magnetic field of the Earth, it is logical that it is mainly a direct current that acts in the Earth, and since thermal current is a direct current by nature, logically it must be caused by high temperature of the Earth centre.

The presence of carbonate materials in the Earth is beyond question – almost all rocks include, as a rule, limestones, dolomites and other carbonates. In the present work by carbonates are meant all minerals, as well as to one extent or other oxidized carbon compounds.

Thus, we have indicated the presence of all conditions for the electric reduction of carbonates in the Earth's crust – it is electrically conductive, there is an electric current flowing in it and a large amount of carbonate minerals.

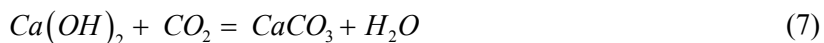
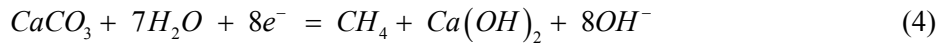
It is known [9] that the largest number of oil deposits is located at the boundaries of tectonic plates separated by spaces filled with liquid magma the external manifestations of which are volcanoes, geysers, mud volcanoes, the sources of hot or warm waters. In other words, these are the areas on the Earth's surface where the largest heat flow from the Earth's interior is found. According to the concepts of nonlinear nonequilibrium thermodynamics, if there is at least one flow in some direction, there are all the other possible flows. In this case we are interested in the theoretical possibility of electric current flow from the Earth's centre to its surface. The last achievements of thermodynamic theory, to be more precise, the principle of totality of flows, which is one of conclusions from the linear nonequilibrium thermodynamics developed, as mentioned above, by professor M. Mamedov, also confirms the theoretical possibility of thermal current.

From these considerations the reason for preferable location of oil deposits at the boundaries of geological tectonic plates becomes apparent. Naturally, all other factors being equal, the greater is the flow of heat, hence, of electricity, the greater is the amount of oil and gas.

Thus, the foregoing information suggests the following logical conclusion: oil is formed in the Earth's interior due to passing of the Earth's electric currents through carbonates and water. In other words, under the influence of the Earth's electric currents created by high temperature of the Earth's interior there is a transition of inorganic carbonates to organic, called "fossil fuels".

Basic equations of hydrocarbon formation

For clarity, let us consider full cycle of formation, combustion with generation of energy on the Earth's surface and absorption of combustion products (CO_2) by the Earth for methane which is the simplest hydrocarbon following the way proposed in this theory:



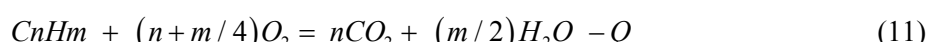
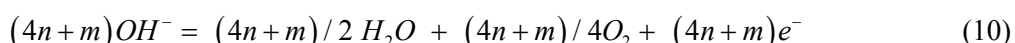
Let us comment on the schematic and equations (3 – 7).

Schematic (3) means that the Earth's heat which actually is a variety of energy denoted by Q , gives in the Earth a flow of electrons $8e^-$, or just an electric current. Later on, this electron flow, having passed through calcium carbonate and water (4), reduces carbonate carbon and hydrogen of water with formation of methane, calcium hydroxide and hydroxyl group.

Hydroxyl groups are passed by “relay-race reactions” through the drainage shell of the Earth and through the oceans they are carried out to the Earth's surface as oxygen and water, preliminarily subject to recombination reaction, and electron in this case also comes back to the initial point in (4). The resulting methane in the form of natural gas is carried out to the Earth's surface and used as energy (6). As this takes place, the initial energy E is released which, in fact, is the Earth's heat converted into thermal current and then methane as the energy of chemical bonds in methane molecule. In so doing, carbon dioxide and water are also formed. Then the resulting water joins total water circulation in nature, and carbon dioxide through the water surfaces and the Earth's drainage shell finally gets to that place in the Earth from where it was retrieved as methane. Naturally, in this case it will be immediately trapped by calcium hydroxide with formation of calcium carbonate. The equations (3), (4), (5) and (7) describe processes occurring in the Earth's interior, and the process described by equation (6) occurs on the Earth's surface.

Thus, our “travel” through equations (3 – 7) has led us to the initial equation (3) on which basis it is quite natural to believe that we deal with a cyclic process.

Equations (3 – 7) yield a precise material balance, which is a further argument in favour of proposed theory. Described by equations (3 – 7), processes for methane as a particular case of the variety of fossil fuel formation processes can be denoted by the following equations (8 – 12) for all fossil fuels:



In the above equations (8) – (12) all kinds of fossil fuels are denoted by one formula $CnHm$, not quite clear for non-specialists, hence small comment is needed.

First of all, n and m are only positive integers.

Formula $CnHm$, as a rule, means:

1. $m = 2n + 2$ – aliphatic hydrocarbons – methane homologues;
2. $m = 2n$ – olefinic or cycloaliphatic hydrocarbons;
3. $m = n$ – aromatic hydrocarbons;
4. $m \rightarrow 0$ or $m = 0$ – coal.

Genesis revisited

One of the main problems of Charles Darwin's theory of the origin of species is the absence in nature of the so-called "intermediate biological species", i.e. living organisms between the fish and reptiles, fish and birds, reptiles and birds and so on, which according to evolution theory once existed and resulted in current variety of biological species. Finding in nature of metamorphized remains of similar hypothetical animals would confirm this theory and, possibly, would lead to its recognition. However, they are absent in the nature, at least up to now no paleontological excavation in the world has ever discovered them, casting doubt upon the validity of this theory.

The theory of the origin of species deals with genesis of biological species, and the theory of the origin of fossil fuels offered for consideration of scientists and specialists covers the problems of genesis of oil and other fossil fuels. So, drawing certain analogy between these theories in order to eliminate the disadvantages of the former theory in the latter one seems quite natural.

Thus, putting it in plain language, this theory asserts that oil is formed from any carbonate-comprising rock (stone).

Carbonates are salts of carbonic acid H_2CO_3 ($CaCO_3$ – calcite, limestone, marble; $CaCO_3 \cdot MgCO_3$ – dolomites, etc. are part of many rocks) and comprise acid residual, namely a fragment of CO_3^{2-} which is the object of electric reduction by the Earth's currents, and logic suggests that oil must comprise oxygen-containing compounds. But is it confirmed by facts?

Indeed, oil comprises a variety of oxygen-containing compounds – "these oil components are represented by R-COOH acids, ArOH phenols, ketones, RCOOR ethers and lactones, less frequently by anhydrides and furan compounds, and their total content is 5 – 10 % "[10].

It counts in favour of the idea that a progenitor of oil is oxygen-containing carbon compound, such as carbonates.

The universally known English name for oil is "stone oil". Another English word for oil is petroleum. The geological dictionary says that "petro" means stone, and "oleum" – oil. Again we have come to stone oil! Why did people call this oil stone and not iron, aluminum, wooden or earthen? Why are these two names – stone and oil – inseparable?

One thing is indisputable: if your family name is Ivanov, your ancestor's name was Ivan! And, similarly, if material is called "stone oil", "stone" is of essential, if not major importance in the origin of this "oil".

There is a city called Balkanabat in Turkmenistan previously called "Nebitdag". "Nebit" in Turkmen means "oil", "dag" means "mountain", which is translated into Russian as "Neftegorsk" (Oil Mountain City). But mountain, as a rule, is stones, and again "stone" and "oil" are inseparable. May be, all these are accidents? It should be borne in mind that there are no accidents in nature!

Shales (Fig. 1) belong to terrigenous rocks with a parallel (layered) arrangement of low-temperature minerals. As is evident from the figure below, it is just a stone.

Visual comparison of these two shales shows that combustible shale has plenty of organic carbon which has certainly formed from its inorganic mate. However, are there inorganic carbonates in combustible shales?

Note the following information:

“Combustible shale (Fig. 2) consists of predominant mineral (calcites ($CaCO_3$), dolomite ($CaCO_3 \cdot MgCO_3$), illites, montmorillonite, kaolin, feldspars, quartz, pyrite, etc.) and organic parts (kerogen), the latter making 10 to 30 % of the rock mass and achieving 50 – 70 % only in top quality shales” [11]. As the phrase goes, comment is needless.

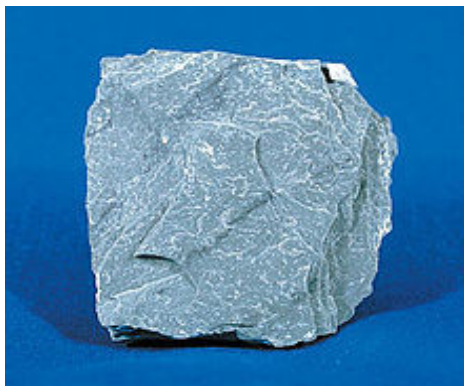


Fig. 1. Shale.



Fig. 2. Combustible shale.

We finish the etymology (etymology is a section of linguistics studying the derivation of words) of the word “oil” with the words of a great Russian chemist D.I. Mendeleyev: “Of crucial importance are positions of oil areas close to mountain ranges” [12, p. 239].

These perfectly correct notes of the great scientist could be supported and substantiated as follows: almost all rocks comprise carbonates. Mountains, basically, are a product of volcano activity which had abated after a lapse of great time intervals. At the present time the echoes of this abated activity are manifested in mountain regions as the hot sources of water – geysers, mud volcanoes or even active volcanoes. In other words, in the mountains or their vicinity there are oil-forming minerals and heat flow from the Earth’s interior which also account for electric current performing the main oil formation work. However, it does not necessarily mean that oil cannot be found beyond mountains! Fossil fuels shall be there where carbonate minerals are available (and they may be also in the Earth’s interior!), as well as heat flow and, hence, electric current from the Earth’s interior!

Yet another example. It is known that “...Norway is the second largest net exporter of gas in the world and the sixth largest exporter of oil” [13]. But for us the most important is that this Scandinavian country with the world hydrocarbon supplies is near Iceland, otherwise called “The country of geysers and volcanoes”. Naturally, the proximity of places of huge heat flows from the Earth’s interior and the abundance of hydrocarbons is not an accidental geographical phenomenon. Such examples are numerous: the point is that practically all large hydrocarbon deposits are located at the fractures of geological tectonic plates.

Global energy cycle

Processes described above by equations (8 – 12) can be represented in the form of a cyclic process, as shown below. Since this cycle describes formation and use of all conventional fossil fuels

and in view of the fact that they make the basis for practically all (nearly 90 %) power supplies used by mankind, it is reasonable to call it "Global energy cycle" (Fig. 3).

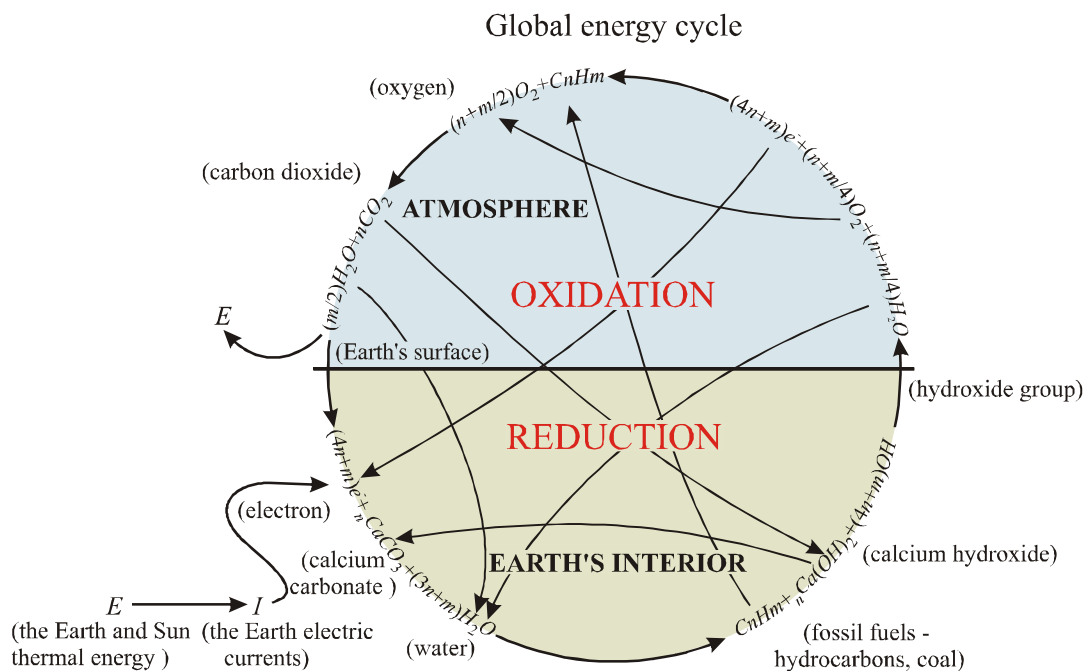
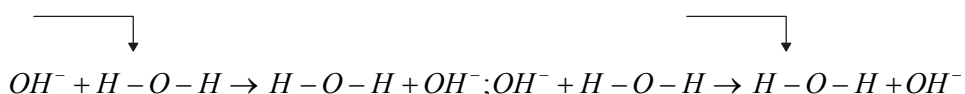


Fig. 3. Global energy cycle.

Letters n and m in the indexes and coefficients have identical values. It is natural to assume that coefficients n and m are functions of parameters characterizing conditions of process origin. It is also logical that coal is also formed according to the above scheme with a large deficit or in the absence of water in electric reduction zone. Thus, oil formation theory that consists in formation of oil and other fossil fuels in the Earth's interior by electric reduction of inorganic carbonates to "organic carbonates" (otherwise called fossil fuels) by terrestrial currents (thermal current) formed by the high temperature of the Earth centre answers all the questions that had been raised in the Introduction. Besides, this theory, on the one hand, predicts oxygen release from the Earth's interior, on the other hand – carbon dioxide absorption by the Earth, both these processes having no relation to photosynthetic process. But is there any oxygen release from the Earth? Yes, this process takes place in nature. Note the following information: "It is known that the main supplier of oxygen to the atmosphere is the world ocean, rather than vegetation" [14, 15]. It is quite reasonable to ask: where it comes to the ocean from?

As can be seen from the above picture and equations, a hydroxyl group which is a charged chemical particle is formed as a product of electric reduction of carbonates. Just like proton H^+ , this particle can be passed along the water chain for huge distances owing to the so-called "relay-race reactions" [16] along the Earth's drainage shell [17, 18] according to the scheme:



and so on, till hydroxyl groups reach the water surface to be discharged with oxygen formation according to known scheme:



and, finally, oxygen comes to atmosphere through the water surfaces.

Is carbon dioxide absorbed by the Earth? Yes, it is. Let's get down to facts.

"Ponds and other small freshwater bodies absorb carbon from atmosphere in much larger quantities than is considered to be the case. John Downing and his colleagues from the University of Iowa demonstrated this by an example of small "farmer ecosystems". They came to conclusion that, first, on the cultivated lands of the USA small ponds absorb 20 – 50 times more carbon atoms than trees planted on the same area. And, second, in the ratio between absorption and area, ponds are well ahead of large lakes.

According to estimates of scientists, there are nearly 300 million natural ponds and lakes in the world, of total area about 4.2 million km², which is twice the figures reported earlier. More than 90 % of these water bodies have areas less than a hectare. According to Downing, ponds and lakes contribute to carbon circulation no less than oceans with all their weeds [19].

Naturally, carbon dioxide dissolved in water also moves to the Earth's interior along the Earth's drainage shell and, finally, gets to that place from where it was retrieved in the form of fossil fuels.

Confinedness of hydrocarbon deposits and earthquakes to the boundaries of geological (also called "tectonic") plates, in conformity with the theses of this oil formation theory, suggests the idea that, possibly, earthquakes occur in the cases when oxygen carryover from the electric reduction zone is complicated or impossible due to formation of oxygen-fuel "explosive mixture".

Summarizing the foregoing, it can be stated that this theory claims to establish theoretically the existence of some earlier unknown natural phenomena, namely the presence of thermal current in the Earth due to high temperature in its centre, formation of fossil fuels by passing of the Earth's currents through carbonates and water. It also explains previously known natural phenomena, such as the entry of the bulk of oxygen to atmosphere through the oceans, absorption of carbon dioxide by the Earth and logically substantiates a new standpoint for earthquakes.

Thus, if the Earth's heat does not decline, and it will not decline, then oil, gas, coal will be everlasting! This is the principle of endlessness of the Earth's energy resources. This is the main conclusion from the theory proposed in this study. In this connection, the concept of "nonrenewable energy sources" to which fossil fuels have been referred to this date, becomes meaningless, since they are shown to be renewed. And, logically, repeated formation of hydrocarbons and coal will take place mainly in the same geographical coordinates where they have been formed before and are still formed today.

Thus, one can state the discovery of earlier unknown natural phenomenon the essence of which is that fossil fuels are formed of inorganic carbonates electrically reduced to "organic" carbonate (coal) or its compounds (oil, gas) by the Earth's currents (thermal current) formed by high temperature of the Earth's centre.

Therefore, the earlier hypothesis [20, 21] and theory [22] of formation of oil and all fossil fuels can be considered completely proved.

Logically, the Earth is a natural converter of its own heat via thermoelectricity to the energy of fossil fuels and simultaneously produces oxygen and passes it through the water surfaces to the Earth atmosphere, being its main supplier.

References

1. Global Energetic Trends. www.rcb.ru
2. M.M. Mamedov, N.M. Mamedov, The Law of Reversibility of Steady-State Nonequilibrium Processes – the Fundamental Law of Nature Following from the Second Principle of Thermodynamics, *Yestestvennyye i Tekhnicheskiye Nauki* 2, 18-19 (2008).

3. M.M. Mamedov, B.M. Mamedov, Fundamentals of Universal Nonequilibrium Thermodynamics, *Aktualnyye Problemy Sovremennoi Nauki*, 1, 115-118 (2012).
4. *Intensification of Electrochemical Processes* (Moscow: Nauka, 1988), p. 149.
5. L.P. Shulgin, *Electrochemical Processes on Alternating Current* (Leningrad: Nauka, 1974), p. 16 – 29.
6. A.P. Krayev, *Fundamentals of Geoelectricity* (Leningrad: Nedra, 1965).
7. S.Yu. Balasanyan, *Dynamic Geoelectricity* (Novosibirsk: Nauka, 1990).
8. *Big Encyclopedia of Kirill and Mefodiy. Electronic version.* 2007.
9. M.K. Kalinko, *Inorganic Origin of Oil in the Light of Present-Day Knowledge* (Moscow: Nedra, 1968).
10. <http://dic.academic.ru/>
11. Combustible Shale www.wikipedia.ru
12. D.I. Mendeleyev, *Oil Industry in the North American State of Pennsylvania and in the Caucasus* (Saint-Petersburg: Printing House of “Social Benefit” Partnership, 1877).
13. Oil and Gas. www.norvegia.ru/About_Norway/business/industries/oilgas/
14. World Ocean as Oxygen Supplier. www.astronet.ru www.okeanavt.ru
15. Oxygen from the Earth Depths. www.rust.su
16. I.A. Khairetdinov, *Introduction to Electrgeochemistry* (Moscow: Nauka, 1980).
17. V.I. Vernadsky, *Selected Works, Vol.1-5* (Moscow: AN SSSR Publ., 1954-1960).
18. S.M. Grigoryev, *The Role of Water in Formation of the Earth's Crust (Drainage Sheath of the Earth's Crust)* (Moscow: Nedra, 1971).
19. Ponds Absorb Carbon, “*Neutral Turkmenistan*” *Newspaper*, 04.06.2008, p.3, with reference to Internet-site “*Izvestiya Nauki*” www.gazeta.ru
20. On the Physics and Chemical Version of Carbonaceous Energy Substances Formation in the Earth's Crust, *Nauka i Tekhnika v Turkmenistane* 4, 35 – 43 (2005).
21. On the Physics and Chemical Version of Fossil Fuels Formation in the Earth's Crust, *Yestestvennyye i Tekhnicheskiye Nauki* 2, 166-170 (2005).
22. Electrochemical Theory of Oil Formation, *Yestestvennyye i Tekhnicheskiye Nauki* 2, 253 – 255 (2001).

Submitted 11.06.2011.

ARTICLE PREPARATION RULES

The article shall conform to the journal profile. The article content shall be legible, concise and have no repetitions.

The article shall be submitted to the editorial board in electronic version.

The text shall be typed in text editor not lower than MS Word 6.0/7.0.

Page setup: “mirror margins”- top margin – 2.5 cm, bottom margin – 2.0 cm, inside – 2.0 cm, outside– 3.0 cm, from the edge to page header – 1.27 cm, page footer – 1.27 cm.

Graphic materials, pictures shall be submitted in color or, as an exception, black and white, in .ojp or .cdr formats, .jpg or .tif formats being also permissible. According to author’s choice, the tables and partially the text can be also in color.

The article shall be submitted in English on A4 paper sheets; the number of pages shall not exceed 12. By agreement with the editorial board, the number of pages can be increased.

To accelerate publication of the article, please adhere to the following rules:

- the authors’ initials and names are arranged in the centre of the first page at the distance of 1 cm from the page header, font Times New Roman, size 12 pt, line spacing 1.2;
- the name of organization, address (street, city, postal code, country) – indent 1 cm below the authors’ initials and names, font Times New Roman, size 11 pt, line spacing 1.2, center alignment;
- the title of the article is arranged 1 cm below the name of organization, in capital letters, semi-bold, font New Roman, size 12 pt, line spacing 1.2, center alignment. The title of the article shall be concrete and possibly concise;
- the abstract is arranged 1 cm below the title of the article, font Times New Roman, size 10 pt, in italics, line spacing 1.2 ,center alignment;
- key words are arranged below the abstract, font Times New Roman, size 10 pt, line spacing 1.2, justified alignment. The title “Key words” – font Times New Roman, size 10 pt, semi-bold;
- the main text of the article is arranged 1 cm below the abstract, indent 1 cm, font Times New Roman. size 11 pt, line spacing 1.2, justified alignment;
- formulae are typed in formula editor, fonts Symbol, Times New Roman. Font size is “normal” – 12 pt, “large index” – 7 pt, “small index” – 5 pt, “large symbol” – 18 pt, “small symbol” – 12 pt. The formula is arranged in the text, centre aligned and shall not occupy more than 5/6 of the line width, formulae are numbered in round brackets right;
- dimensions of all quantities used in the article are represented in the International System of Units (SI) with the explication of the symbols employed;
- figures are arranged in the text. The figures and pictures shall be clear and contrast; the plot axes – parallel to sheet edges, thus eliminating possible displacement of angles in scaling;
- tables are arranged in the text. The width of the table shall be 1 cm less than the line width. Above the table its ordinary number is indicated, right alignment. Continuous table numbering throughout the text. The title of the table is arranged below its number, center alignment;
- references should appear at the end of the manuscript. References within the text should be enclosed in square brackets. References should be numbered in order of first appearance in the text. Examples of various reference types are given below.

- L.I. Anatychuk, *Thermoelements and Thermoelectric Devices: Handbook* (Kyiv: Naukova Dumka, 1979), p.766. (Book)
- T.M. Tritt, Thermoelectric Phenomena, Materials, and Applications, *Annual Review of Materials Research* **41**, 433 (2011). (Journal paper)
- U. Ghoshal, *Proceedings of the XXI International Conference on Thermoelectrics* (N.Y., USA, 2002), p. 540. (Proceedings Conference)

The article should be supplemented by:

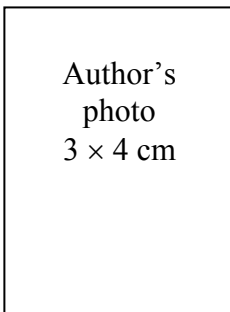
- letter from the organization where the work was performed or from the authors of the work applying for the publication of the article;
- information on the author (authors): last name and initials; full name and postal address of the institution where the author works; academic degree; position; telephone number; E-mail;
- author's (authors') photo in color or, as an exception, in black and white. With the number of authors more than two their photos are not given;
- author's application to the following effect:

We, the undersigned authors, ... transfer to the founders and editors of "Journal of Thermoelectricity" the right to publish the article...in Ukrainian, Russian and English. This is to confirm that the present publication does not violate the copyright of other persons or organizations.

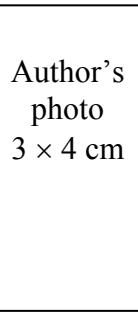
Date

Signatures

Below is given an example of article preparation.



A.I. Casian¹, B.M. Gorelov²



¹Technical University of Moldova,
168, Stefan cel Mare Ave.,
Chisinau, MD-2004, Moldova;
²Institute of Surface Chemistry of National Academy
of Sciences of Ukraine, 17, Gen. Naumov Str.,
Kyiv, 03164, Ukraine

STATE OF THE ART AND PROSPECTS OF THERMOELECTRICITY ON ORGANIC MATERIALS

The aim of the paper is to analyze the expected thermoelectric opportunities of organic materials, including some highly conducting quasi-one-dimensional crystals. It is shown that interest of investigators in these materials has been growing recently. Quasi-one-dimensional organic crystals have high prospects for thermoelectric applications. These materials combine the properties of multi-component systems with more diverse internal interactions and of quasi-one-dimensional quantum wires with increased density of electronic states. It is shown that the values of the thermoelectric figure of merit $ZT \sim 1.3 - 1.6$ at room temperature are expected in really existing organic crystals of tetrathiotetracene-iodide, TTT_2I_3 , if the crystal parameters are approaching the optimal ones.

Keywords: thermoelectricity, tetrathiotetracene-iodide, polarizability.

Introduction

It is known that conducting organic materials usually have much lower thermal conductivity than the inorganic materials. Moreover, the organic materials can be fabricated by simpler chemical methods, and it is expected that such materials will be less expensive in comparison with the inorganic ones. Exactly these properties attracted attention to such materials for the use in thermoelectric (TE) applications long time ago [1, 2]. In spite of relatively high value of the thermoelectric figure of merit $ZT = 0.15$ at room temperature observed in polycopper phthalocyanine [2] as early as 1980, the thermoelectric properties of organic materials are still weakly investigated. This situation has the only explanation that thermoelectricians are still weakly interested in organic materials, and organic chemists are also weakly interested in thermoelectric materials. Moreover, in order to seek good organic thermoelectrics, it is necessary to organize multidisciplinary consortiums of physicists, organic chemists and engineers in the field of thermoelectricity.

The aim of this paper is to present briefly the state-of-the-art of investigations in the area of new organic thermoelectric materials and to describe the nearest expected results for really existing quasi-one-dimensional organic crystals of tetrathiotetracene-iodide, TTT_2I_3 .

Quasi-one-dimensional organic crystals of TTT_2I_3

The structure of quasi-one-dimensional organic crystals of tetrathiotetracene-iodide, TTT_2I_3 , has been briefly described in [34]. These needle-like crystals are formed of segregate chains or stacks of planar molecules of tetrathiotetracene TTT , and iodine ions. The chemical compound TTT_2I_3 is of mixed-valence: two molecules of TTT give one electron to the iodine chain which is formed from I_3^- ions. The

conductivity of iodine chains is negligibly small, so that only *TTT* chains are electrically conductive and holes serve as carriers. The electrical conductivity σ along *TTT* chains at room temperature varies between 10^3 and $10^4 \Omega^{-1}\text{cm}^{-1}$ for crystals grown by gas phase method [35], and between 800 and $1800 \Omega^{-1}\text{cm}^{-1}$ for crystals grown from solution [36]. Thus, the conductivity is very sensitive to crystal impurity and perfection which depends on growth method. In the direction perpendicular to chains σ is by three orders of magnitude smaller than in the longitudinal direction and is neglected.

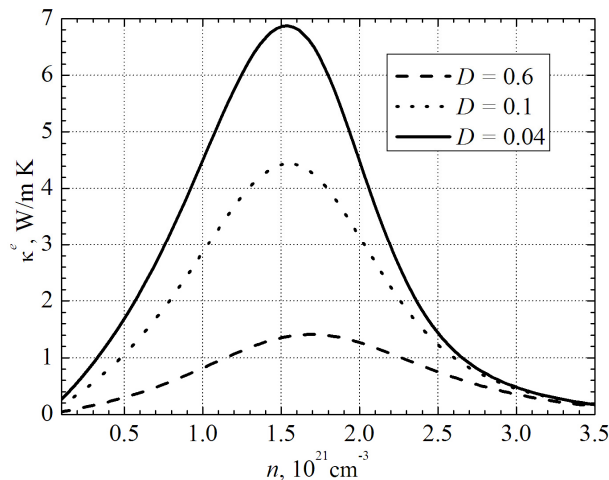


Fig. 1. Dependences of electron thermal conductivity κ^e on n .

$$\sigma = R_0, S = R_1 / eTR_0, \kappa^e = (e^2 T)^{-1} \left(R_2 - R_1^2 / R_0 \right), \quad (1)$$

Thermoelectric properties

Expressions (2) – (3) have been calculated in order to determine the thermoelectric properties of quasi-one-dimensional organic crystals of TTT_2I_3 with different degrees of purity....

Conclusions

The state-of-the-art of research on new organic materials for thermoelectric applications is analyzed. It is shown that the interest of investigators in these materials has been growing in recent years. The highest value of $ZT \sim 0.38$ at room temperature has been measured in doped acetylene, with the only problem that this material is not stable. Accurate control of the oxidation level in poly (3, 4-ethylenedioxythiophene) (PEDOT) gave the power factor $324 \mu\text{W}\cdot\text{m}^{-1}\text{K}^{-2}$ and in combination with its low intrinsic thermal conductivity ($\kappa = 0.37 \text{ W}\cdot\text{m}^{-1}\text{K}^{-1}$) yielded $ZT = 0.25$ at room temperature, and this material is air-stable....

References

- Ali Shakouri, Recent Developments in Semiconductor Thermoelectric Physics and Materials, *Annu. Rev. Mater. Res.* **41**, 399–431 (2011).
- L.I. Anatychuk, *Thermoelectricity, Vol.2, Thermoelectric Power Converters* (Kyiv, Chernivtsi: Institute of Thermoelectricity, 2003), 376p.
- M.E. Bengen, *German Patent Appl. OZ 123, 438, 1940; German Patent 869,070, 1953, Tech. Oil Mission Reel, 143,135, 1946.*